Chapter 9

On the Indicatrixes of Waves Scattering from the Random Fractal Anisotropic Surface

Alexander A. Potapov

Additional information is available at the end of the chapter

http://dx.doi.org/10.5772/intechopen.68187

Abstract

Millimeter and centimeter wave scattering from the random fractal anisotropic surface has been theoretically investigated. Designing of such surfaces is based on the modifications of non-differentiable two-dimensional Weierstrass function. Wave scattering on a random surface is interesting for many sections of physics, mathematics, biology, and so on. Questions of a radar location and radio physics take the predominating position here. There are many real surfaces and volumes in the nature that can be carried to fractal objects. At the same time, the description of processes of waves scattering of fractal objects differs from classical approaches markedly. There are many monographs in the world on the topic of classical methods of wave scattering but the number of books devoted to waves scattering on fractal stochastic surfaces is not enough. These results of estimation of three-dimensional scattering functions are a priority in the world and are important in radar of low-contrast targets near the surface of the earth and the sea.

Keywords: fractal, fractal surfaces, Kirchhoff approach, radio waves scattering, Weierstrass function, radar, low-contrast targets

1. Introduction

There are a lot of scientific and engineering problems, which can be successfully solved only with deep understanding of wave-scattering characteristics for statistically rough surface (see, e.g., [1–3] and references). In this section, we consider the main issues of theory of fractal wave scattering on the statistically rough surface as applied to problems of image creation by radar methods (RMs). These issues are crucial for radio location of low-contrast targets on the background of earth and sea surface.

In the general case, RM can be interpreted as a scattering specific effective squares (SESs), as a σ_* card (matrix) or as a signature (portrait) of object being sounded for the high angular resolution. SES card with fuzzy bounds corresponds to real RM for the wide-probing beam. RM resolution increase necessitates the use of complicated probing signals. Subject detail digital radar maps (DDRM or etalons) are often results of current image processing [4–8].

Currently, there are two general approaches of scattering on the statistically rough surface: method of small perturbation (SP) and Kirchhoff approach (tangent plane method (TPM)). These methods relate to two extreme cases of very small flat irregularities or smooth and large irregularities, respectively. Two-scale scattering model becomes a generalization of these methods. The model is a combination of small ripple (computations using SP) and large irregularities (computations using TPM). Review of these methods evolution is represented in Refs. [1–3].

Thus, before the present diffraction problems for the statistically rough surfaces took into account irregularities of only a single scale. Soon, it had been realized that multiscale surfaces lead to better fitting. As we have found out [6, 7] fractality accounting makes theoretical and experimental scattering patterns for earth cover in microwaves range closer. This fact is always interpreted (and has been interpreted now) as results of pure instrumental errors.

The aim of this work is to report systematically and consistently about theoretical solution of scattering problem for the random fractal anisotropic surface using Kirchhoff approach for the first time, to calculate scattering indicatrixes for radio microwaves, and to analyze the ensemble of indicatrixes obtained.

2. Formulation of the problem

Idea of fractal radio systems in the framework of fractal radio physics and radio electronics that was proposed and now is being consistently developed in the Institute of Radio Engineering and Electronics of the RAS (see, e.g., [5–48] and references) allows us to look at conventional radio physics methods in a new fashion. Currently, fractal radio physics and fractal radio location are the very active investigation areas, where significant applications have been obtained.

New problems that arise and being formulated are very important for every branch of science in the sense of its evolution. During the last 35 years, we succeeded in developing a number of important sections of fractal radio physics and fractal radio electronics that almost completes its main structure [6–8]. At once, these results reveal perspective of its modern applications and new relations between fractal physics and classical radio physics and electronics. It is necessary to note that for this course several monographs and more than 800 studies and 23 monographs were published (e.g., look at Refs. [5–48] and references).

Figure 1 shows us the main courses of works that are being carried out in the Institute of Radio Engineering and Electronics of the RAS and also information about the moment of its intensive growth beginning is demonstrated (for details, see Refs. [6, 7]). For such a "fractal" approach, it

http://dx.doi.org/10.5772/intechopen.68187

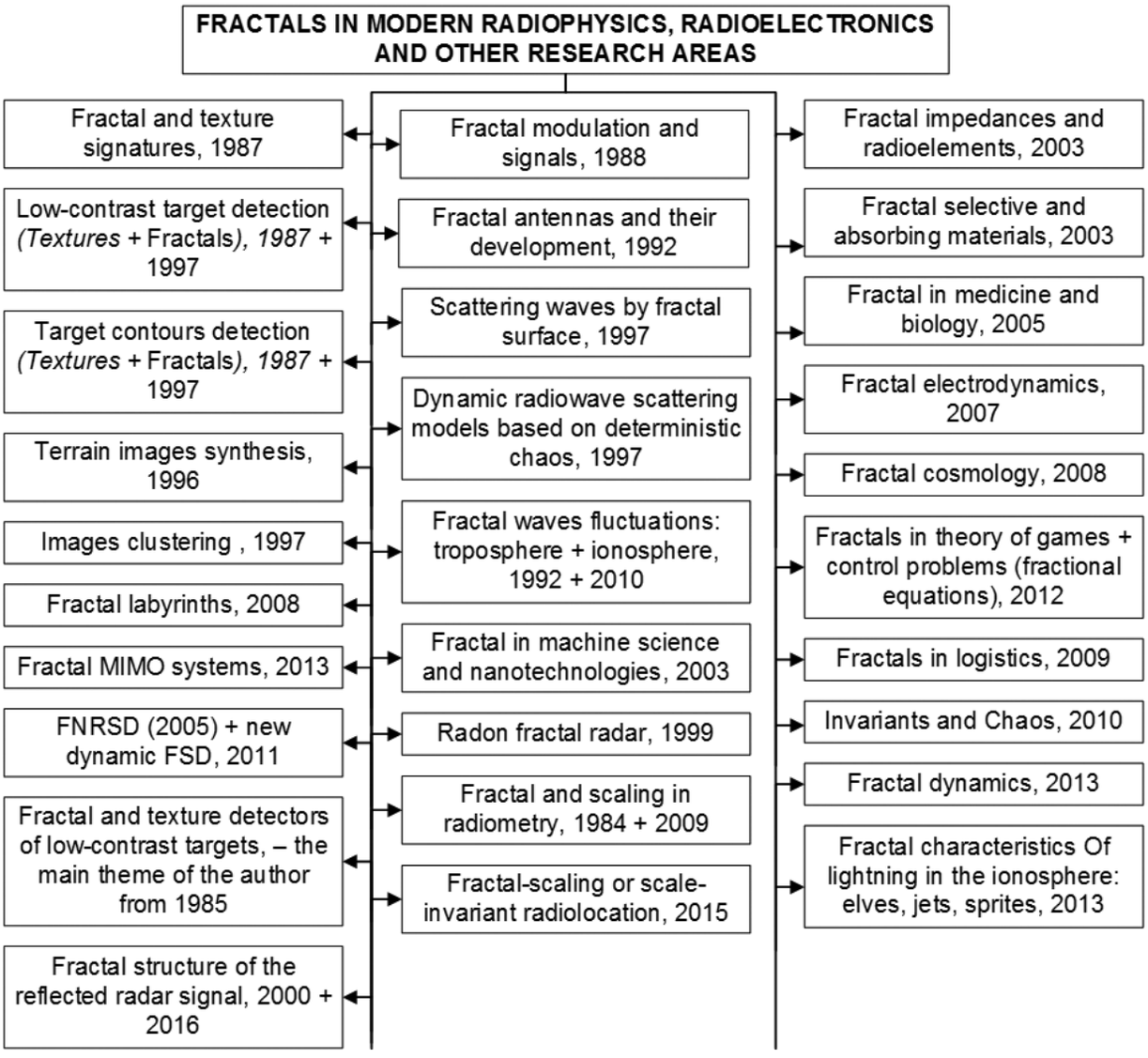

Figure 1. Sketch of development of a new information technology.

is natural to focus on analysis and also on the processing of radio physical signals (fields) only in space of fractional measuring using hypothesis of scaling and distributions with "heavy tales" or stable distributions. Note that scale transformations using scaling effects are widespread in up-to-date physics when different relations between thermodynamical values in renormgroup theory of phase changes are setting up [49].

Fractals belong to sets, which have extremely branched and irregular structure. In December 2005 in the USA, Mandelbrot approved [34] fractal classification that was developed by the author and is presented in **Figure 2**, where fractal features are characterized so long as there is a fractal structure with fractal dimension D in the space with topological dimension. Physical mathematical problems of the fractals theory and fractional measuring are represented in monographs [6–8] in detail.

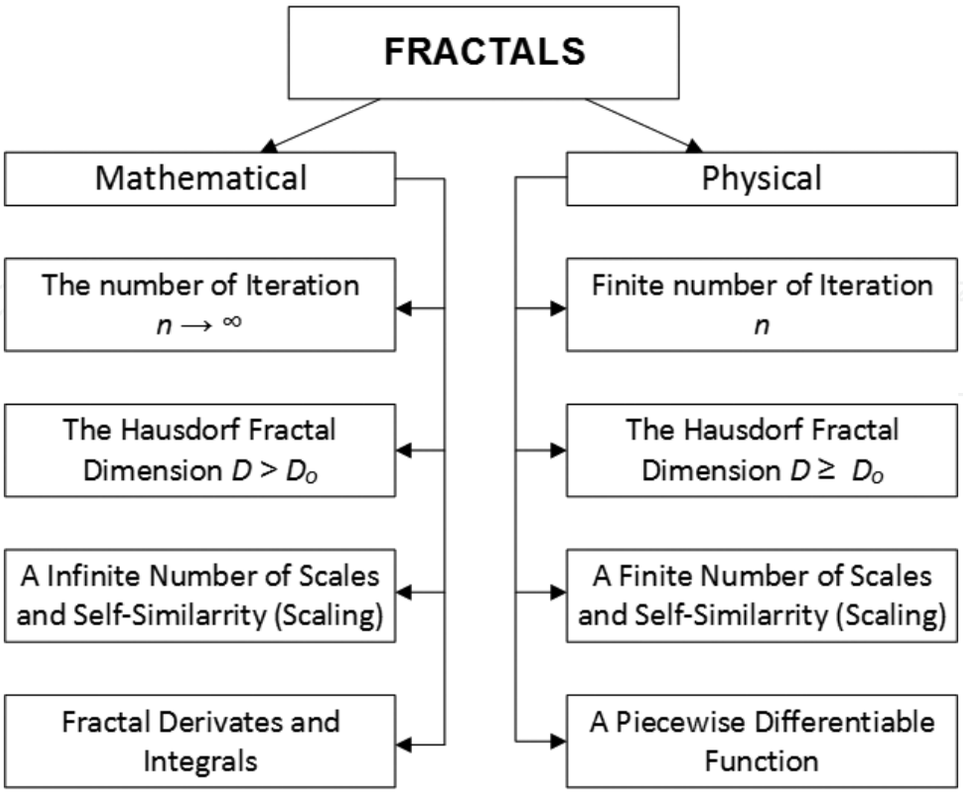

Figure 2. Classification and morphology of fractal sets and fractal set signatures.

In case of RM formation, the structure and parameters of wave field, which is generated by remote random surface at the field analysis area, depend on receiving point location and surface parameters. By taking into account these facts, we have to analyze the scattered field in a time-spatial continuum [5]. Therefore in the late 1970s of the XX century, the author formulated the problem of creating a theoretical modeling the band of millimeter and centimeter waves (MMW and CMW, respectively) for radar time-spatial signal by taking into account radio channel "antenna's aperture–atmosphere–targets–chaotic covering without vegetation" and the problem of creating of new features classes for radar targets recognition or radar signatures [5].

3. "Diffraction by fractals" ≠ "classical diffraction"

Effectiveness of radio physical investigations can be significantly improved by taking into account fractality of wave phenomena that are progressing at every stage of wave radiation, scattering, and propagation in different medium. In spite of pure scientific interest, there are practical applications to the radar and telecommunications problems solution and also to problems of mediums monitoring at different time-spatial scales.

Recently, interest to investigate wave scattering by rough surfaces that have non-Gaussian statistics has also grown. They often argue that correlation spatial coefficient of dispersive surface $\rho(\Delta x = x_2 - x_1, \Delta y = y_2 - y_1)$ cannot be exponential due to non-differentiability of respective random process. Sometimes in this case they use regularizing function about a zero

http://dx.doi.org/10.5772/intechopen.68187

point. Fundamental physical foundation of non-differentiable functions application for wave-scattering analysis was developed only after taking into account fractal theory, fractional-measuring theory, operators of integro-differentiation, and scaling relations in radio physical problems [6, 7, 20].

It is significant to note that Gaussian model is parabolic near the angle of incidence $\theta \approx 0$, while the exponential model is linear near the same point. Below, we consider in detail the approach to scattering of MMW and CMW by fractal random surface [5–7, 20, 39–44, 47].

At the present time, many works of foreign authors are related with wave interaction with fractal structures (see, e.g., respective chapters in monographs [6, 7]). Fractal surface implies the presence of irregularities of all scales with respect to scattered wavelength. Therefore, fractal wave front being non-differentiable does not have normal. In that way, conceptions of "ray trajectory" and "ray optics effects" are excluded. However, chords, which connect values of typical irregularity heights at the certain horizontal distances, still have finite root-mean-square slope. For this case, "topoteza" of fractal random surface is introduced; it is equal to the length of surface slope closeness to the unity [6, 7, 20].

Subject to all features, there are scattering models in the west of author works: (1) model of fractal heights and (2) model of fractal irregularities slopes. Thus, model No. 2 is once differentiable and has a slope that is changing continuously from point to point. This model leads to ray optics or to effects that are described using the conception of "ray." Such a kind of scattering was investigated together with radio waves propagation in the ionosphere [6, 7].

Electromagnetic waves scattering by fractal surfaces was investigated in detail in Refs. [50–58]. In Ref. [50], it was shown that diffraction by fractal surfaces fundamentally differs from diffraction by conventional random surfaces and some of classical statistical parameters like correlation length and root-mean-square deviation go to infinity. It is due to self-similarity of fractal surface. In Ref. [52], band-limited Weierstrass function was used. Less restrictions were imposed than the ones in Ref. [50]. The proposed function possesses both self-similarity property and still finite number of derivatives over a certain range under consideration. This relaxation of conditions of Weierstrass function allows performing analytical and numerical calculations.

Though there are many works on the creation and analysis of chaotic surfaces with the fractal structure [6, 7, 55–58], only few of them consider two-dimensional (2D) fractal surfaces. Corrugated surfaces that possess fractal properties only for one dimension (1D) were characterized in some works [52, 53, 59, 60]. In Refs. [39–44, 47, 61–63], modified Weierstrass function was used for designing 2D fractal chaotic surface. This function was derived from band-limited Weierstrass function. General solution for scattered field was obtained using Kirchhoff theory [1–3, 5–7, 61–65]. On this basis, we will carry out further calculations.

4. Fractal model of 2D chaotic surface

Modified 2D band-limited Weierstrass function has the view [6, 7, 20, 39–44, 47, 61–63]

$$W(x,y) = c_w \sum_{n=0}^{N-1} q^{(D-3)n} \sum_{m=1}^{M} \sin\left\{ Kq^n \left[x \cdot \cos\left(\frac{2\pi m}{M}\right) + y \cdot \sin\left(\frac{2\pi m}{M}\right) \right] + \phi_{nm} \right\}, \quad (1)$$

where c_w is the constant that provides unit normalization; $q > 1$- is the fundamental spatial frequency; D is the fractal dimension ($2<D<3$); K is the fundamental wave number; N and M are the number of tones; ϕ_{nm}- is an arbitrary phase that has a uniform distribution over the interval $[-\pi, \pi]$.

Eq. (1) is a combination of random structure and determined period. Function $W(x, y)$ is anisotropic in two directions if M and N are not very large. It has derivatives, and at the same time, it is self-similar. Respective surface is multiscale and roughness can vary depending on the scale being considered. Since the natural surfaces are neither purely random nor periodical and are often anisotropic [5, 40], the function that was proposed above is a good candidate for characterizing natural surfaces.

5. Relationships between statistical parameters of roughness measurements and fractal surface parameters

Such parameters as correlation length Γ, mean-root-square deviation σ, and spatial autocorrelation coefficient $\rho(\tau)$ are conventionally used for numerical characterization of rough surface. In this section of our work, these statistical parameters are introduced for the estimation of fractal dimension D influence and other fractal parameters influence on the surface roughness. Similar relationships are presented in Refs. [6, 7, 20] for 1D fractal surfaces. Derivations of σ and $\rho(\tau)$ for 2D fractal surfaces are cumbersome and tedious [61], and so we present here only some final results.

5.1. Mean square deviation

The mean-root-square deviation $\boldsymbol{\sigma}$ is determined as

$$\sigma = \left(\langle W^2(\vec{r}) \rangle_{\mathbf{s}} \right)^{1/2} \quad (2)$$

where $W(\vec{r}) = W(x, y)$; $\vec{r} = x\vec{\mathbf{I}} + y\vec{\mathbf{J}}$. Angle bracket implies ensemble averaging.

From Eqs. (1) and (2), we have

$$\sigma = \mathrm{c}_w \left[\frac{M\left(1 - q^{2(D-3)N}\right)}{2\left(1 - q^{2(D-3)}\right)} \right]^{\frac{1}{2}}. \quad (3)$$

If $\sigma = 1$, then Eq. (3) is as follows:

http://dx.doi.org/10.5772/intechopen.68187

$$c_w = \left[\frac{2\left(1-q^{2(D-3)}\right)}{M\left(1-q^{2(D-3)N}\right)}\right]^{\frac{1}{2}}. \tag{4}$$

Thus, Eqs. (1) and (4) are as follows:

$$W_{\text{н}}(x,y) = \left[\frac{2(1-q^{2(D-3)})}{M(1-q^{2(D-3)N})}\right]^{1/2} \sum_{n=0}^{N-1} q^{(D-3)n} \sum_{m=1}^{M} \sin\left\{Kq^n\left[x\cdot\cos\left(\frac{2\pi m}{M}\right)+y\cdot\sin\left(\frac{2\pi m}{M}\right)\right]+\phi_{nm}\right\}. \tag{5}$$

Eq. (5) is normalized with $\sigma = 1$. A normalized function will be used in the following sections for the analysis and modeling of wave field scattered by fractal surfaces. Surface becomes more isotropic with the increase of N and M. It is important to notice that $W_u(x, y)$ characterizes mathematical fractals only if $N \to \infty$ и $M \to \infty$.

5.2. Coefficient of spatial autocorrelation and of correlation length

Now, let us turn to the consideration of spatial autocorrelation coefficient $\rho(\tau)$ and correlation length Γ. By definition

$$\rho(\tau) = \frac{\langle W_{\text{н}}(\vec{r}+\vec{\tau})W_{\text{н}}(\vec{r})\rangle_s}{\sigma^2} \tag{6}$$

$$\text{where } \tau = (\Delta x^2 + \Delta y^2)^{\frac{1}{2}}. \tag{7}$$

From Eqs. (5) and (6), we have

$$\rho(\tau) = \left[\frac{\left(1-q^{2(D-3)}\right)}{M\left(1-q^{2(D-3)N}\right)}\right] \sum_{n=0}^{N-1} q^{2(D-3)n} \sum_{m=1}^{M} \cos\left[Kq^n\tau\cdot\cos\left(\theta-\frac{2\pi\cdot m}{M}\right)\right], \tag{8}$$

$$\text{where } \sin\theta = \frac{\Delta y}{\tau},\ \cos\theta = \frac{\Delta x}{\tau}. \tag{9}$$

The average spatial autocorrelation coefficient

$$\tilde{\rho}(\tau) = \langle\rho(\tau)\rangle_s = \left[\frac{\left(1-q^{2(D-3)}\right)}{\left(1-q^{2(D-3)N}\right)}\right] \sum_{n=0}^{N-1} q^{2(D-3)n} J_0(Kq^n\tau), \tag{10}$$

where $J_0(Kq^n\tau)$ is the zero-order Bessel function of the first kind.

Correlation length Γ is defined as the first root of $\rho(\tau) = 1/e$ when τ increases from zero. From relationship (8)

$$\left[\frac{(1-q^{2(D-3)})}{M(1-q^{2(D-3)N})}\right]\sum_{n=0}^{N-1}q^{2(D-3)n}\sum_{m=1}^{M}\cos\left[Kq^{n}\Gamma\cdot\cos\left(\theta-\frac{2\pi\cdot m}{M}\right)\right]=1/e. \tag{11}$$

Similarly from Eq. (10), the average correlation length is defined $\breve{\Gamma}$:

$$\frac{(1-q^{2(D-3)})}{M(1-q^{2(D-3)N})}\sum_{n=0}^{N-1}q^{2(D-3)n}J_0(Kq^{n}\tilde{\Gamma})=1/e. \tag{12}$$

From Eqs. (10)–(12), one can find relationships between average correlation length $\breve{\Gamma}$, fractal dimension D, and also q. There are dependences $\breve{\Gamma}$ on q and D shown in **Figures 3** and **4**, respectively. It is shown that with an increased value of D, $\breve{\Gamma}$ decreases more rapidly for the same variation of q. It is shown in **Figure 4** that the value of $\breve{\Gamma}$ reduces steadily with the increase of D value. However, $\breve{\Gamma}$ does not change when q = 1.01.

Consequently, the mean correlation length $\breve{\Gamma}$ is sensitive to fractal dimension D with the exception of cases when q is close to unity. These results imply that the value of fractal surface irregularities is mainly determined by fractal parameter D.

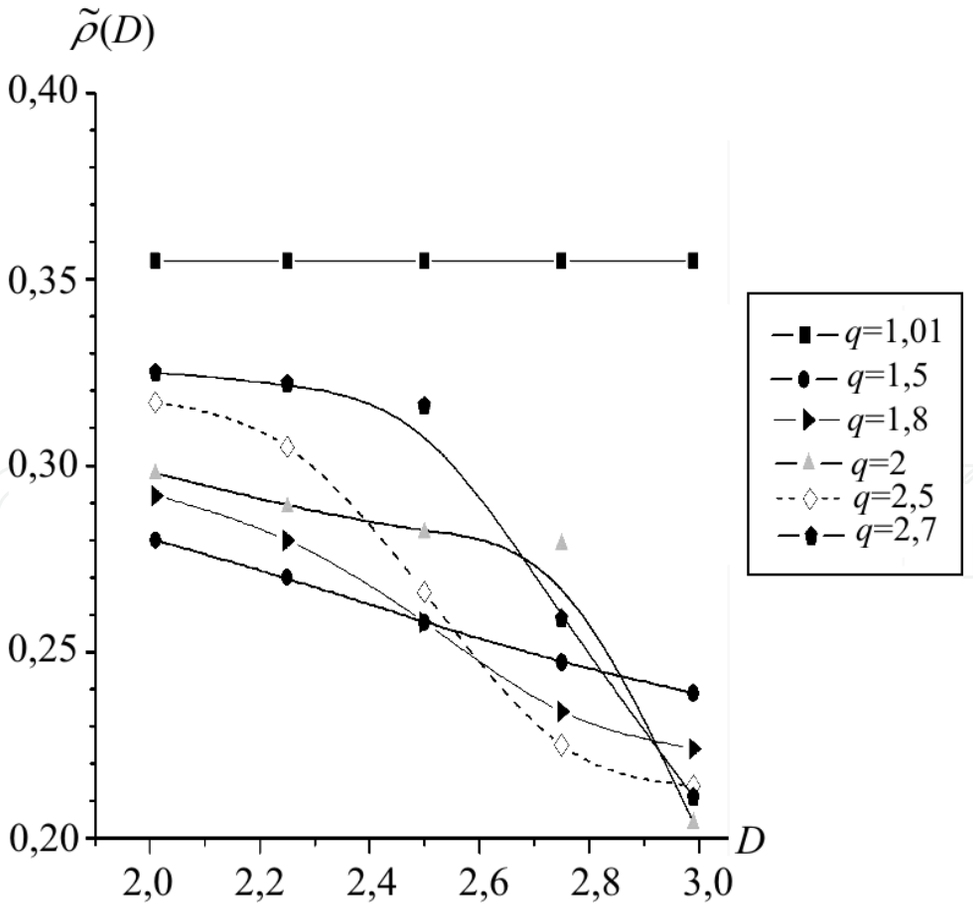

Figure 3. Average correlation length $\tilde{\Gamma}$ as function of q.

http://dx.doi.org/10.5772/intechopen.68187

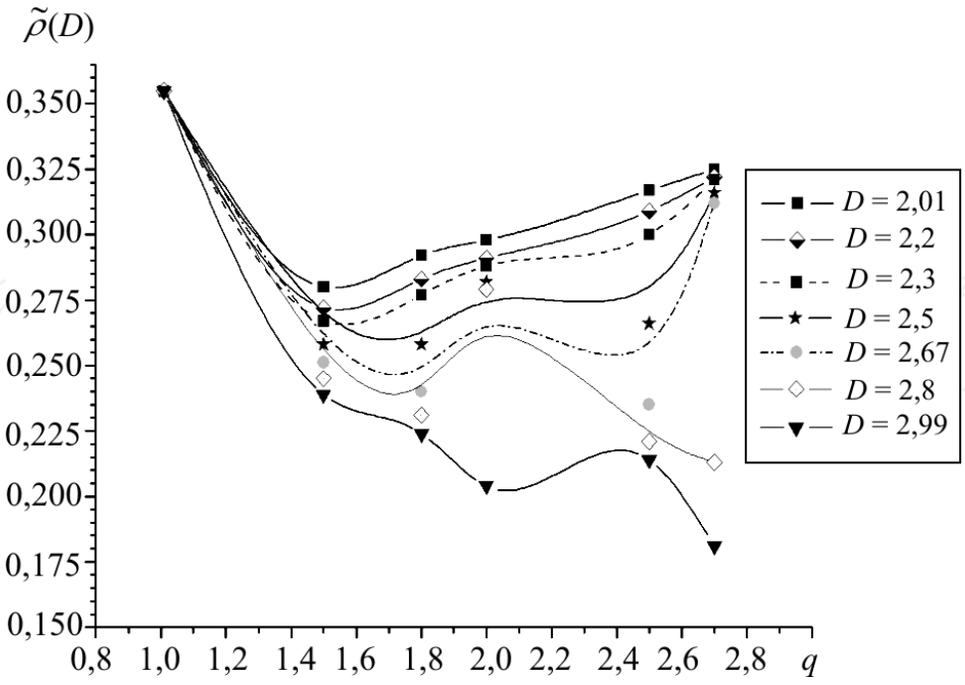

Figure 4. Average correlation length $\tilde{\Gamma}$ as function of D.

6. Memoir about the basic foundation of wave-scattering theory by fractal surfaces

As mentioned above, Kirchhoff approach has been already used for the analysis of wave scattering by fractal surfaces [6, 7, 20, 39–44, 47, 50–63]. This theory will be used in our work for numerical analysis of a field scattered by fractal chaotic surfaces. Conventional conditions of Kirchhoff approach are the following: irregularities are large scale, irregularities are smooth and flat. In the following calculations, we assume that observation is carried out from Fraunhofer zone, incident wave is plane and monochromatic, there are no points with infinite gradient on the surface, Fresnel coefficient V_0 is constant for this surface, and surface scales are much greater than incident wavelength.

6.1. Scattered field

Scattering geometry is presented in **Figure 5**. Then, *scattered field* $\psi_p(\vec{r})$ that interacts with surface square S of $\mathbf{2}\boldsymbol{L_x} \times \mathbf{2}\boldsymbol{L_y}$ when $-\boldsymbol{L_x} \le \boldsymbol{x} \le \boldsymbol{L_x}$ and $-\boldsymbol{L_y} \le \boldsymbol{y} \le \boldsymbol{L_y}$ are equal to [1–3, 5–7, 20, 61]:

$$\psi_p(\vec{r}) = -\frac{ik \cdot \exp(ikr)}{4\pi \cdot r} 2F(\theta_1, \theta_2, \theta_3) \int_S \exp[ik\phi(x_0, y_0)] dx_0 dy_0 + \psi_\kappa. \tag{13}$$

In Eq. (13), we used the following notations:

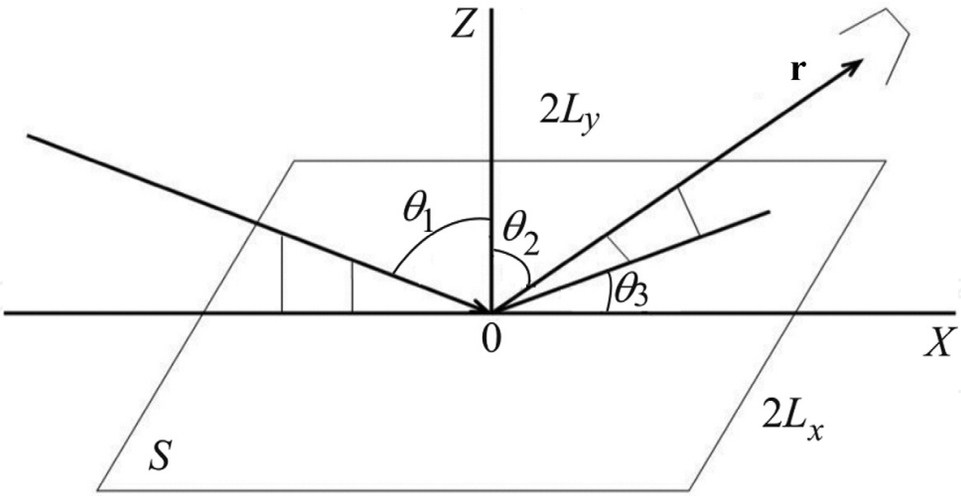

Figure 5. Scattering geometry: θ_1, incident angle; θ_2– scattering angle; and θ_3 azimuth angle.

$$F(\theta_1, \theta_2, \theta_3) = \frac{1}{2}\left(\frac{Aa}{C} + \frac{Bb}{C} + c\right), \tag{14}$$

$$\phi(x_0, y_0) = Ax_0 + By_0 + Ch(x_0, y_0), \tag{15}$$

$$h(x_0, y) = \sigma \cdot W_{\text{н}}(x_0, y_0), \tag{16}$$

$$a = V_0(\sin\theta_1 - \sin\theta_2\cos\theta_3), \tag{17}$$

$$b = V_0(\sin\theta_2 \cdot \sin\theta_3), \tag{18}$$

$$c = V_0(\cos\theta_1 + \cos\theta_2), \tag{19}$$

$$A = \sin\theta_1 - \sin\theta_2\cos\theta_3, \tag{20}$$

$$B = -\sin\theta_2\sin\theta_3, \tag{21}$$

$$C = -(\cos\theta_1 + \cos\theta_2), \tag{22}$$

$$\psi_{\text{к}} = -\frac{ik \cdot \exp(ikr)}{4\pi \cdot r}\left\{\frac{ia}{kc}\int [\exp(ik\phi(X, y_0)) - \exp(ik\phi(-X, y_0))] \cdot dy_0 + \right.$$
$$\left. + \frac{ib}{kc}\int \left[\exp\left(ik\phi(x_0, Y)\right) - \exp\left(ik\phi(x_0, -Y)\right)\right] \cdot dx_0 \right\}. \tag{23}$$

Component $\psi_{\text{к}}$ relates to edge effect. From Eqs. (15) and (16), we have

$$\exp[ik\phi(x_0, y_0)] = \exp\left\{ik[Ax_0 + By_0 + C\sigma \cdot W_u(x_0, y_0)]\right\}. \tag{24}$$

In Eq. (24), the third exponent is expressed as

http://dx.doi.org/10.5772/intechopen.68187

$$\exp[ikC\sigma \cdot W_u(x_0, y_0)] = \exp\left\{ ikC\sigma \left[\frac{2\left(1-q^{2(D-3)}\right)}{M\left(1-q^{2(D-3)N}\right)} \right]^{1/2} \sum_{n=0}^{N-1} q^{(D-3)n} \sum_{m=1}^{M} \times \right.$$
$$\left. \times \cos\left[Kq^n \cdot \left(x_0 \cdot \cos\left(\frac{2\pi \cdot m}{M}\right) + y_0 \sin\left(\frac{2\pi \cdot m}{M}\right) + \phi_{nm} - \frac{\pi}{2} \right) \right] \right\} =$$
$$= \prod_{n=1}^{N-1} \prod_{m=1}^{M} \exp\left\{ ikC\sigma \left[\frac{2\left(1-q^{2(D-3)}\right)}{M\left(1-q^{2(D-3)N_0}\right)} \right]^{1/2} q^{(D-3)n} \times \right.$$
$$\left. \times \cos\left[x_0 \cdot \cos\left(\frac{2\pi \cdot m}{M}\right) + y_0 \sin\left(\frac{2\pi \cdot m}{M}\right) + \phi_{nm} - \frac{\pi}{2} \right] \right\}. \tag{25}$$

From expression (Eq. (25)) and by taking into account expansion (Eq. (26)) and relationship (Eq. (27)):

$$\exp(iz\cos\varphi) = \sum_{u=-\infty}^{+\infty} iuJ_u(z)\exp(iu\varphi), \tag{26}$$

$$c_f = kC\sigma \left[\frac{2\left(1-q^{2(D-3)}\right)}{M\left(1-q^{2(D-3)N}\right)} \right]^{1/2}. \tag{27}$$

we obtain

$$\exp[ikC\sigma \cdot W_u(x_0, y_0)] = \prod_{n=0}^{N-1} \prod_{m=1}^{M} \sum_{u=-\infty}^{+\infty} J_{u_{nm}}\left(c_f q^{(D-3)n}\right) \times$$
$$\times \exp\left\{ iu \left[Kq^n \cdot \left(x_0 \cdot \cos\left(\frac{2\pi \cdot m}{M}\right) + y_0 \sin\left(\frac{2\pi \cdot m}{M}\right) + \phi_{nm} - \frac{\pi}{2} \right) \right] \right\}. \tag{28}$$

Eq. (28) can be written as

$$\exp[ikC\sigma \cdot W_u(x_0, y_0)] = \sum_{u_{1,0}=-\infty}^{+\infty} \cdots \sum_{u_{1,0}=-\infty}^{+\infty} \cdots \sum_{u_{1,0}=-\infty}^{+\infty} \cdots \sum_{u_{1,0}=-\infty}^{+\infty} \cdots \sum_{u_{1,0}=-\infty}^{+\infty} \times$$
$$\times \left[\prod_{n=0}^{N-1} \prod_{m=1}^{M} J_{u_{nm}}\left(c_f q^{(D-3)n}\right) \right] \cdot \exp\left\{ iK \left[\sum_{n=0}^{N-1} q^{(D-3)n} \sum_{m=1}^{M} u_{nm} \cos\left(\frac{2\pi \cdot m}{M}\right) \right] x_0 \right\} \times$$
$$\times \exp\left\{ iK \left[\sum_{n=0}^{N-1} q^{(D-3)n} \sum_{m=1}^{M} u_{nm} \sin\left(\frac{2\pi \cdot m}{M}\right) \right] y_0 \right\} \times$$
$$\times \exp\left(i \sum_{n=0}^{N-1} \sum_{m=1}^{M} u_{nm} \phi_{nm} \right). \tag{29}$$

As result from Eqs. (13)–(23) and (29) ***field*** $\psi_p(\vec{r})$ ***scattered*** from finite site S is

$$\psi_{\mathrm{p}}(\vec{r}) = -\frac{iL_xL_yk\cdot\exp(ikr)}{\pi r}2F(\theta_1,\theta_{2,}\theta_3)$$
$$\times\sum_{u_{1,0}=-\infty}^{+\infty}\cdots\sum_{u_{1,N-1}=-\infty}^{+\infty}\cdots\sum_{u_{2,0}=-\infty}^{+\infty}\cdots\sum_{u_{2,N-1}=-\infty}^{+\infty}\cdots\sum_{u_{M,N-1}=-\infty}^{+\infty}\times \tag{30}$$
$$\times\left[\prod_{n=0}^{N-1}\prod_{m=1}^{M}J_{u_{mn}}(c_jq^{(D-3)n})\right]\exp\left(i\sum_{n=0}^{N-1}\sum_{m=1}^{M}u_{mn}\phi_{mn}\right)\times$$
$$\times\mathrm{sinc}(\varphi_cL_x)\cdot\mathrm{sinc}(\varphi_{\mathrm{s}}L_{\mathrm{y}})+\psi_{\kappa},$$

$$\mathrm{sinc}(x)\equiv\frac{\sin(x)}{\mathrm{x}}, \tag{31}$$

$$\varphi_c = kA + K\sum_{n=0}^{N-1}q^n\sum_{m=1}^{M}u_{nm}\cos\left(\frac{2\pi\cdot m}{M}\right),\ \varphi_s = kB + K\sum_{n=0}^{N-1}q^n\sum_{m=1}^{M}u_{nm}\sin\left(\frac{2\pi\cdot m}{M}\right). \tag{32}$$

6.2. Average-scattered field

A more convenient parameter for the characterization of scattered field properties is *average-scattered field* $\tilde{\psi}_{\mathrm{p}}(\vec{r})$:

$$\tilde{\psi}_{\mathrm{p}}(\vec{r}) = \langle\psi_{\mathrm{p}}(\vec{r})\rangle_s \tag{33}$$

Eqs. (32) and (33) are defined as follows:

$$\tilde{\psi}_{\mathrm{p}}(\vec{r}) = -\frac{iL_xL_yk\cdot\exp(ikr)}{\pi r}2F(\theta_1,\theta_2,\theta_3)\left[\prod_{n=0}^{N-1}J_0^M(c_fq^{(D-3)n})\right]\mathrm{sinc}(kAL_x)\mathrm{sinc}(kBL_y)+\psi_{\kappa} \tag{34}$$

Assume that the outside area $-L_x \le x_0 \le L_x$ и $-L_y \le y_0 \le L_y$ surface S is smooth, that is,

$$h(\pm X,\ \pm Y)\equiv 0, \tag{35}$$

$$\text{where } X > L_x,\ Y > L_y. \tag{36}$$

Then, Eq. (23) can be written as

$$\psi_{\kappa} = -\frac{ik\cdot\exp(ikr)}{\pi\cdot r}\left(\frac{Aa}{C}+\frac{Bb}{C}\right)\lim_{X\to L_x^+}X\cdot\mathrm{sinc}(kAX)\cdot\lim_{Y\to L_y^+}Y\cdot\mathrm{sinc}(kBY). \tag{37}$$

6.3. Scattering indicatrixes for field

Scattering indicatrixes for field $\boldsymbol{\rho}_{\psi}$ is defined as

$$\rho_{\psi} = \frac{\psi_{\mathrm{p}}(\vec{r})}{\psi_{\mathrm{p0}}(\vec{r})}), \tag{38}$$

where field scattered from perfectly smooth surface $\psi_{\mathrm{p0}}(\vec{r})$ in a specular direction is expressed as

$$\psi_{p0}(\vec{r}) = -\frac{2L_xL_yik\cdot\exp(ikr)\cos\theta_1}{\pi\cdot r}. \tag{39}$$

Average-scattering indicatrix $\tilde{\rho}_\psi$ can be obtained after normalization:

$$\tilde{\rho}_\psi = \frac{\tilde{\psi}_{sc}(\mathbf{r})}{\psi_{sc0}(\mathbf{r})}. \tag{40}$$

Assume that surface gradients much less than incident angle is θ_1, then from Eqs. (30), (37)–(39) we have

$$\begin{aligned}\tilde{\rho}_\psi = {} & \frac{F(\theta_1,\theta_2,\theta_3)}{\cos\theta_1}\left[\prod_{n=0}^{N-1}J_0^M\left(c_f q^{(D-3)n}\right)\right]\mathrm{sinc}(kAL_x)\mathrm{sinc}(kBL_y)+\\ & +\frac{1}{2L_xL_y\cos\theta_1}\left(\frac{Aa}{C}+\frac{Bb}{C}\right)\lim_{X\to L_x^+}X\cdot\mathrm{sinc}(kAX)\cdot\lim_{Y\to L_y^+}Y\cdot\mathrm{sinc}(kBY).\end{aligned} \tag{41}$$

In specular direction $\theta_1 = \theta_2, \theta_3 = 0$ and coefficients are the $A = 0$, $B = 0$, $a = 0$, $b = 0$. Using Eqs. (17)–(22), we can write average-scattering indicatrixes $\tilde{\rho}_\psi$, which was defined in Eq. (40), as

$$\tilde{\rho}_\psi = \left[\prod_{n=0}^{N-1}J_0^M(c_f q^{(D-3)n})\right], \tag{42}$$

$$\text{where } c_f = -2k\sigma\cdot\cos\theta_1\left[\frac{2\left(1-q^{2(D-3)}\right)}{M\left(1-q^{2(D-3)N}\right)}\right]^{\frac{1}{2}}. \tag{43}$$

Thus, $\tilde{\rho}_\psi$ relates to parameters k, σ, θ_1, q, D, N, M. If $c_f q^{(D-3)n} < 1$, then in second approximation $\tilde{\rho}_\psi$ we have

$$\tilde{\rho}_\psi = 1 - 2(k\sigma\cdot\cos\theta_1)^2. \tag{44}$$

Eq. (44) shows that in specular direction $\tilde{\rho}_\psi$ depends on the wavelength of incident radiation, σ of rough surface, and incident angle θ_1. This result coincides with conventional results for Gaussian random surfaces [1]. Thus, fractal surfaces have diffraction properties that are similar to the ones of Gaussian random surfaces in a specular direction. This result involves a previous one [26], which was used as main assumption for mean-root-square scattering cross section measurement on this surface with specular ray measurement.

6.4. Average field intensity

Now, let us find *scattering indicatrixes for average field intensity* $\tilde{\rho}_I$. The intensity of scattered field is defined as

$$\boldsymbol{I}(\vec{r}) = \psi_{\mathrm{p}}(\vec{r})\psi_{\mathrm{p}}^{*}(\vec{r}). \tag{45}$$

The average intensity of scattered field is obtained by Eq. (45) averaging:

$$\tilde{I}(\vec{r}) = \langle I(\vec{r})\rangle_{S}. \tag{46}$$

From Eqs. (30), (45), and (46), we have

$$\begin{aligned}\tilde{I}(\vec{r}) = &\left[\frac{L_x L_y k}{\pi\cdot r}2F(\theta_1,\theta_2,\theta_3)\right]^2\times\\ &\times\sum_{u_{1,0}=-\infty}^{+\infty}\cdots\sum_{u_{1,N-1}=-\infty}^{+\infty}\cdots\sum_{u_{2,0}=-\infty}^{+\infty}\cdots\sum_{u_{2,N-1}=-\infty}^{+\infty}\cdots\sum_{u_{M,N-1}=-\infty}^{+\infty}\times\\ &\times\left[\prod_{n=0}^{N-1}\prod_{m=1}^{M}J_{u_{mn}}(c_j q^{(D-3)n})\right]^2\times\\ &\mathrm{sinc}^2(\varphi_c L_x)\cdot\mathrm{sinc}^2(\varphi_{\mathrm{s}} L_{\mathrm{y}}).\end{aligned} \tag{47}$$

6.5. Scattering indicatrix for average field intensity

In a similar manner as stated above, here we define ***scattering indicatrix for average field intensity*** $\tilde{\rho}_I \equiv g$:

$$g(\vec{r}) \equiv \tilde{\rho}_I = \frac{\tilde{I}(\vec{r})}{I_0}, \tag{48}$$

$$\text{where } I_0 = \psi_{\mathrm{p}0}(\vec{r})\cdot\psi_{\mathrm{p}0}^{*}(\vec{r}). \tag{49}$$

Based on the assumptions that were proposed in the beginning of this section, we can write Eq. (48) as

$$\begin{aligned}g \approx \frac{F^2(\theta_1,\theta_2,\theta_3)}{\cos^2\theta_1}&\left\{\left[1-\frac{1}{2}(kC\sigma)^2\right]\cdot\mathrm{sinc}^2(kAL_x)\mathrm{sinc}^2(kBL_y)\right.\\ &+\frac{1}{4}C_f^2\sum_{n=0}^{N-1}\sum_{m=1}^{M}q^{2(D-3)n}\mathrm{sinc}^2\left[\left(kA+Kq^n\cos\frac{2\pi\cdot m}{M}\right)L_x\right]+\\ &\left.+\mathrm{sinc}^2\left[\left(kB+Kq^n\sin\frac{2\pi\cdot m}{M}\right)L_y\right]\right\},\end{aligned} \tag{50}$$

where values with the order higher than $c_f^2 q^{2(D-3)n}$ in Eqs. (48) and (49) are negligible.

Statistical parameter of scattered field σ_I is defined as

$$\frac{\sigma_I = \tilde{I}(\vec{r}) - \tilde{\psi}_{\mathrm{p}}^{2}(\vec{r})}{I_{0,}} \tag{51}$$

that here corresponds to the mean-root-square value of average-scattered field.

http://dx.doi.org/10.5772/intechopen.68187

Let us compare the view of Eq. (34) with the first term in Eq. (50). It is obvious that the first term in Eq. (50) is equal to the expression for $\tilde{\psi}_{\mathrm{p}}^{2}(\vec{r})$ that represents specular ray and side lobes. Thus, δ_I is determined only by the second term in Eq. (50) that relates to scattering by surface roughness. The second moment of scattered field σ_I can be useful for diffraction studying away from specular direction and also for the determination of the influence of fractal parameters on inverse-scattering pattern. The advantage of such a presentation is that in the consideration it is sufficient to discount only average coefficients. Thus, it is necessary to measure phase components that relate with scattered wave front.

6.6. Results clarification

In Ref. [52], *approximate formula of average field intensity for the problem of scattering by fractal phase screen* was presented. As it is explained in Ref. [61], this formula includes some errors. Below, details are explained and presented in Ref. [61]. Surface model in Ref. [52] is specified by *Weierstrass function* (see also expression (6.77) in monograph [7]:

$$\phi(x) = \frac{\sqrt{2\sigma_{\phi}[1 - b^{(2D-4)}]^{1/2}}}{[b^{(2D-4)N_1} - b^{(2D-4)(N_2+1)}]^{1/2}} \sum_{n=N_1}^{N_2} b^{(D-2)n} \cos(2\pi s b^n x + \phi_n), \tag{52}$$

where b is the fundamental spatial frequency; D is the fractal dimension, which varies over interval from 1 to 2; s is the scaling factor; ϕ_n is the phase that is distributed uniformly over the $[0, 2\pi]$. Number of harmonics in function (Eq. (52)) is determined by $N = N_2 - N_1 + 1$.

Average-scattered field intensity is determined by Eq. (22) in Ref. [52] (or by Eq. (6.96) in monograph [7] in the form of weighted array of Bessel functions):

$$\begin{aligned} \langle I(x) \rangle = {} & \frac{L^4}{\lambda^2 z^2} \sum_{q_1=-\infty}^{\infty} \sum_{q_2=-\infty}^{\infty} \dots \sum_{q_N=-\infty}^{\infty} J_{q_1}^2(C_{N_1}) J_{q_2}^2(C_{N_1+1}) \dots J_{q_N}^2(C_{N_2}) \times \\ & \times \operatorname{sinc}^2\left[L\left(\frac{x}{\lambda_z} - s q_1 b - s q_2 b^{N_1+1} - \dots s q^{N_2}\right)\right] \operatorname{sinc}^2\left(\frac{Lx}{\lambda z}\right), \end{aligned} \tag{53}$$

$$\text{where } \mathrm{C}_n = \frac{\sqrt{2\sigma_{\phi}[1 - b^{(2D-4)} b^{(D-2)n}]^{1/2}}}{[b^{(2D-4)N_1} - b^{(2D-4)(N_2+1)}]^{1/2}} \tag{54}$$

L is the phase screen size, x, y are the coordinate values in intensity observation plane at a distance of z from the phase screen, and λ is the incident wavelength.

In Eqs. (B2) and (B3) in Ref. [52], typographical errors were made. In Eq. (53), term sq_1b must be: $sq_1b^{N_1}$, which is clear from expression (6.95) in monograph [7]. In line with Eq. (B2), Eq. (B3) must be

$$C_n = \frac{\sqrt{2\sigma_{\phi}[1 - b^{(2D-4)}]^{1/2} b^{(D-2)n}}}{[b^{(2D-4)N_1} - b^{(2D-4)(N_2+1)}]^{1/2}}. \tag{55}$$

Approximate expression for the average intensity is derived from Eq. (22) in Ref. [12] (see also expression (6.97) in monograph [6]):

$$\langle I(x)\rangle = \frac{L^4}{\lambda^2 z^2}\left\{(1-\sigma_\phi^2)\mathrm{sinc}^2(Lx/\lambda z) + \sum_{n=-\infty}^{+\infty}(C_n^2/4)\mathrm{sinc}^2[L(x/\lambda z - sb^n)]\right\}\mathrm{sinc}^2(Ly/\lambda z). \quad (56)$$

After the correction, we have

$$\langle I(x)\rangle = \frac{L^4}{\lambda^2 z^2}\left\{(1-\sigma_\phi^2)\mathrm{sinc}^2(Lx/\lambda z) + \sum_{n=N_1}^{N_2}(C_n^2/4)\mathrm{sinc}^2[L(x/\lambda z - sb^n)]\right\}\mathrm{sinc}^2(Ly/\lambda z). \quad (57)$$

Accurate derivation of Eq. (57) looks like this [61]:

$$\left.\begin{aligned} J_{u_i}(C_n) &= \left(\tfrac{C_n}{2}\right)^u \sum_{j=-\infty}^{\infty}\frac{(-1)^j(C_n/2)^{2j}}{j!(u+j)!} \\ J_{u_i}^2(C_n) &= \left(\tfrac{C_n}{2}\right)^{2u}\left[\sum_{j=-\infty}^{\infty}\tfrac{(-1)^j(C_n/2)^{2j}}{j!(u+j)!}\right]^2 \end{aligned}\right\}, \quad (58)$$

where u_i is the integer and $u_i \in (q_1, \ldots, q_N)$.

Since terms with the order higher than C_n^2 are negligible, then $u_i \in \{0, 1\}$, $\sum u_i = 0$ or 1.

Thus

$$\left.\begin{aligned} J_0(C_n) &= \left(\tfrac{C_n}{2}\right)^u \sum_{j=-\infty}^{\infty}\frac{(-1)^j(C_n/2)^{2j}}{j!(u+j)!} \approx 1 - \frac{1}{4}C_n^2 \\ J_0^2(C_n) &= 1 - \frac{1}{2}C_n^2 \end{aligned}\right\}, \quad (59)$$

$$J_1^2(C_n) \approx \frac{1}{4}C_n^2. \quad (60)$$

From Eqs. (53), (59), and (60), we have

$$\begin{aligned} \langle I(x)\rangle = \frac{L^4}{\lambda^2 z^2}\Bigg[& J_0^2(C_{N_1})\ldots J_0^2(C_{N_2})\mathrm{sinc}^2\left(\frac{Lx}{\lambda z}\right) + \\ & + J_1^2(C_n)J_0^2(C_{N_1+1})\ldots J_0^2(C_{N_2})\mathrm{sinc}^2\left(\frac{Lx}{\lambda z} - sb^{N_1}\right) + \\ & + J_0^2(C_{N_1})J_1^2(C_{N_1+1})\ldots J_0^2(C_{N_2})\mathrm{sinc}^2\left(\frac{Lx}{\lambda z} - sb^{N_1+1}\right) + \\ & + \ldots + J_0^2(C_{N_1})\ldots J_1^2(C_{N_2})\mathrm{sinc}^2\left(\frac{Lx}{\lambda z} - sb^{N_2}\right)\Bigg]\mathrm{sinc}^2\left(\frac{Ly}{\lambda z}\right), \end{aligned} \quad (61)$$

where

$$J_0^2(C_{N_1})\ldots J_0^2(C_{N_2}) \approx \left(1 - \frac{1}{2}C_{N_1}^2\right)\ldots\left(1 - \frac{1}{2}C_{N_2}^2\right) \approx 1 - \frac{1}{2}\sum_{n=N_1}^{N_2}C_n^2 = 1 - \sigma_\phi^2, \quad (62)$$

http://dx.doi.org/10.5772/intechopen.68187

$$\left.\begin{array}{l} J_1^2(C_{N_1})\ldots J_0^2(C_{N_2}) \approx \frac{1}{4} C_{N_1}^2 \\ \cdot \\ \cdot \\ \cdot \\ J_0^2(C_{N_1})\ldots J_1^2(C_{N_2}) \approx \frac{1}{4} C_{N_2}^2 \end{array}\right\}. \tag{63}$$

So, from Eqs. (61)–(63) finally we obtain the expression for average intensity in Fraunhofer zone:

$$\langle I(x)\rangle = \frac{L^4}{\lambda^2 z^2}\left\{\left(1-\sigma_\phi^2\right)\mathrm{sinc}^2(Lx/\lambda z) + + \sum_{n=N_1}^{N_2}\left(C_n^2/4\right)\mathrm{sinc}^2[(L(x/\lambda z - sb^n)]\right\}\mathrm{sinc}^2(Ly/\lambda z). \tag{64}$$

7. Results of the theoretical investigations of scattering indicatrixes in MW range

In **Figures 6–80**, we present a thorough array of typical kinds of dispersing fractal surfaces with the basis of Weierstrass function, and also 3D-scattering indicatrixes and their cross sections that

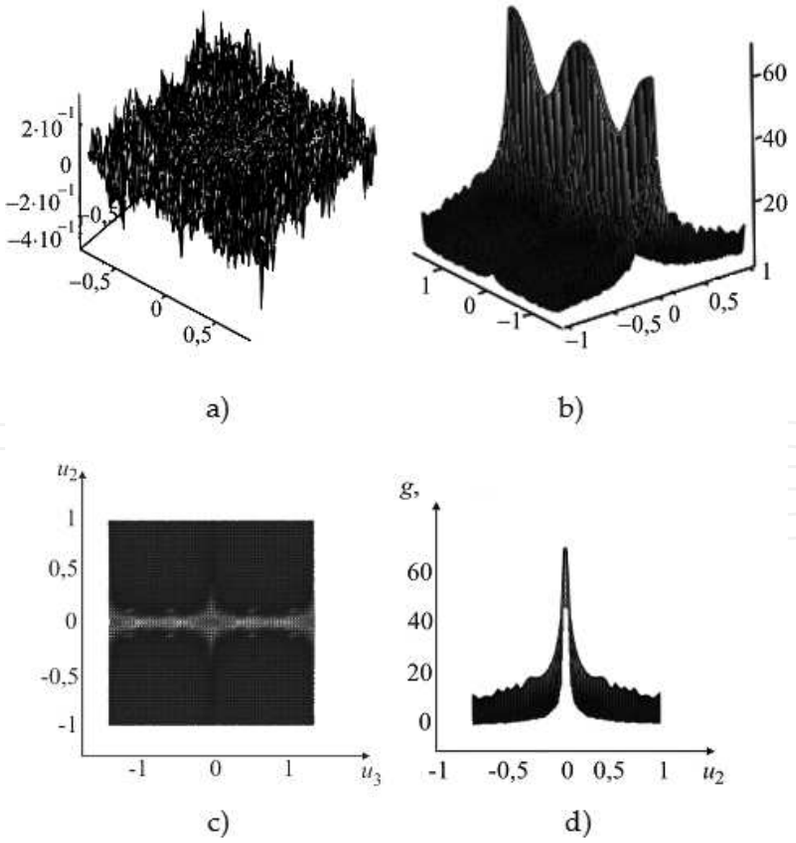

Figure 6. The fractal surface and the scattering indicatrix $g(\theta_2, \theta_3)$ when λ = 2.2 mm and $\theta_1 = 0°$: (a) fractal surface for D = 2.2; $N = M$ = 10; q = 2.7; (b) $g(\theta_2, \theta_3)$; (c) $g(\theta_2, \theta_3)$, top view; (d) $g(\theta_2, \theta_3)$, side view.

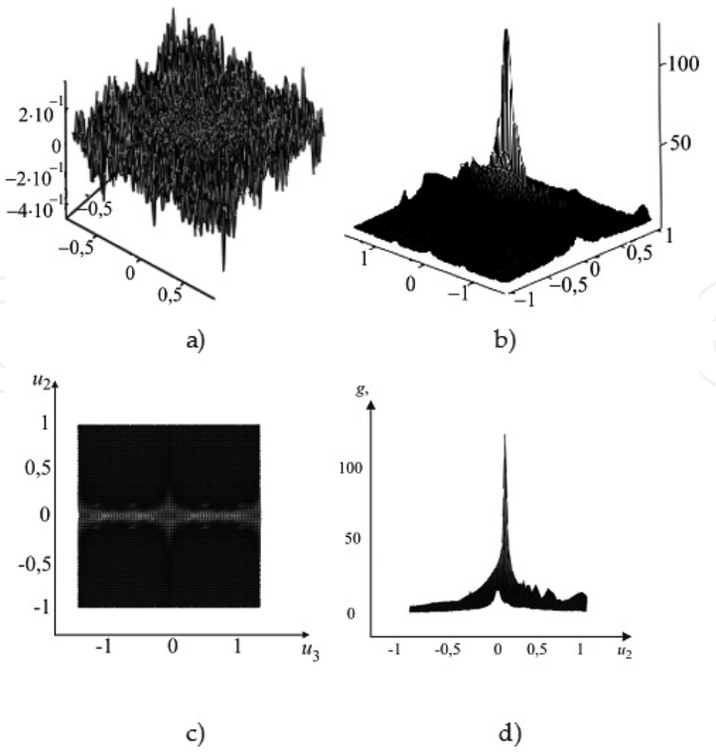

Figure 7. The fractal surface and the scattering indicatrix $g(\theta_2, \theta_3)$ when $\lambda = 2.2$ mm and $\theta_1 = 5°$: (a) fractal surface for $D = 2.2$; $N = M = 10$; $q = 2.7$; (b) $g(\theta_2, \theta_3)$; (c) $g(\theta_2, \theta_3)$, top view; (d) $g(\theta_2, \theta_3)$, side view.

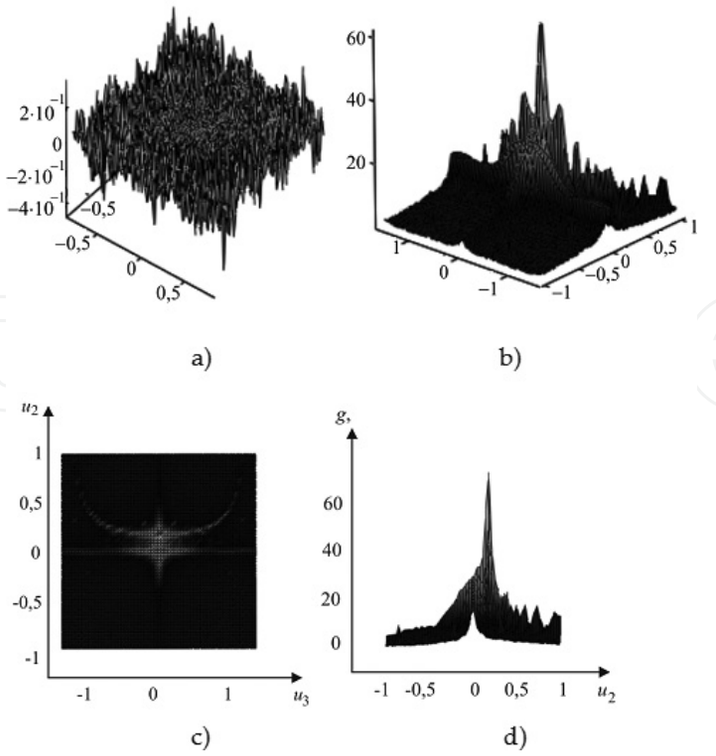

Figure 8. The fractal surface and the scattering indicatrix $g(\theta_2, \theta_3)$ when $\lambda = 2.2$ mm and $\theta_1 = 10°$: (a) fractal surface for $D = 2.2$; $N = M = 10$; $q = 2.7$; (b) $g(\theta_2, \theta_3)$; (c) $g(\theta_2, \theta_3)$, top view; (d) $g(\theta_2, \theta_3)$, side view.

http://dx.doi.org/10.5772/intechopen.68187

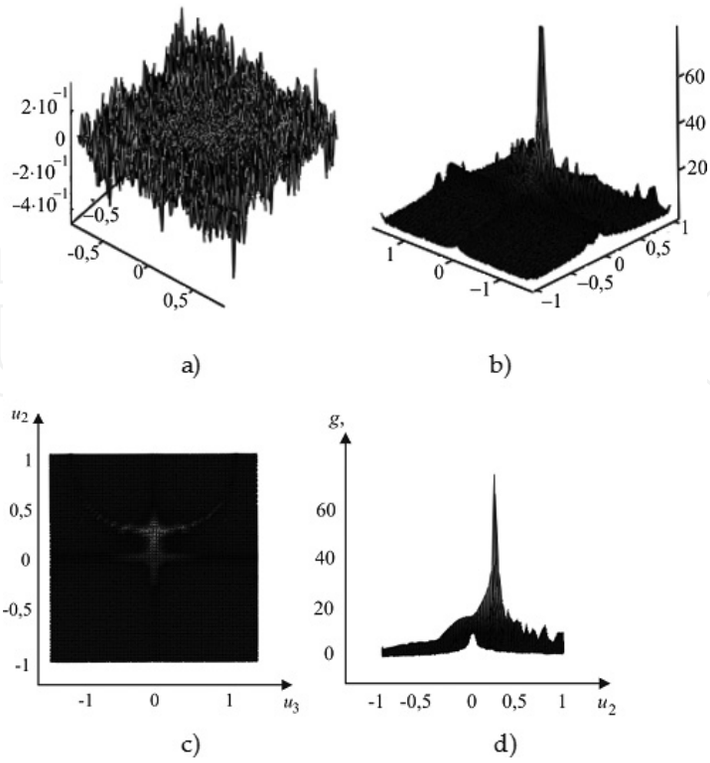

Figure 9. The fractal surface and the scattering indicatrix g(θ2, θ3) when λ = 2.2 mm and θ_1 = 15°: (a) fractal surface for D = 2.2; $N = M$ = 10; q = 2.7; (b) g(θ2, θ3); (c) g(θ2, θ3), top view; (d) g(θ2, θ3), side view.

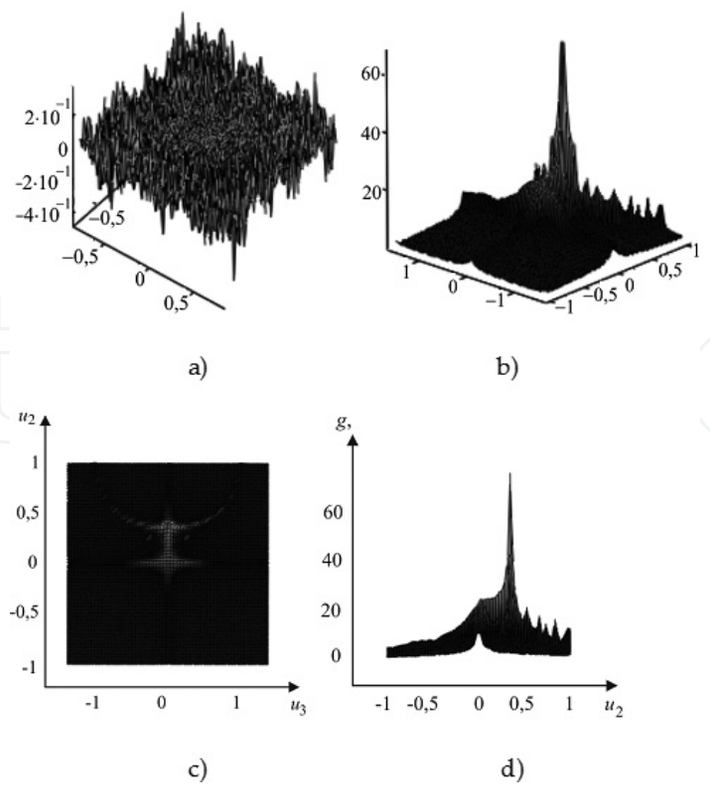

Figure 10. The fractal surface and the scattering indicatrix $g(\theta_2, \theta_3)$ when λ = 2.2 mm and θ_1 = 20°: (a) fractal surface for D = 2.2; $N = M$ = 10; q = 2.7; (b) $g(\theta_2, \theta_3)$; (c) $g(\theta_2, \theta_3)$, top view; (d) $g(\theta_2, \theta_3)$, side view.

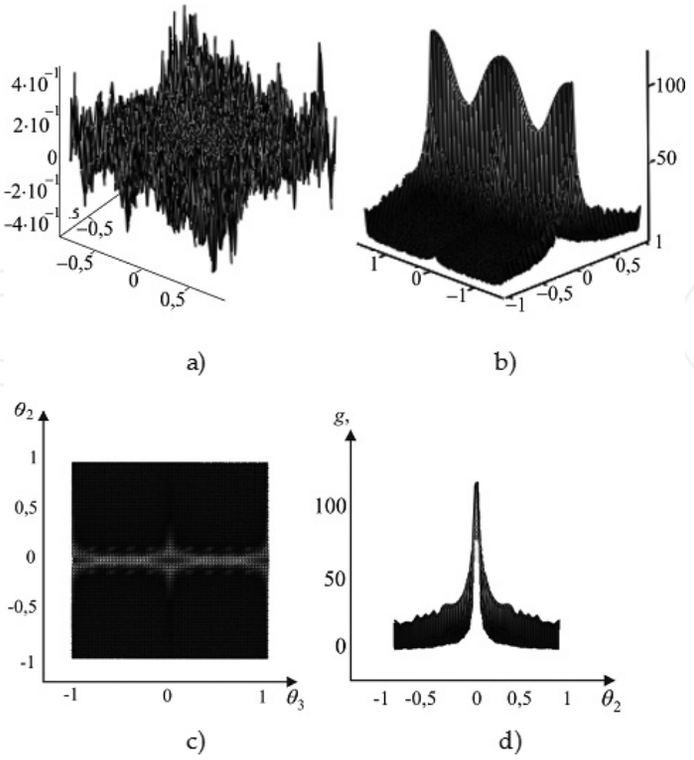

Figure 11. The fractal surface and the scattering indicatrix $g(\theta_2, \theta_3)$ when $\lambda = 2.2$ mm and $\theta_1 = 0°$: (a) fractal surface for $D = 2.2$; $N = M = 20$; $q = 2.7$; (b) $g(\theta_2, \theta_3)$; (c) $g(\theta_2, \theta_3)$, top view; (d) $g(\theta_2, \theta_3)$, side view.

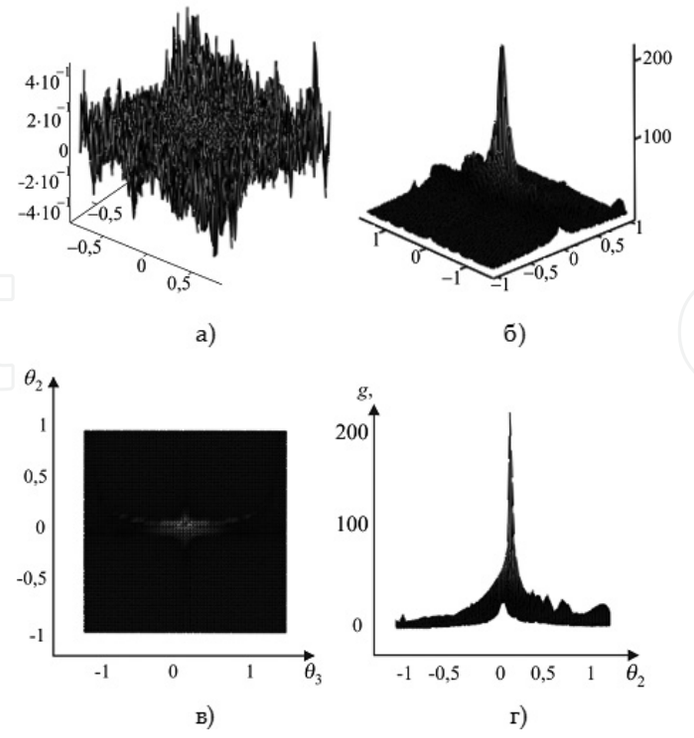

Figure 12. The fractal surface and the scattering indicatrix $g(\theta_2, \theta_3)$ when $\lambda = 2.2$ mm and $\theta_1 = 5°$: (a) fractal surface for $D = 2.2$; $N = M = 20$; $q = 2.7$; (b) $g(\theta_2, \theta_3)$; (c) $g(\theta_2, \theta_3)$, top view; (d) $g(\theta_2, \theta_3)$, side view.

http://dx.doi.org/10.5772/intechopen.68187

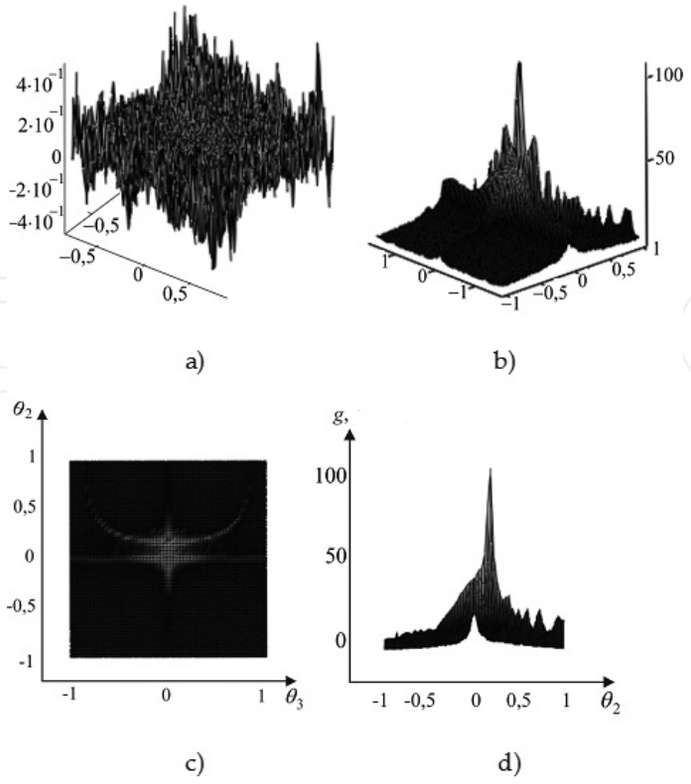

Figure 13. The fractal surface and the scattering indicatrix $g(\theta_2, \theta_3)$ when $\lambda = 2.2$ mm and $\theta_1 = 10°$: (a) fractal surface for $D = 2.2$; $N = M = 20$; $q = 2.7$; (b) $g(\theta_2, \theta_3)$; (c) $g(\theta_2, \theta_3)$, top view; (d) $g(\theta_2, \theta_3)$, side view.

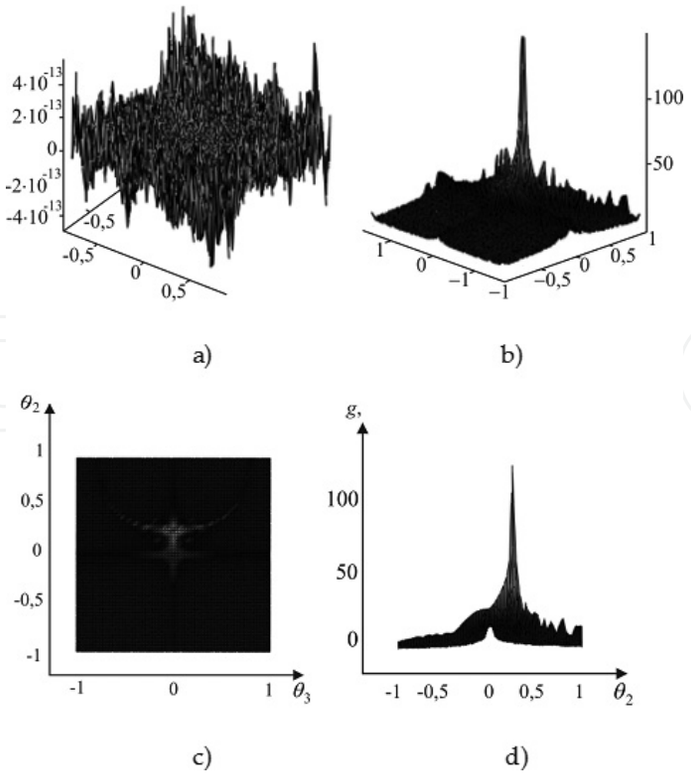

Figure 14. The fractal surface and the scattering indicatrix $g(\theta_2, \theta_3)$ when $\lambda = 2.2$ mm and $\theta_1 = 15°$: (a) fractal surface for $D = 2.2$; $N = M = 20$; $q = 2.7$; (b) $g(\theta_2, \theta_3)$; (c) $g(\theta_2, \theta_3)$, top view; (d) $g(\theta_2, \theta_3)$, side view.

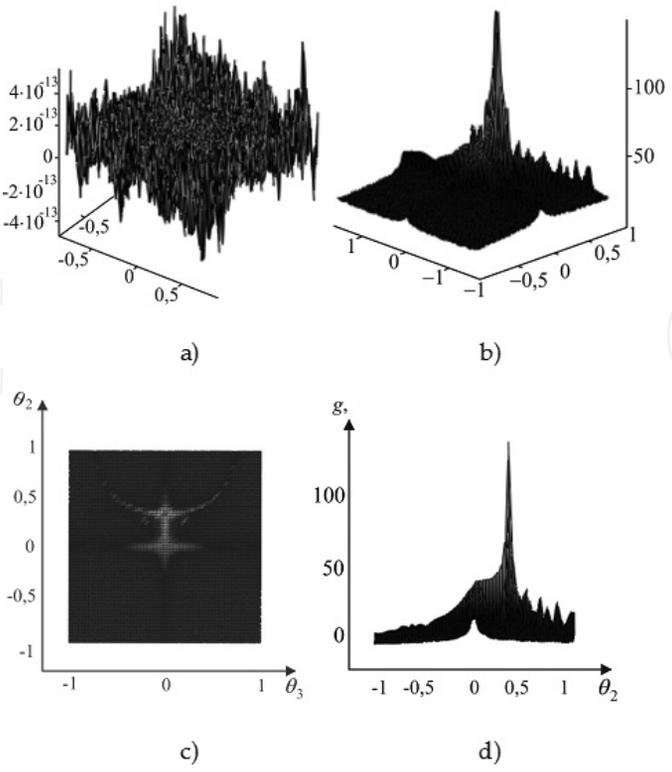

Figure 15. The fractal surface and the scattering indicatrix $g(\theta_2, \theta_3)$ when $\lambda = 2.2$ mm and $\theta_1 = 20°$: (a) fractal surface for $D = 2.2$; $N = M = 20$; $q = 2.7$; (b) $g(\theta_2, \theta_3)$; (c) $g(\theta_2, \theta_3)$, top view; (d) $g(\theta_2, \theta_3)$, side view.

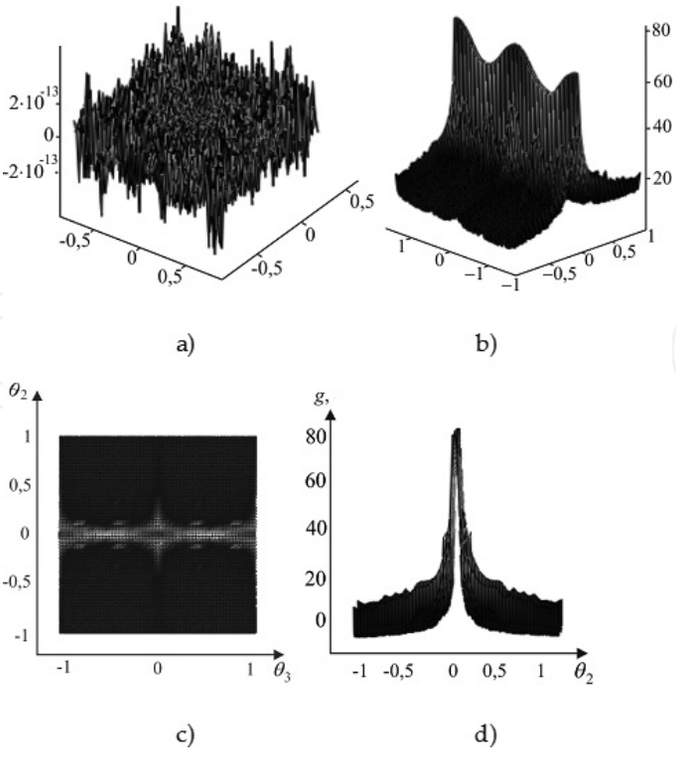

Figure 16. The fractal surface and the scattering indicatrix $g(\theta_2, \theta_3)$ when $\lambda = 2.2$ mm and $\theta_1 = 0°$: (a) fractal surface for $D = 2.5$; $N = M = 10$; $q = 2.7$; (b) $g(\theta_2, \theta_3)$; (c) $g(\theta_2, \theta_3)$, top view; (d) $g(\theta_2, \theta_3)$, side view.

http://dx.doi.org/10.5772/intechopen.68187

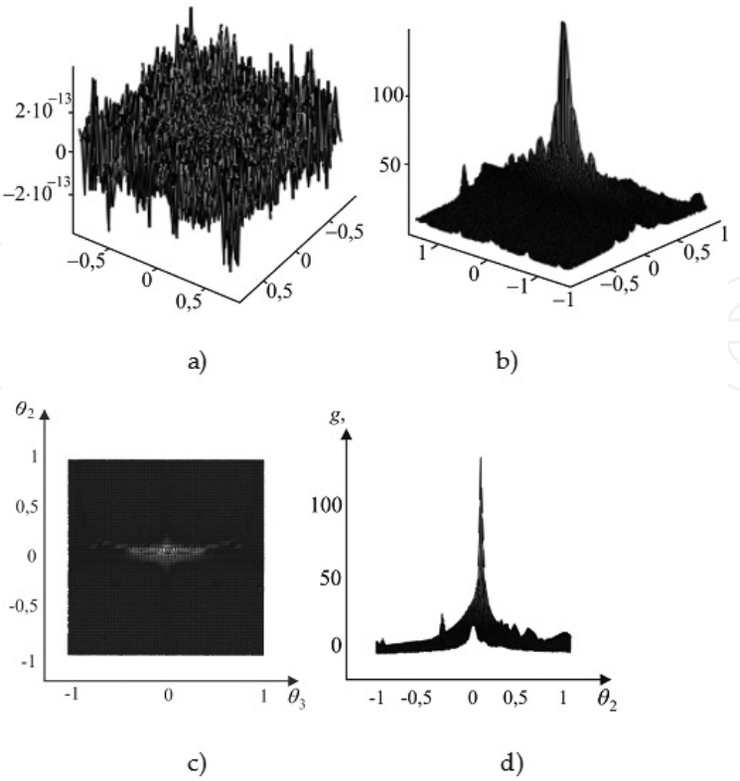

Figure 17. The fractal surface and the scattering indicatrix $g(\theta_2, \theta_3)$ when $\lambda = 2.2$ mm and $\theta_1 = 5°$: (a) fractal surface for $D = 2.5$; $N = M = 10$; $q = 2.7$; (b) $g(\theta_2, \theta_3)$; (c) $g(\theta_2, \theta_3)$, top view; (d) $g(\theta_2, \theta_3)$, side view.

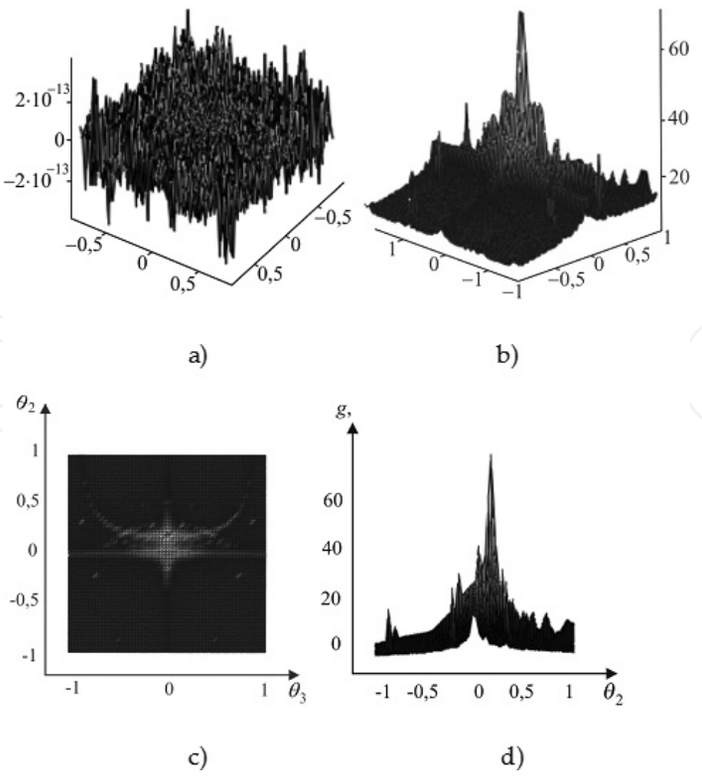

Figure 18. The fractal surface and the scattering indicatrix $g(\theta_2, \theta_3)$ when $\lambda = 2.2$ mm and $\theta_1 = 10°$: (a) fractal surface for $D = 2.5$; $N = M = 10$; $q = 2.7$; (b) $g(\theta_2, \theta_3)$; (c) $g(\theta_2, \theta_3)$, top view; (d) $g(\theta_2, \theta_3)$, side view.

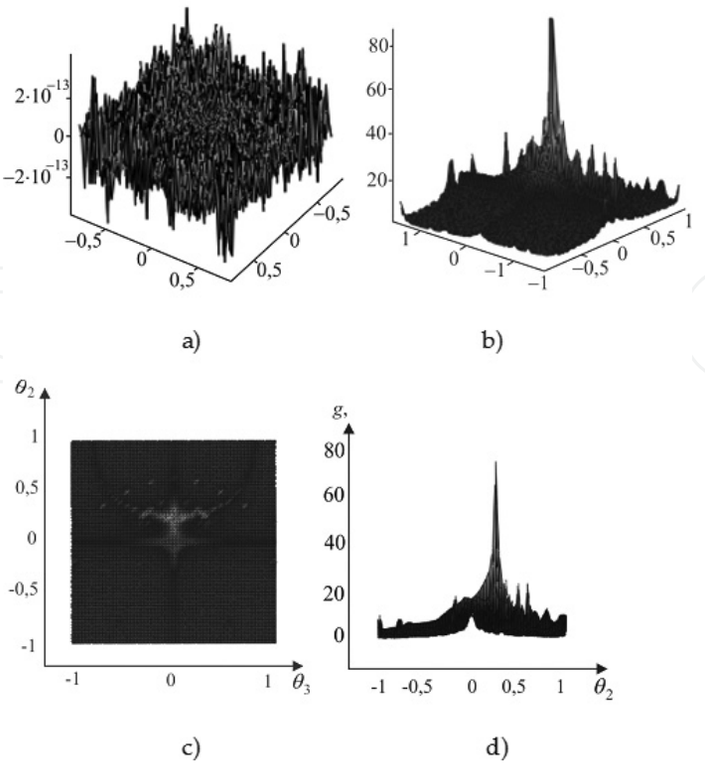

Figure 19. The fractal surface and the scattering indicatrix $g(\theta_2, \theta_3)$ when $\lambda = 2.2$ mm and $\theta_1 = 15°$: (a) fractal surface for $D = 2.5$; $N = M = 10$; $q = 2.7$; (b) $g(\theta_2, \theta_3)$; (c) $g(\theta_2, \theta_3)$, top view; (d) $g(\theta_2, \theta_3)$, side view.

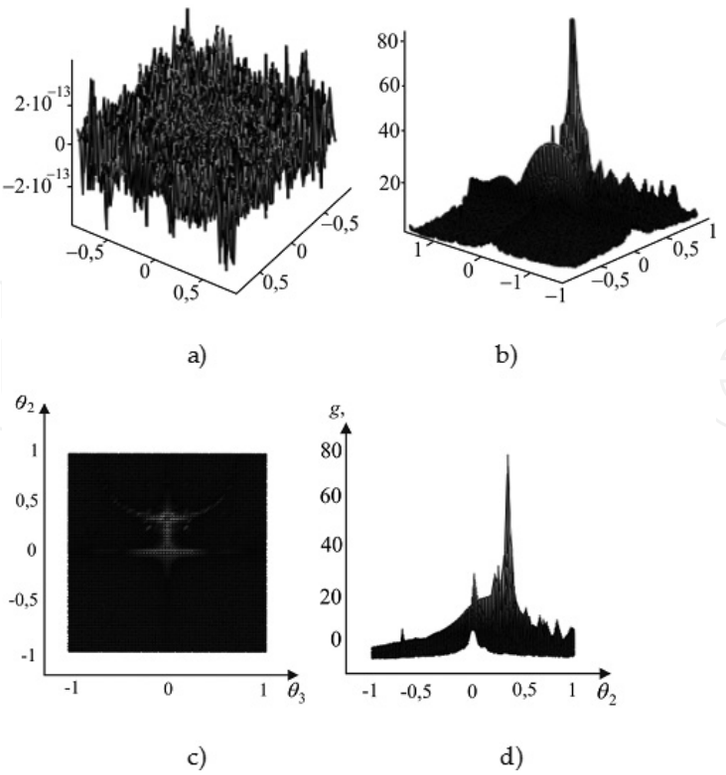

Figure 20. The fractal surface and the scattering indicatrix $g(\theta_2, \theta_3)$ when $\lambda = 2.2$ mm and $\theta_1 = 20°$: (a) fractal surface for $D = 2.5$; $N = M = 10$; $q = 2.7$; (b) $g(\theta_2, \theta_3)$; (c) $g(\theta_2, \theta_3)$, top view; (d) $g(\theta_2, \theta_3)$, side view.

http://dx.doi.org/10.5772/intechopen.68187

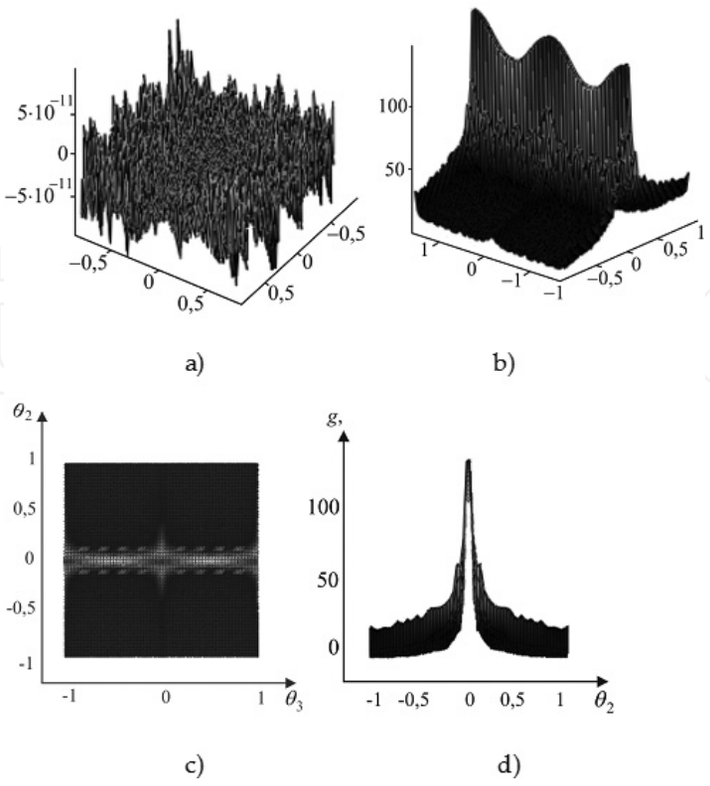

Figure 21. The fractal surface and the scattering indicatrix $g(\theta_2, \theta_3)$ when $\lambda = 2.2$ mm and $\theta_1 = 0°$: (a) fractal surface for $D = 2.5$; $N = M = 20$; $q = 2.7$; (b) $g(\theta_2, \theta_3)$; (c) $g(\theta_2, \theta_3)$, top view; (d) $g(\theta_2, \theta_3)$, side view.

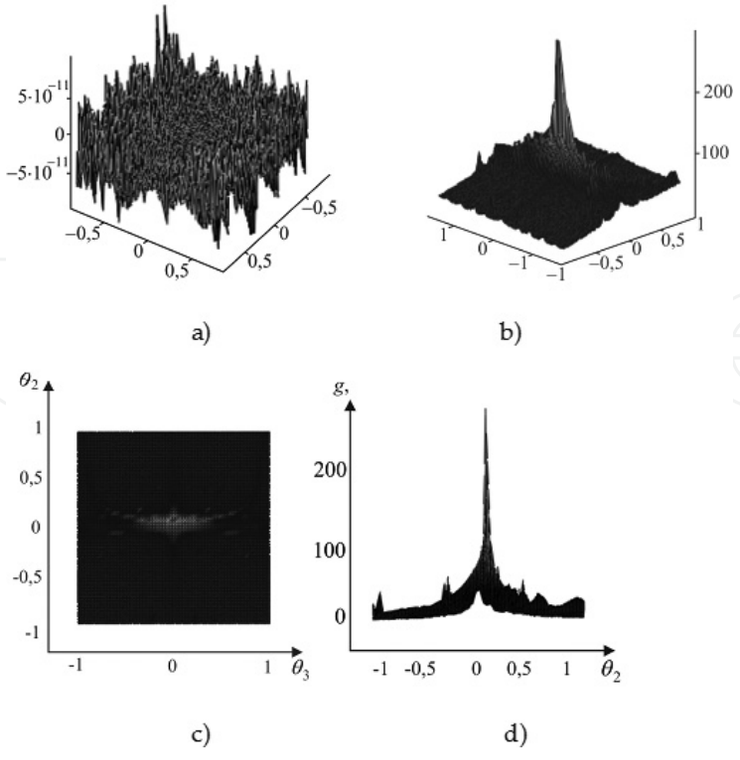

Figure 22. The fractal surface and the scattering indicatrix $g(\theta_2, \theta_3)$ when $\lambda = 2.2$ mm and $\theta_1 = 5°$: (a) fractal surface for $D = 2.5$; $N = M = 20$; $q = 2.7$; (b) $g(\theta_2, \theta_3)$; (c) $g(\theta_2, \theta_3)$, top view; (d) $g(\theta_2, \theta_3)$, side view.

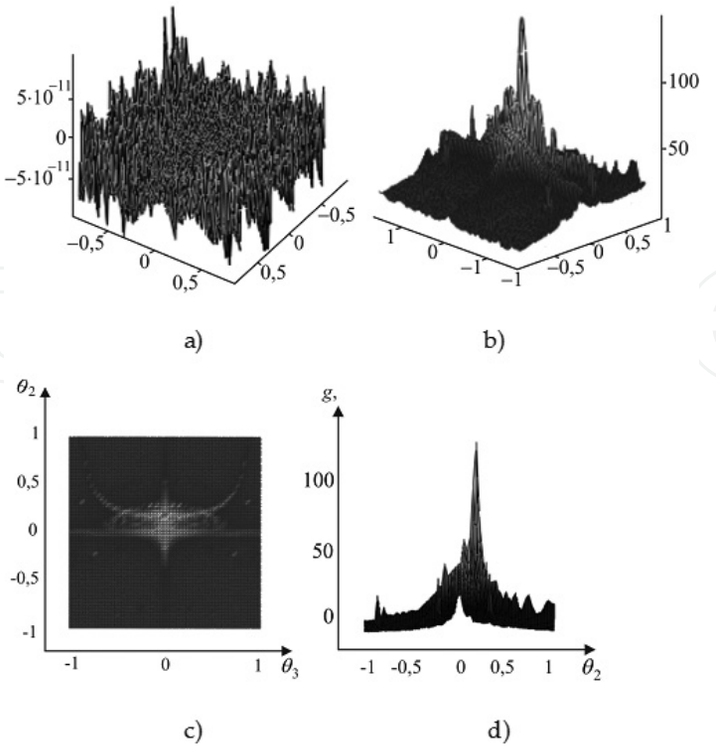

Figure 23. The fractal surface and the scattering indicatrix $g(\theta_2, \theta_3)$ when $\lambda = 2.2$ mm and $\theta_1 = 10°$: (a) fractal surface for $D = 2.5$; $N = M = 20$; $q = 2.7$; (b) $g(\theta_2, \theta_3)$; (c) $g(\theta_2, \theta_3)$, top view; (d) $g(\theta_2, \theta_3)$, side view.

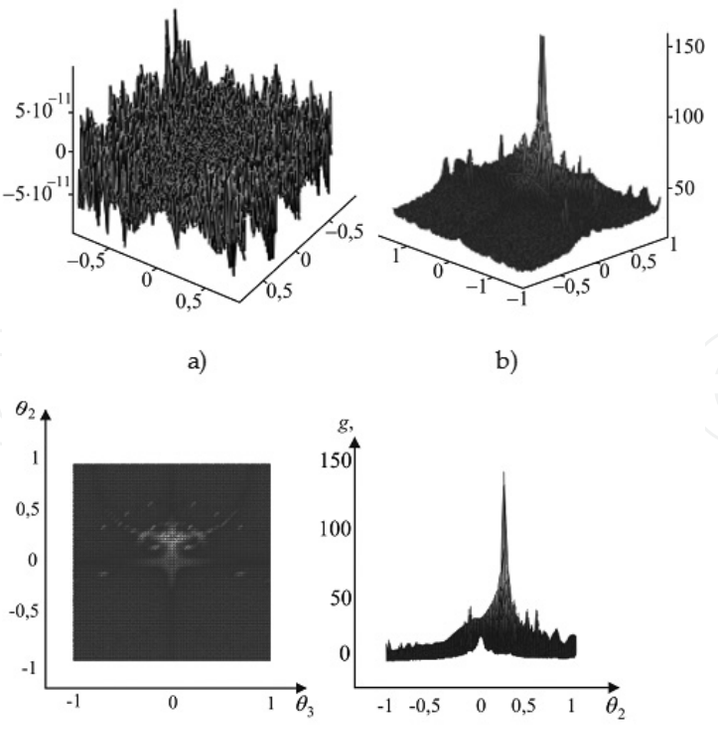

Figure 24. The fractal surface and the scattering indicatrix $g(\theta_2, \theta_3)$ when $\lambda = 2.2$ mm and $\theta_1 = 15°$: (a) fractal surface for $D = 2.5$; $N = M = 20$; $q = 2.7$; (b) $g(\theta_2, \theta_3)$; (c) $g(\theta_2, \theta_3)$, top view; (d) $g(\theta_2, \theta_3)$, side view.

http://dx.doi.org/10.5772/intechopen.68187

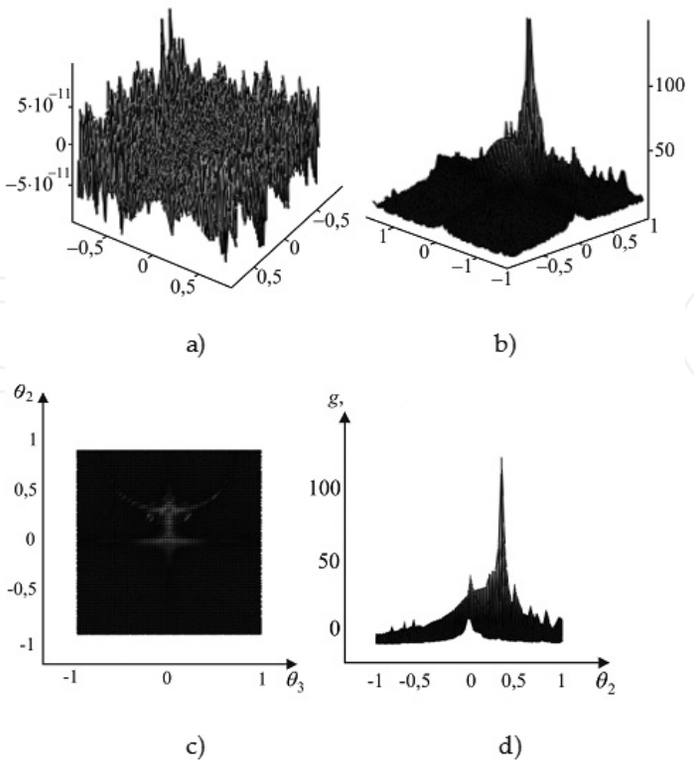

Figure 25. The fractal surface and the scattering indicatrix $g(\theta_2, \theta_3)$ when $\lambda = 2.2$ mm and $\theta_1 = 20°$: (a) fractal surface for $D = 2.5$; $N = M = 20$; $q = 2.7$; (b) $g(\theta_2, \theta_3)$; (c) $g(\theta_2, \theta_3)$, top view; (d) $g(\theta_2, \theta_3)$, side view.

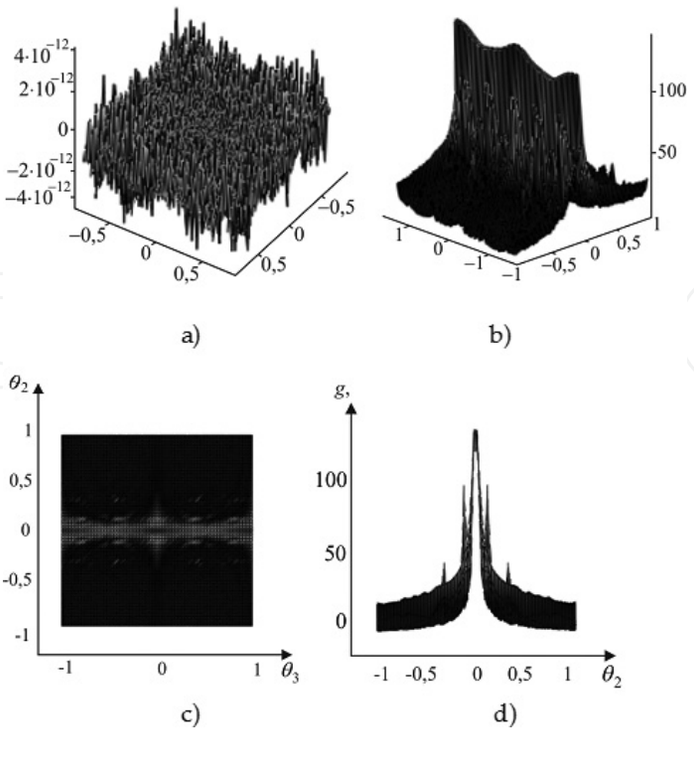

Figure 26. The fractal surface and the scattering indicatrix $g(\theta_2, \theta_3)$ when $\lambda = 2.2$ mm and $\theta_1 = 0°$: (a) fractal surface for $D = 2.8$; $N = M = 10$; $q = 2.7$; (b) $g(\theta_2, \theta_3)$; (c) $g(\theta_2, \theta_3)$, top view; (d) $g(\theta_2, \theta_3)$, side view.

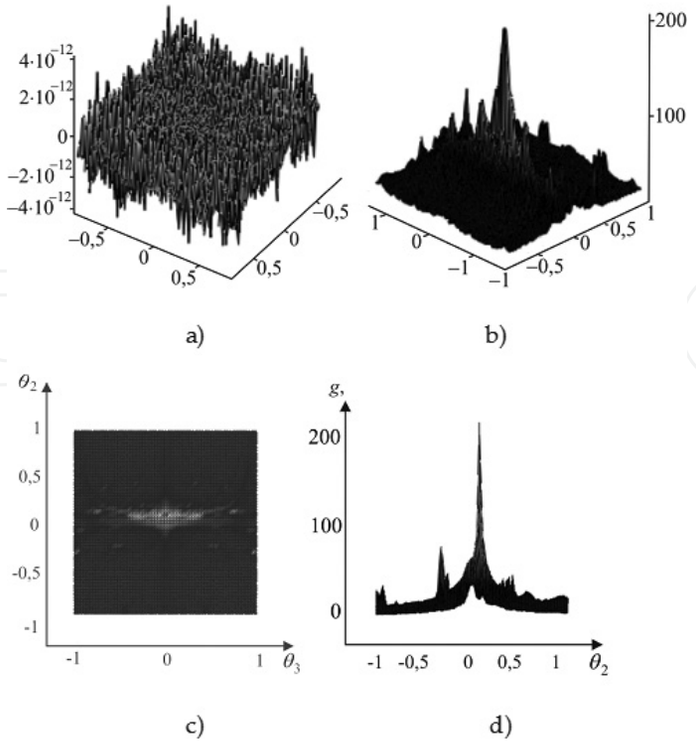

Figure 27. The fractal surface and the scattering indicatrix $g(\theta_2, \theta_3)$ when $\lambda = 2.2$ mm and $\theta_1 = 5°$: (a) fractal surface for $D = 2.8$; $N = M = 10$; $q = 2.7$; (b) $g(\theta_2, \theta_3)$; (c) $g(\theta_2, \theta_3)$, top view; (d) $g(\theta_2, \theta_3)$, side view.

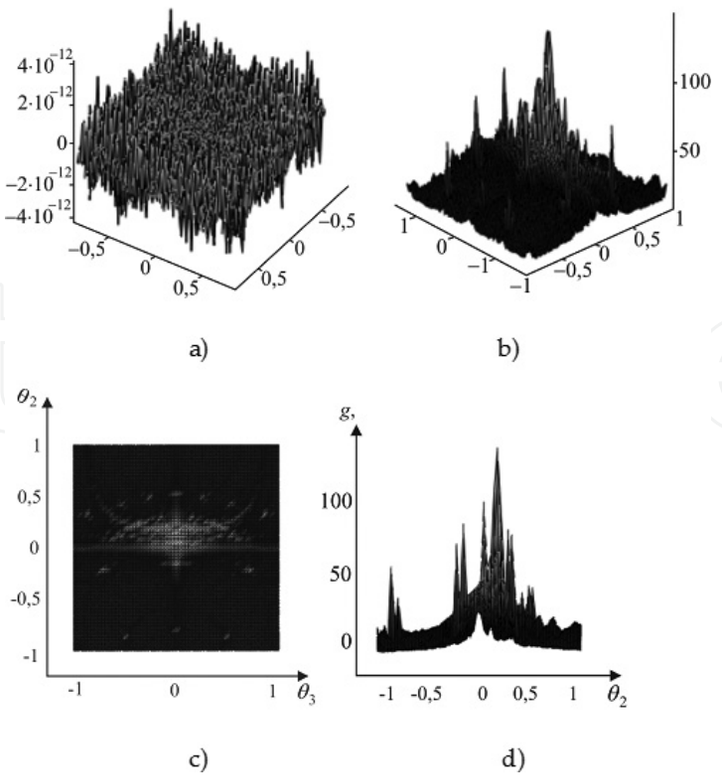

Figure 28. The fractal surface and the scattering indicatrix $g(\theta_2, \theta_3)$ when $\lambda = 2.2$ mm and $\theta_1 = 10°$: (a) fractal surface for $D = 2.8$; $N = M = 10$; $q = 2.7$; (b) $g(\theta_2, \theta_3)$; (c) $g(\theta_2, \theta_3)$, top view; (d) $g(\theta_2, \theta_3)$, side view.

http://dx.doi.org/10.5772/intechopen.68187

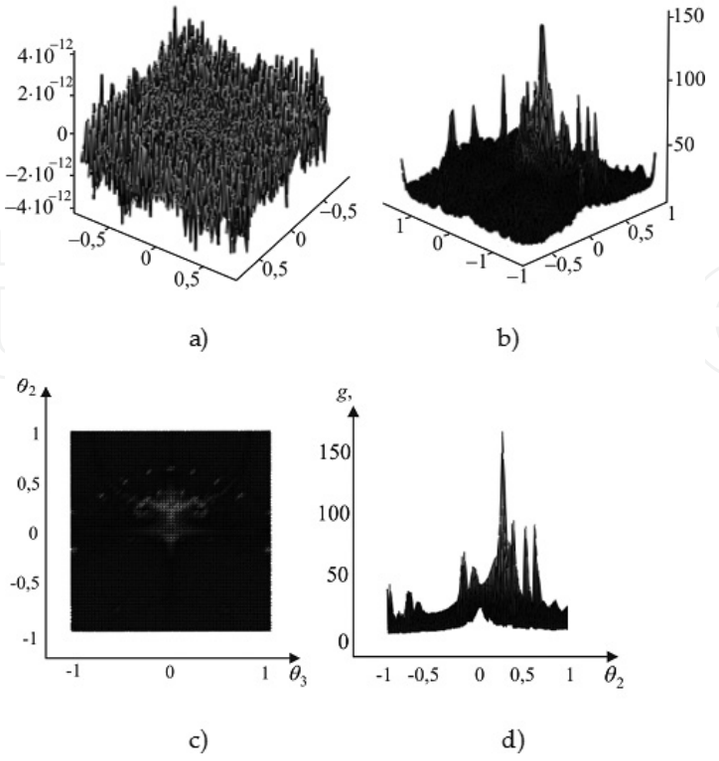

Figure 29. The fractal surface and the scattering indicatrix $g(\theta_2, \theta_3)$ when $\lambda = 2.2$ mm and $\theta_1 = 15°$: (a) fractal surface for $D = 2.8$; $N = M = 10$; $q = 2.7$; (b) $g(\theta_2, \theta_3)$; (c) $g(\theta_2, \theta_3)$, top view; (d) $g(\theta_2, \theta_3)$, side view.

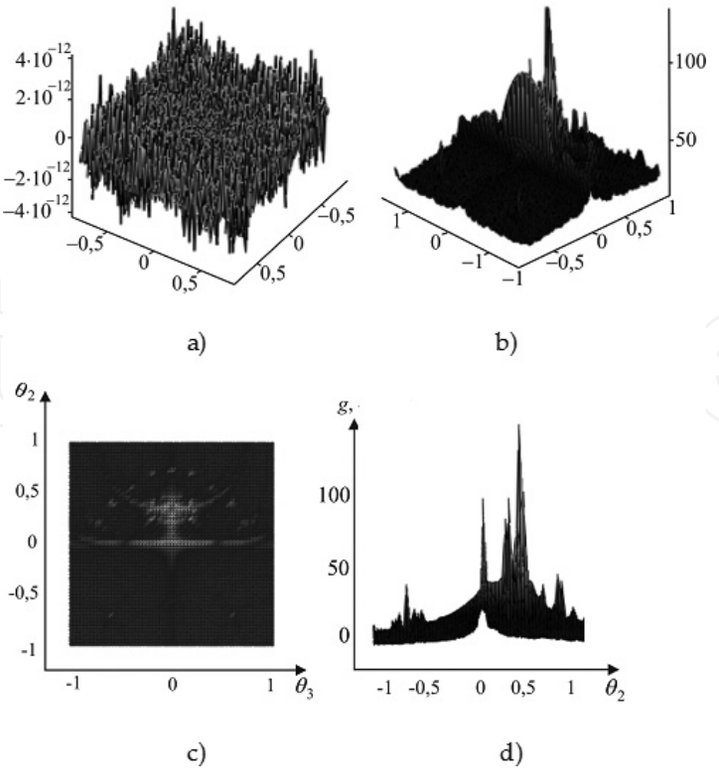

Figure 30. The fractal surface and the scattering indicatrix $g(\theta_2, \theta_3)$ when $\lambda = 2.2$ mm and $\theta_1 = 20°$: (a) fractal surface for $D = 2.8$; $N = M = 10$; $q = 2.7$; (b) $g(\theta_2, \theta_3)$; (c) $g(\theta_2, \theta_3)$, top view; (d) $g(\theta_2, \theta_3)$, side view.

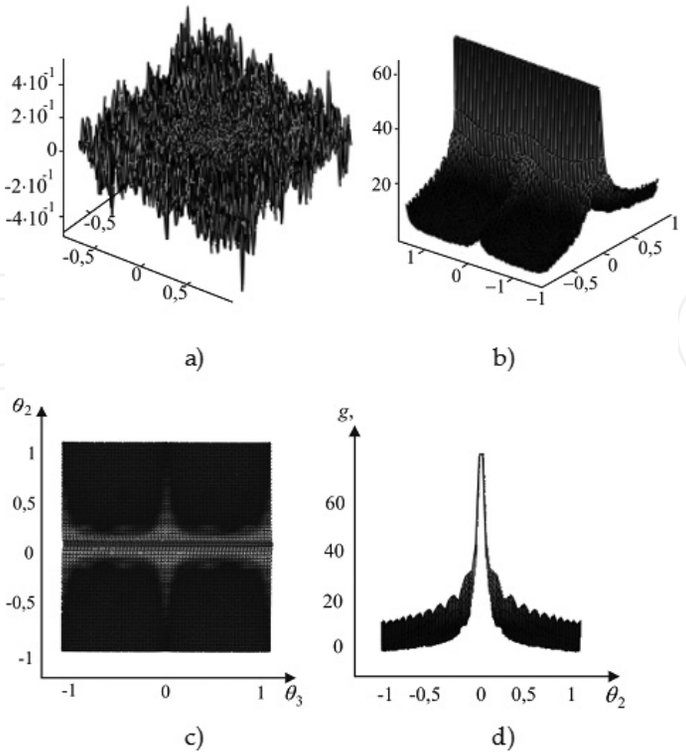

Figure 31. The fractal surface and the scattering indicatrix $g(\theta_2, \theta_3)$ when λ = 8.6 mm and $\theta_1 = 0°$: (a) fractal surface for D = 2.2; $N = M$ = 10; q = 2.7; (b) $g(\theta_2, \theta_3)$; (c) $g(\theta_2, \theta_3)$, top view; (d) $g(\theta_2, \theta_3)$, side view.

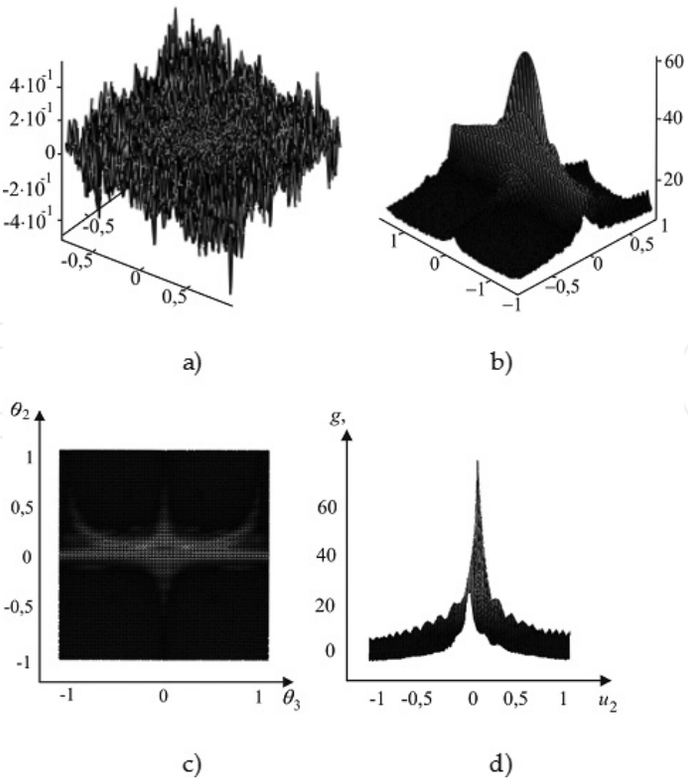

Figure 32. The fractal surface and the scattering indicatrix $g(\theta_2, \theta_3)$ when λ = 8.6 mm and $\theta_1 = 5°$: (a) fractal surface for D = 2.2; $N = M$ = 10; q = 2.7; (b) $g(\theta_2, \theta_3)$; (c) $g(\theta_2, \theta_3)$, top view; (d) $g(\theta_2, \theta_3)$, side view.

http://dx.doi.org/10.5772/intechopen.68187

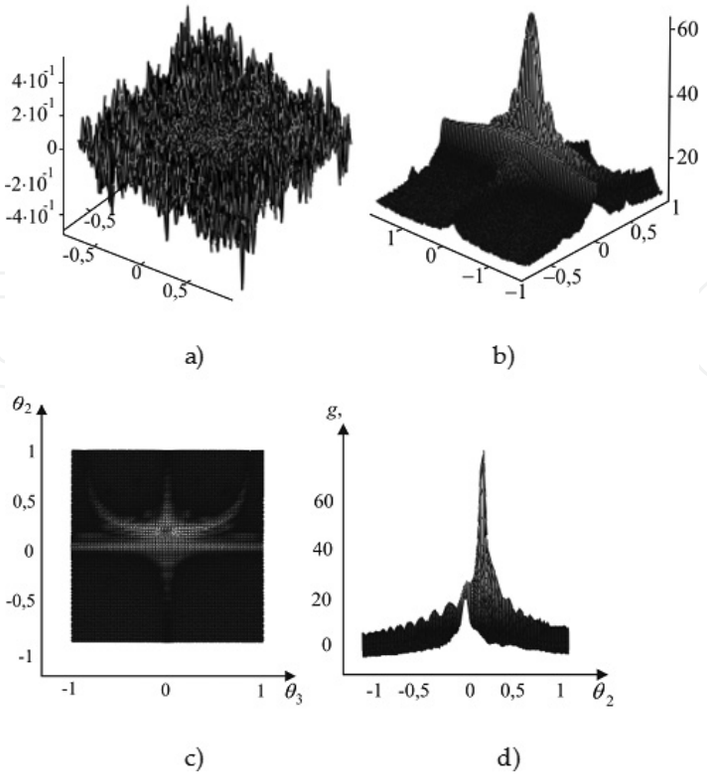

Figure 33. The fractal surface and the scattering indicatrix $g(\theta_2, \theta_3)$ when $\lambda = 8.6$ mm and $\theta_1 = 10°$: (a) fractal surface for $D = 2.2$; $N = M = 10$; $q = 2.7$; (b) $g(\theta_2, \theta_3)$; (c) $g(\theta_2, \theta_3)$, top view; (d) $g(\theta_2, \theta_3)$, side view.

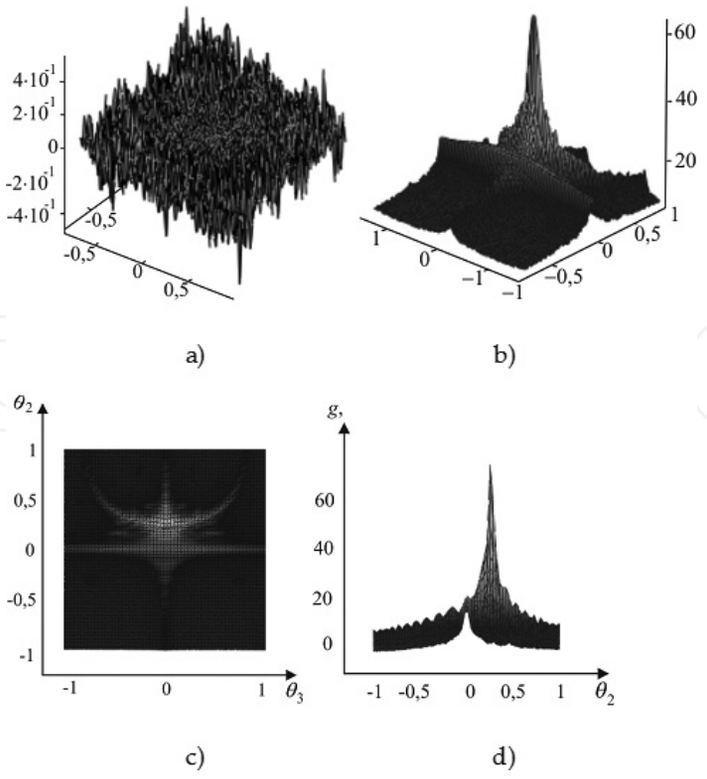

Figure 34. The fractal surface and the scattering indicatrix $g(\theta_2, \theta_3)$ when $\lambda = 8.6$ mm and $\theta_1 = 15°$: (a) fractal surface for $D = 2.2$; $N = M = 10$; $q = 2.7$; (b) $g(\theta_2, \theta_3)$; (c) $g(\theta_2, \theta_3)$, top view; (d) $g(\theta_2, \theta_3)$, side view.

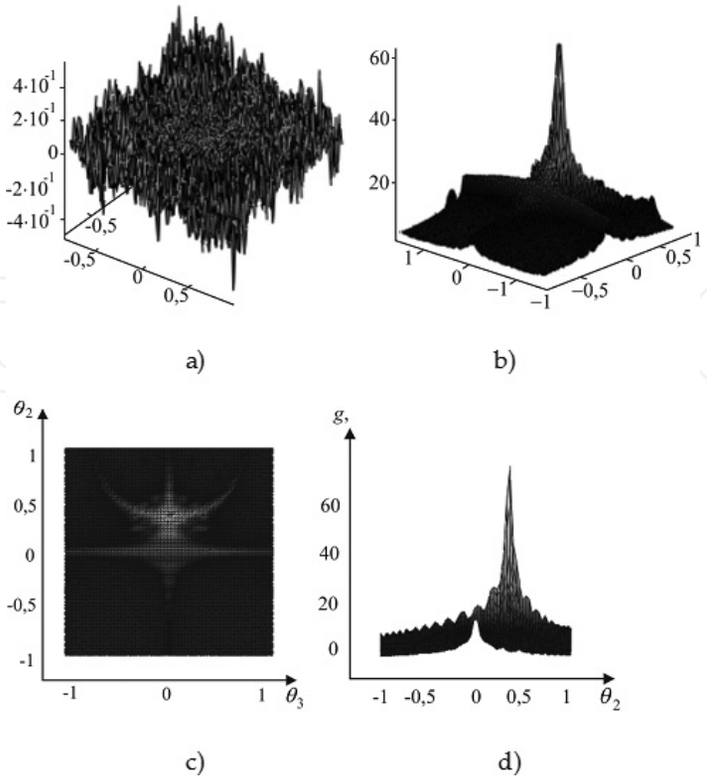

Figure 35. The fractal surface and the scattering indicatrix $g(\theta_2, \theta_3)$ when $\lambda = 8.6$ mm and $\theta_1 = 20°$: (a) fractal surface for $D = 2.2$; $N = M = 10$; $q = 2.7$; (b) $g(\theta_2, \theta_3)$; (c) $g(\theta_2, \theta_3)$, top view; (d) $g(\theta_2, \theta_3)$, side view.

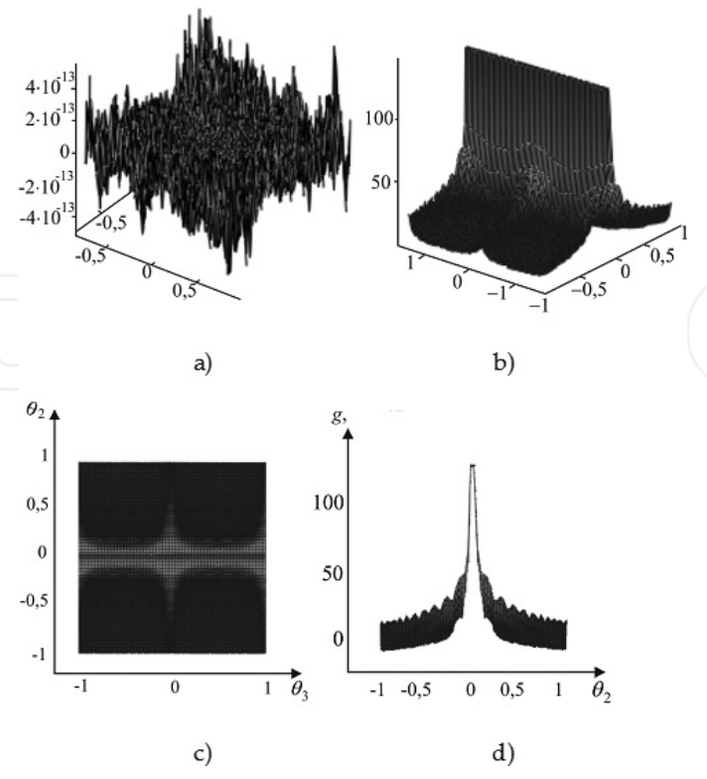

Figure 36. The fractal surface and the scattering indicatrix $g(\theta_2, \theta_3)$ when $\lambda = 8.6$ mm and $\theta_1 = 0°$: (a) fractal surface for $D = 2.2$; $N = M = 20$; $q = 2.7$; (b) $g(\theta_2, \theta_3)$; (c) $g(\theta_2, \theta_3)$, top view; (d) $g(\theta_2, \theta_3)$, side view.

http://dx.doi.org/10.5772/intechopen.68187

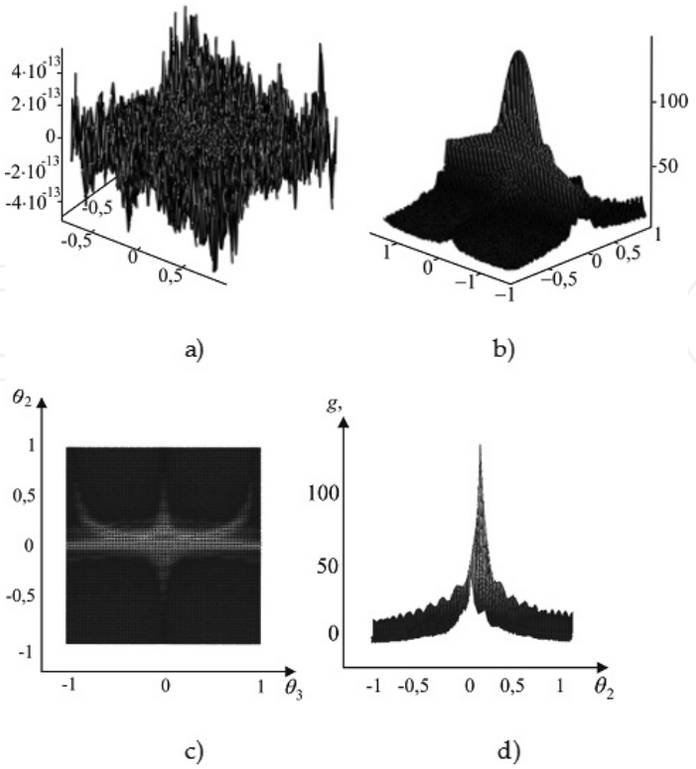

Figure 37. The fractal surface and the scattering indicatrix $g(\theta_2, \theta_3)$ when $\lambda = 8.6$ mm and $\theta_1 = 5°$: (a) fractal surface for $D = 2.2$; $N = M = 20$; $q = 2.7$; (b) $g(\theta_2, \theta_3)$; (c) $g(\theta_2, \theta_3)$, top view; (d) $g(\theta_2, \theta_3)$, side view.

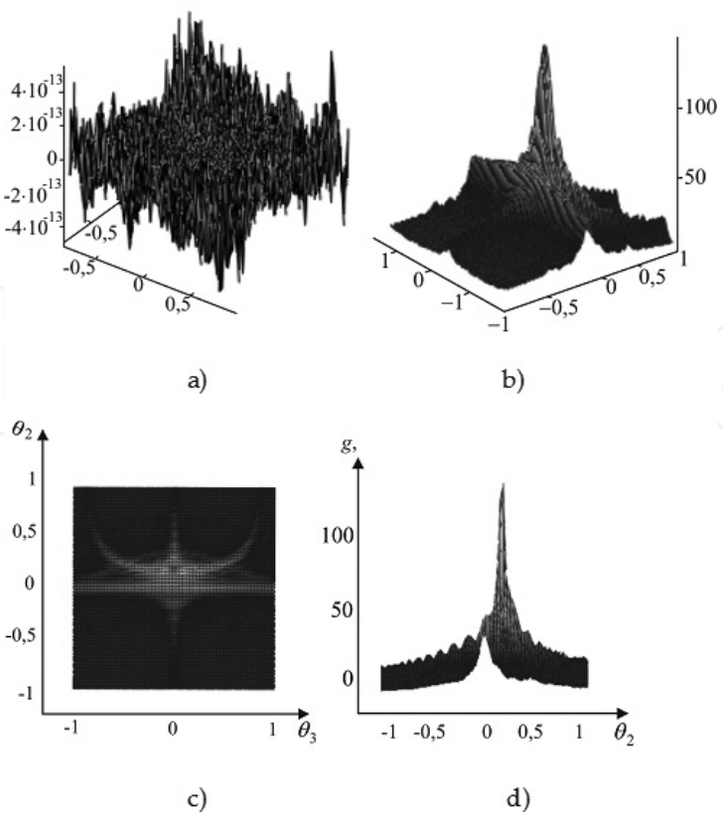

Figure 38. The fractal surface and the scattering indicatrix $g(\theta_2, \theta_3)$ when $\lambda = 8.6$ mm and $\theta_1 = 10°$: (a) fractal surface for $D = 2.2$; $N = M = 20$; $q = 2.7$; (b) $g(\theta_2, \theta_3)$; (c) $g(\theta_2, \theta_3)$, top view; (d) $g(\theta_2, \theta_3)$, side view.

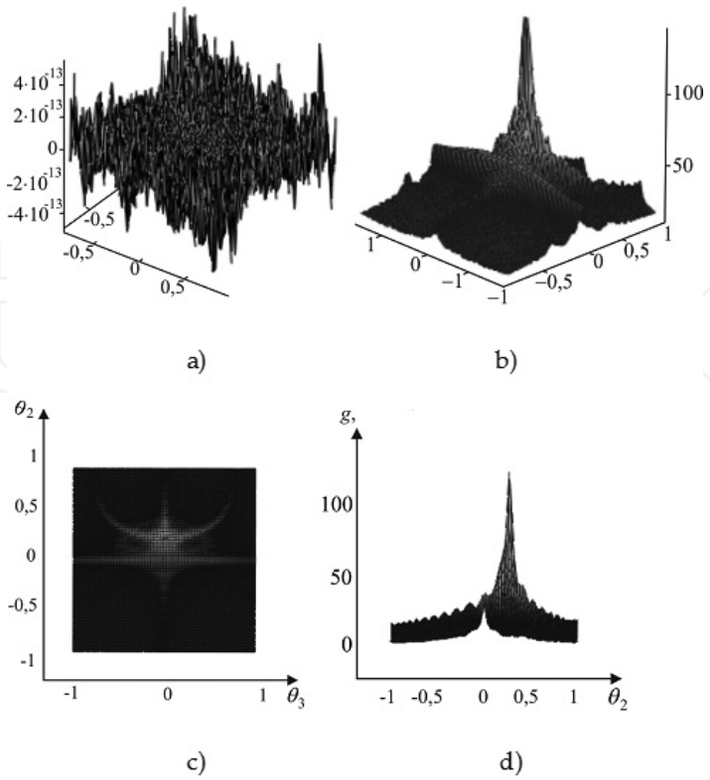

Figure 39. The fractal surface and the scattering indicatrix $g(\theta_2, \theta_3)$ when $\lambda = 8.6$ mm and $\theta_1 = 15°$: (a) fractal surface for $D = 2.2$; $N = M = 20$; $q = 2.7$; (b) $g(\theta_2, \theta_3)$; (c) $g(\theta_2, \theta_3)$, top view; (d) $g(\theta_2, \theta_3)$, side view.

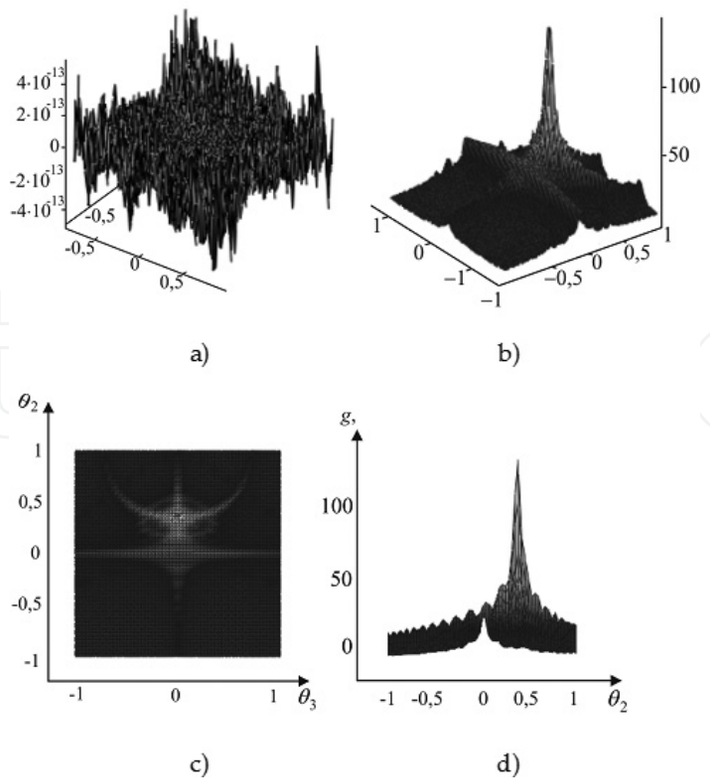

Figure 40. The fractal surface and the scattering indicatrix $g(\theta_2, \theta_3)$ when $\lambda = 8.6$ mm and $\theta_1 = 20°$: (a) fractal surface for $D = 2.2$; $N = M = 20$; $q = 2.7$; (b) $g(\theta_2, \theta_3)$; (c) $g(\theta_2, \theta_3)$, top view; (d) $g(\theta_2, \theta_3)$, side view.

http://dx.doi.org/10.5772/intechopen.68187

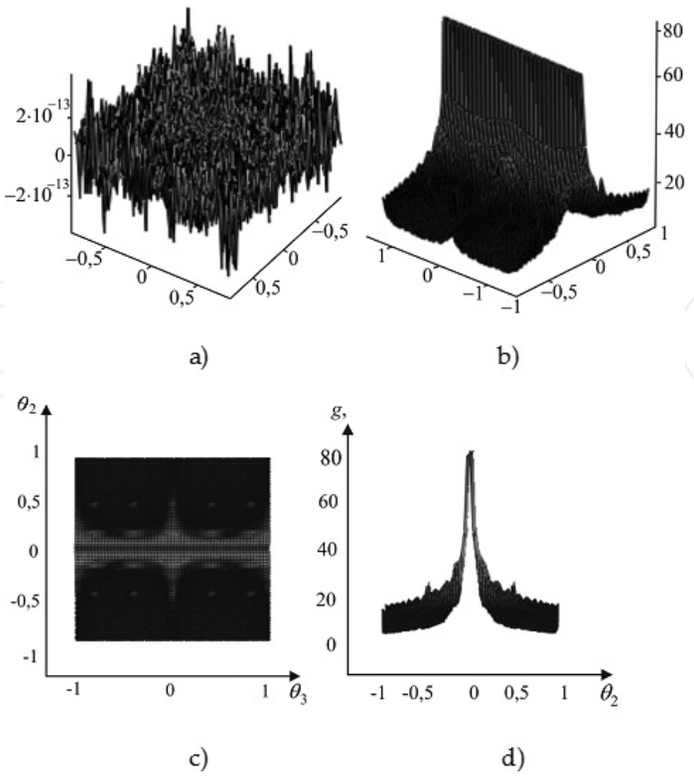

Figure 41. The fractal surface and the scattering indicatrix $g(\theta_2, \theta_3)$ when $\lambda = 8.6$ mm and $\theta_1 = 0°$: (a) fractal surface for $D = 2.5$; $N = M = 10$; $q = 2.7$; (b) $g(\theta_2, \theta_3)$; (c) $g(\theta_2, \theta_3)$, top view; (d) $g(\theta_2, \theta_3)$, side view.

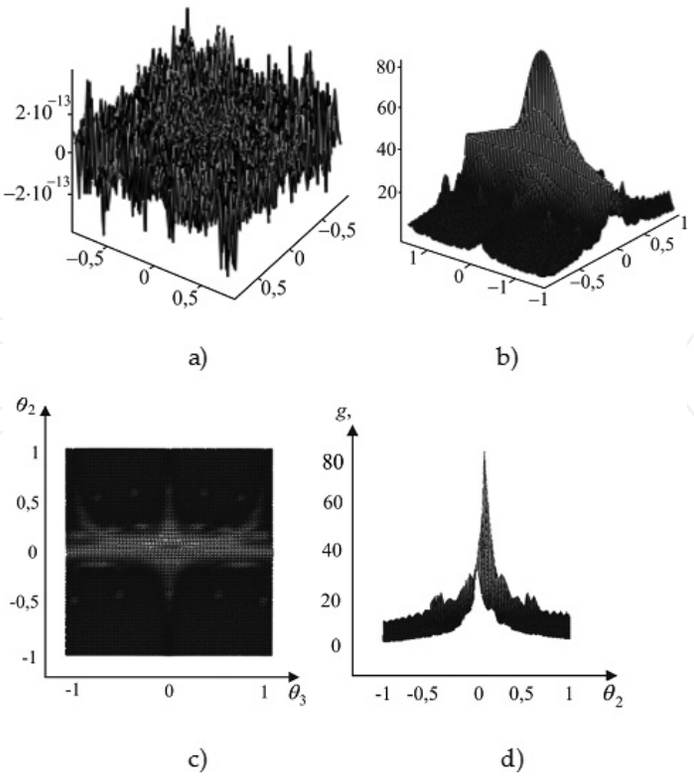

Figure 42. The fractal surface and the scattering indicatrix $g(\theta_2, \theta_3)$ when $\lambda = 8.6$ mm and $\theta_1 = 5°$: (a) fractal surface for $D = 2.5$; $N = M = 10$; $q = 2.7$; (b) $g(\theta_2, \theta_3)$; (c) $g(\theta_2, \theta_3)$, top view; (d) $g(\theta_2, \theta_3)$, side view.

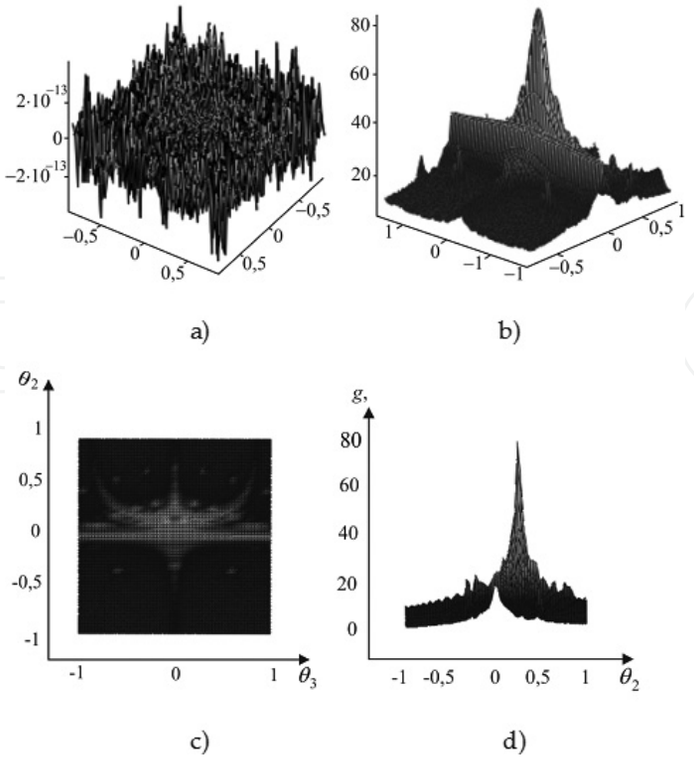

Figure 43. The fractal surface and the scattering indicatrix $g(\theta_2, \theta_3)$ when $\lambda = 8.6$ mm and $\theta_1 = 10°$: (a) fractal surface for $D = 2.5$; $N = M = 10$; $q = 2.7$; (b) $g(\theta_2, \theta_3)$; (c) $g(\theta_2, \theta_3)$, top view; (d) $g(\theta_2, \theta_3)$, side view.

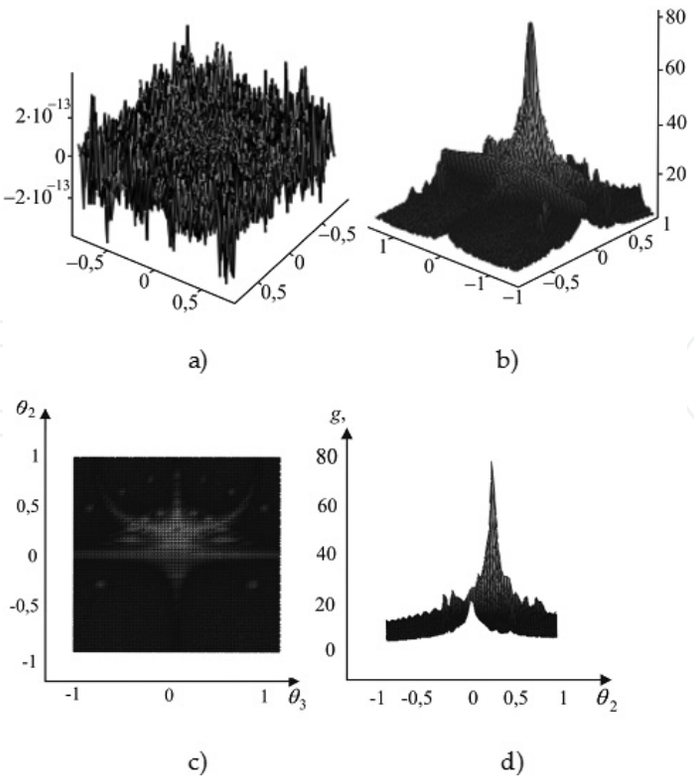

Figure 44. The fractal surface and the scattering indicatrix $g(\theta_2, \theta_3)$ when $\lambda = 8.6$ mm and $\theta_1 = 15°$: (a) fractal surface for $D = 2.5$; $N = M = 10$; $q = 2.7$; (b) $g(\theta_2, \theta_3)$; (c) $g(\theta_2, \theta_3)$, top view; (d) $g(\theta_2, \theta_3)$, side view.

http://dx.doi.org/10.5772/intechopen.68187

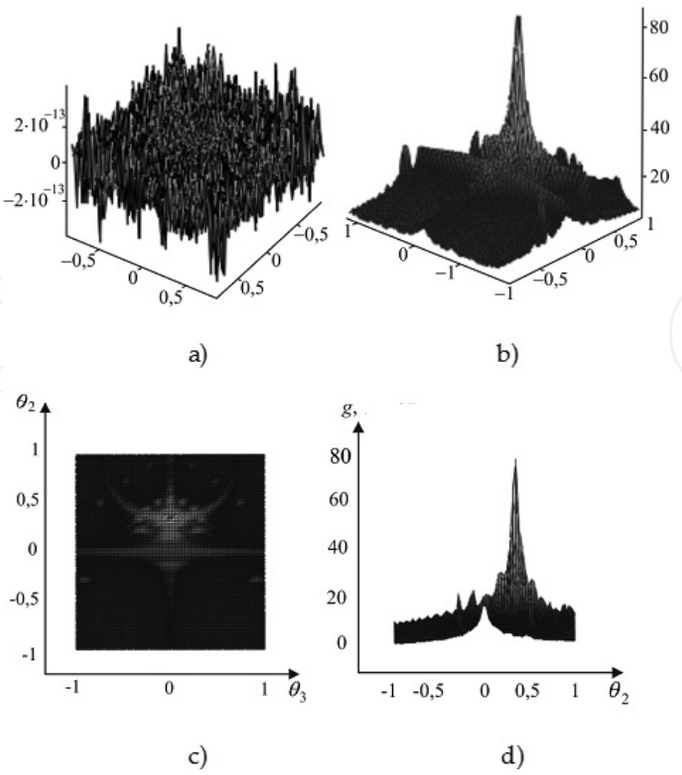

Figure 45. The fractal surface and the scattering indicatrix $g(\theta_2, \theta_3)$ when $\lambda = 8.6$ mm and $\theta_1 = 20°$: (a) fractal surface for $D = 2.5$; $N = M = 10$; $q = 2.7$; (b) $g(\theta_2, \theta_3)$; (c) $g(\theta_2, \theta_3)$, top view; (d) $g(\theta_2, \theta_3)$, side view.

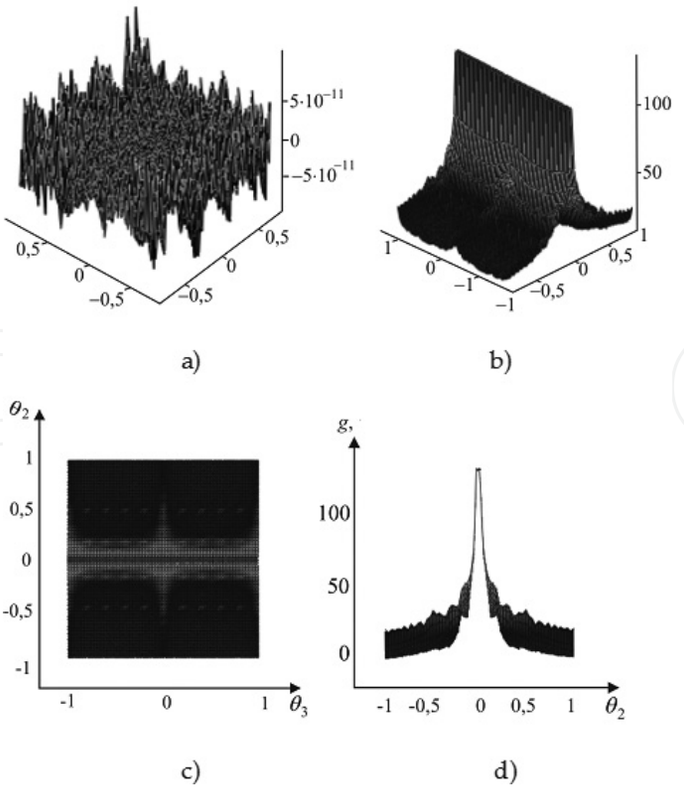

Figure 46. The fractal surface and the scattering indicatrix $g(\theta_2, \theta_3)$ when $\lambda = 8.6$ mm and $\theta_1 = 0°$: (a) fractal surface for $D = 2.5$; $N = M = 20$; $q = 2.7$; (b) $g(\theta_2, \theta_3)$; (c) $g(\theta_2, \theta_3)$, top view; (d) $g(\theta_2, \theta_3)$, side view.

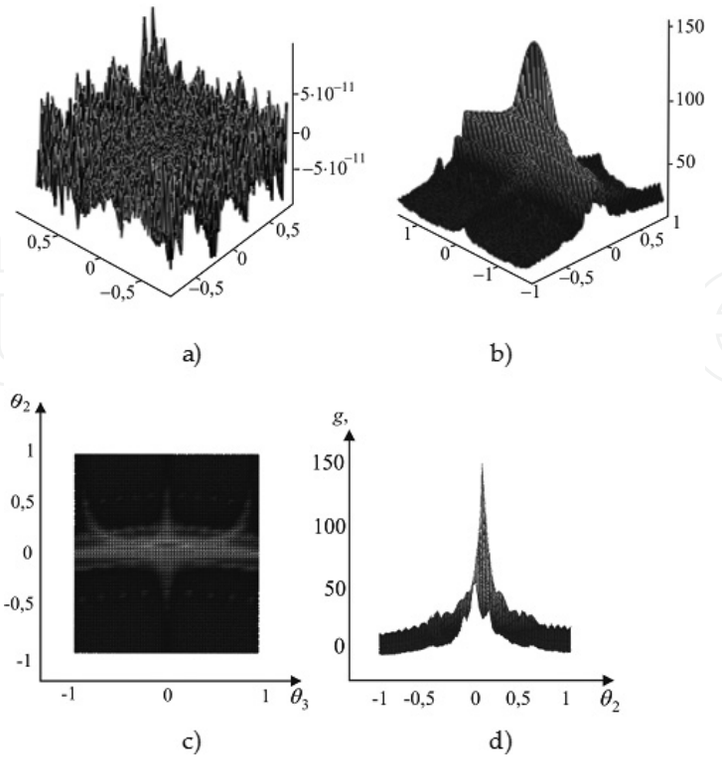

Figure 47. The fractal surface and the scattering indicatrix $g(\theta_2, \theta_3)$ when $\lambda = 8.6$ mm and $\theta_1 = 5°$: (a) fractal surface for $D = 2.5$; $N = M = 20$; $q = 2.7$; (b) $g(\theta_2, \theta_3)$; (c) $g(\theta_2, \theta_3)$, top view; (d) $g(\theta_2, \theta_3)$, side view.

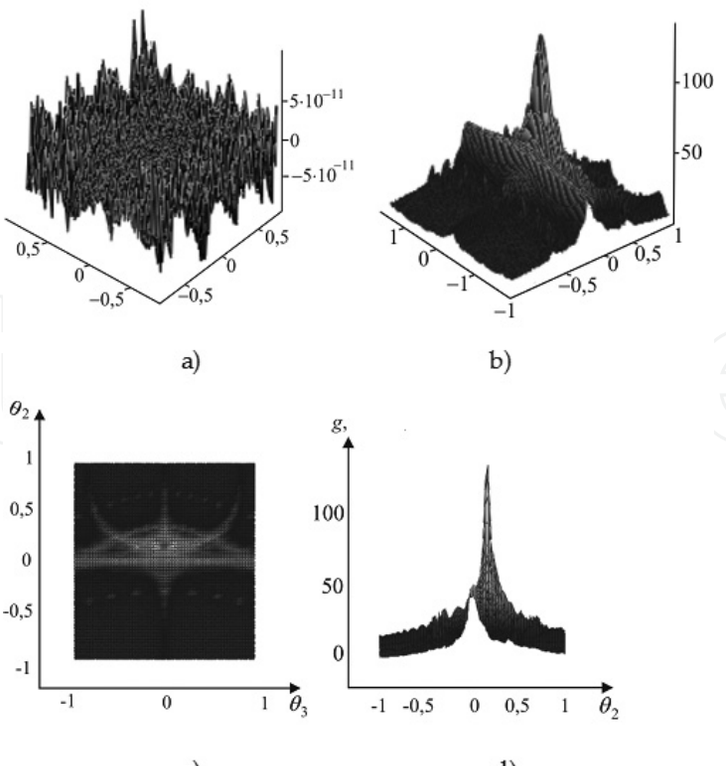

Figure 48. The fractal surface and the scattering indicatrix $g(\theta_2, \theta_3)$ when $\lambda = 8.6$ mm and $\theta_1 = 10°$: (a) fractal surface for $D = 2.5$; $N = M = 20$; $q = 2.7$; (b) $g(\theta_2, \theta_3)$; (c) $g(\theta_2, \theta_3)$, top view; (d) $g(\theta_2, \theta_3)$, side view.

http://dx.doi.org/10.5772/intechopen.68187

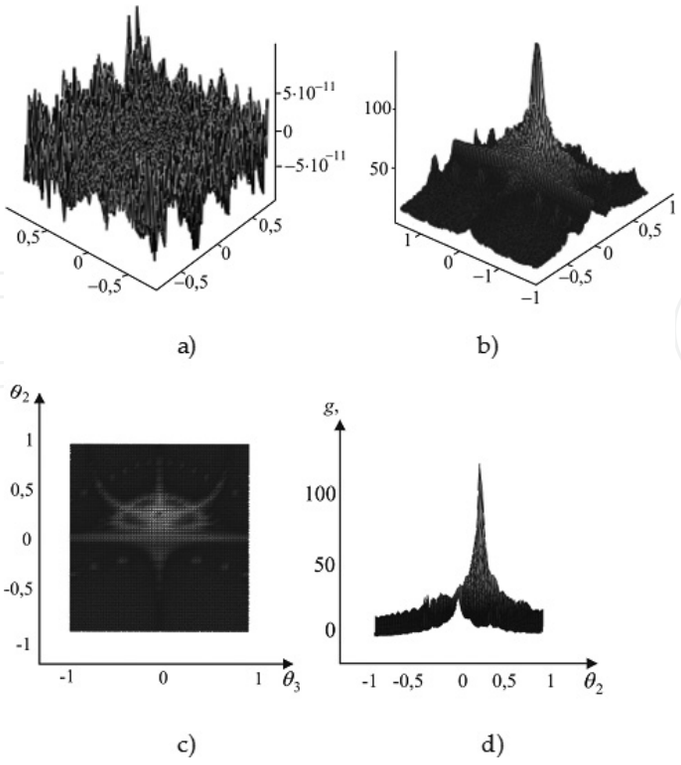

Figure 49. The fractal surface and the scattering indicatrix $g(\theta_2, \theta_3)$ when $\lambda = 8.6$ mm and $\theta_1 = 15°$: (a) fractal surface for $D = 2.5$; $N = M = 20$; $q = 2.7$; (b) $g(\theta_2, \theta_3)$; (c) $g(\theta_2, \theta_3)$, top view; (d) $g(\theta_2, \theta_3)$, side view.

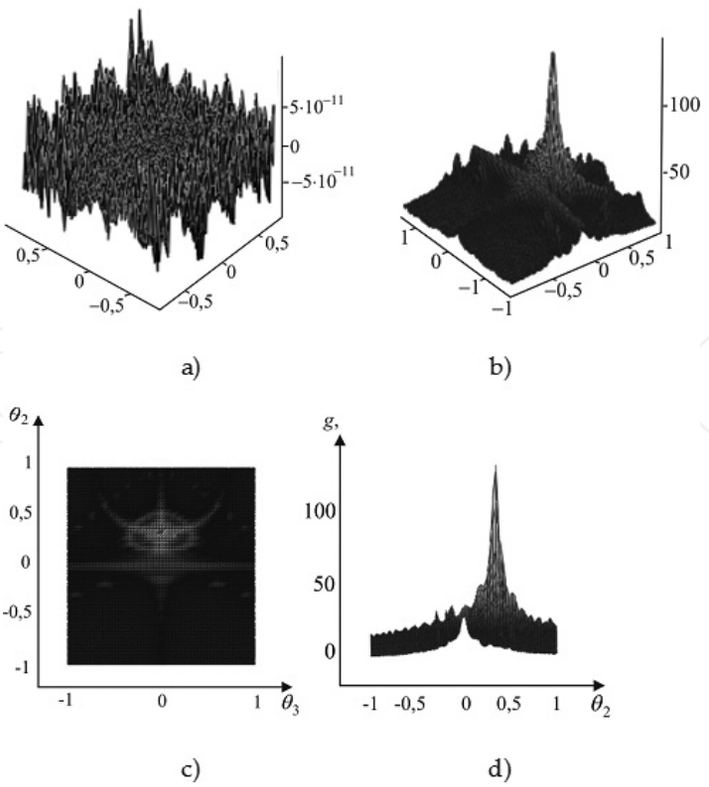

Figure 50. The fractal surface and the scattering indicatrix $g(\theta_2, \theta_3)$ when $\lambda = 8.6$ mm and $\theta_1 = 20°$: (a) fractal surface for $D = 2.5$; $N = M = 20$; $q = 2.7$; (b) $g(\theta_2, \theta_3)$; (c) $g(\theta_2, \theta_3)$, top view; (d) $g(\theta_2, \theta_3)$, side view.

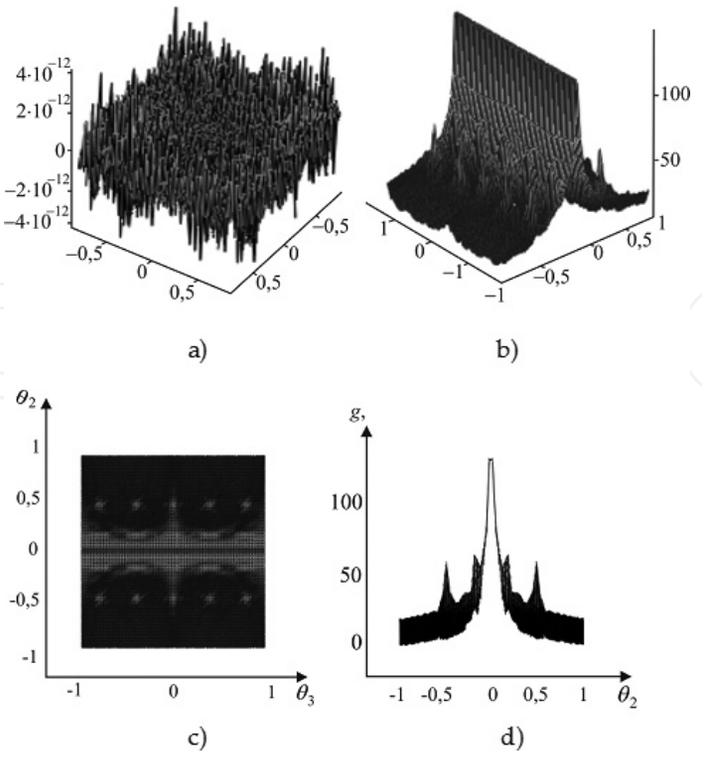

Figure 51. The fractal surface and the scattering indicatrix $g(\theta_2, \theta_3)$ when $\lambda = 8.6$ mm and $\theta_1 = 0°$: (a) fractal surface for $D = 2.8$; $N = M = 10$; $q = 2.7$; (b) $g(\theta_2, \theta_3)$; (c) $g(\theta_2, \theta_3)$, top view; (d) $g(\theta_2, \theta_3)$, side view.

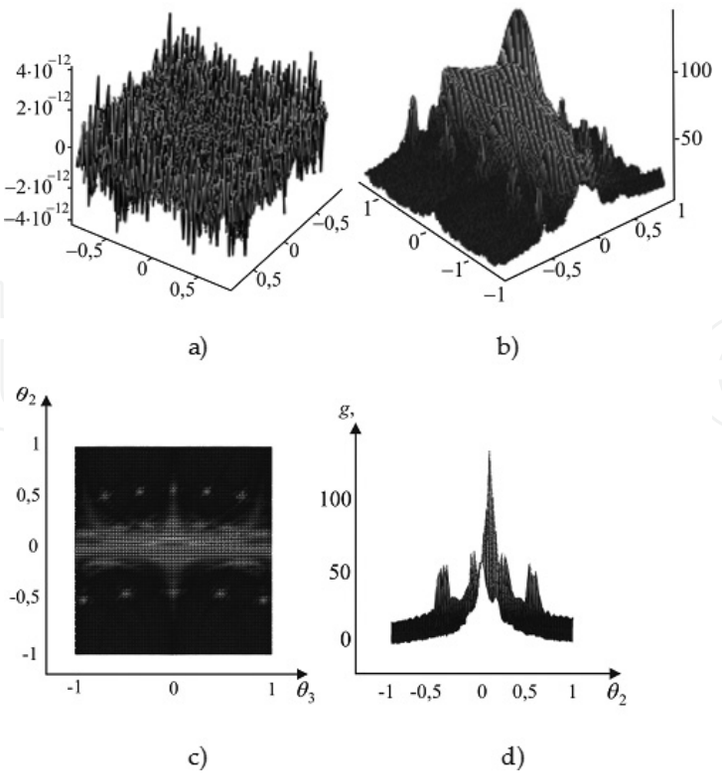

Figure 52. The fractal surface and the scattering indicatrix $g(\theta_2, \theta_3)$ when $\lambda = 8.6$ mm and $\theta_1 = 5°$: (a) fractal surface for $D = 2.8$; $N = M = 10$; $q = 2.7$; (b) $g(\theta_2, \theta_3)$; (c) $g(\theta_2, \theta_3)$, top view; (d) $g(\theta_2, \theta_3)$, side view.

http://dx.doi.org/10.5772/intechopen.68187

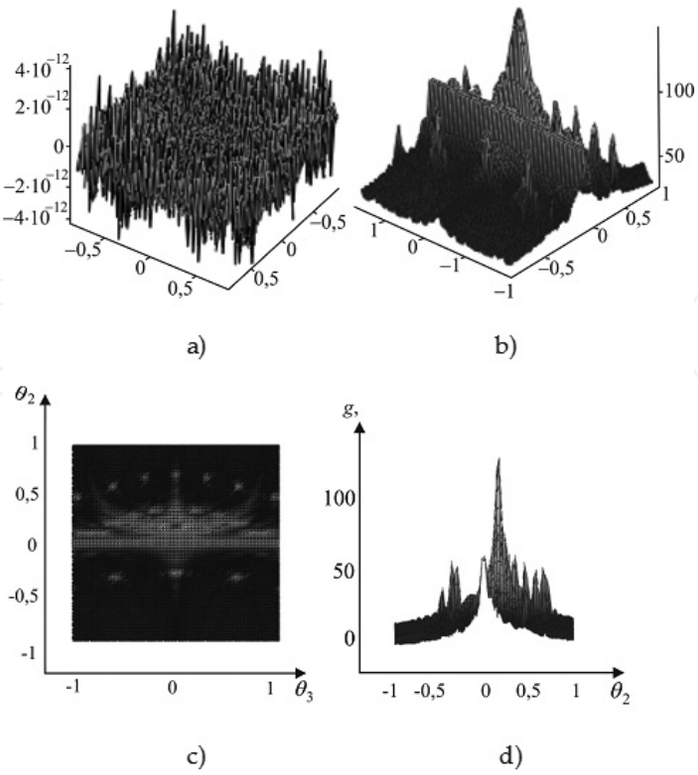

Figure 53. The fractal surface and the scattering indicatrix $g(\theta_2, \theta_3)$ when $\lambda = 8.6$ mm and $\theta_1 = 10°$: (a) fractal surface for $D = 2.8$; $N = M = 10$; $q = 2.7$; (b) $g(\theta_2, \theta_3)$; (c) $g(\theta_2, \theta_3)$, top view; (d) $g(\theta_2, \theta_3)$, side view.

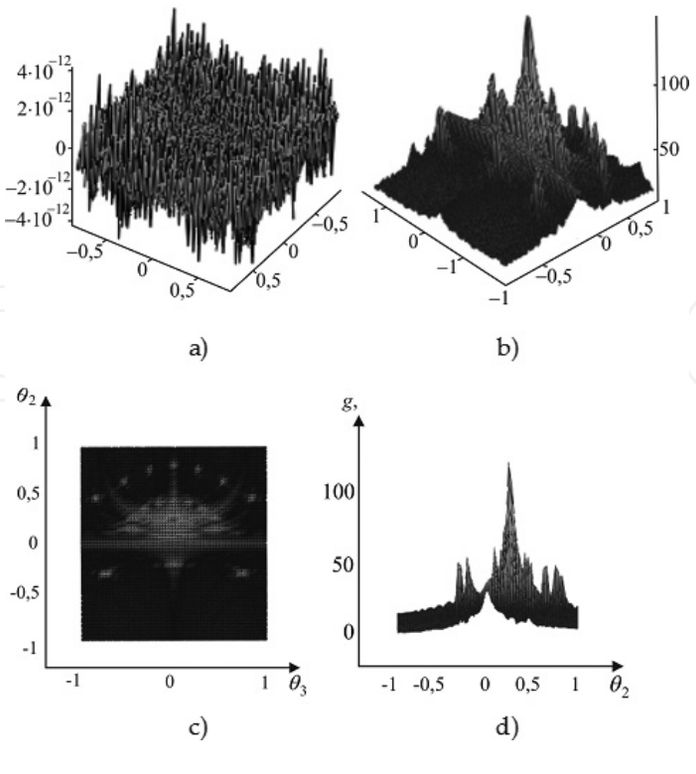

Figure 54. The fractal surface and the scattering indicatrix $g(\theta_2, \theta_3)$ when $\lambda = 8.6$ mm and $\theta_1 = 15°$: (a) fractal surface for $D = 2.8$; $N = M = 10$; $q = 2.7$; (b) $g(\theta_2, \theta_3)$; (c) $g(\theta_2, \theta_3)$, top view; (d) $g(\theta_2, \theta_3)$, side view.

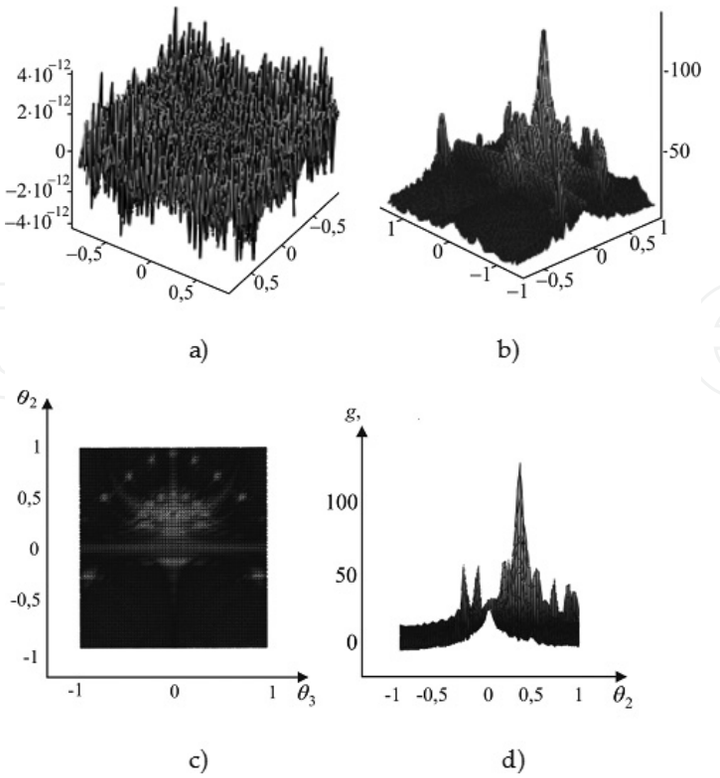

Figure 55. The fractal surface and the scattering indicatrix $g(\theta_2, \theta_3)$ when $\lambda = 8.6$ mm and $\theta_1 = 20°$: (a) fractal surface for $D = 2.8$; $N = M = 10$; $q = 2.7$; (b) $g(\theta_2, \theta_3)$; (c) $g(\theta_2, \theta_3)$, top view; (d) $g(\theta_2, \theta_3)$, side view.

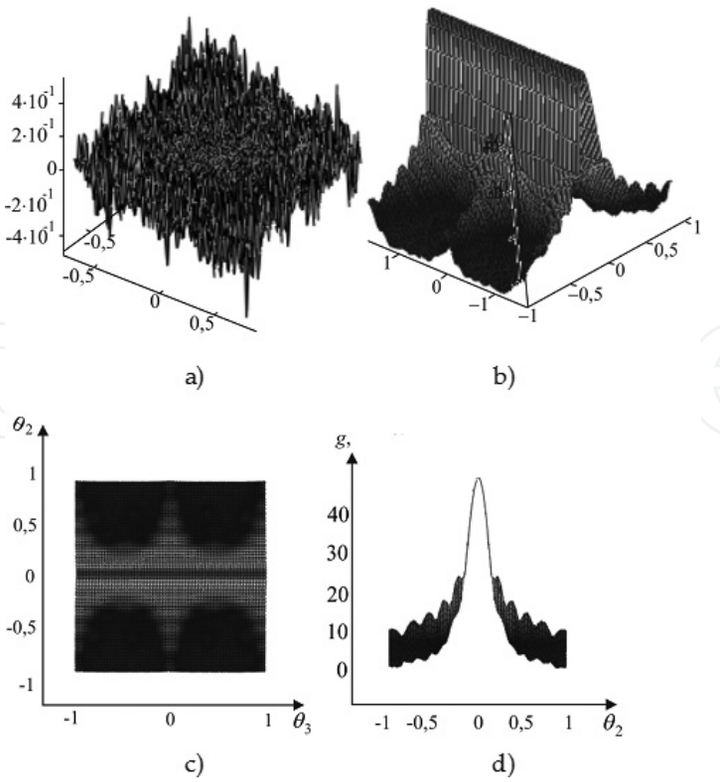

Figure 56. The fractal surface and the scattering indicatrix $g(\theta_2, \theta_3)$ when $\lambda = 30$ mm and $\theta_1 = 0°$: (a) fractal surface for $D = 2.2$; $N = M = 10$; $q = 2.7$; (b) $g(\theta_2, \theta_3)$; (c) $g(\theta_2, \theta_3)$, top view; (d) $g(\theta_2, \theta_3)$, side view.

http://dx.doi.org/10.5772/intechopen.68187

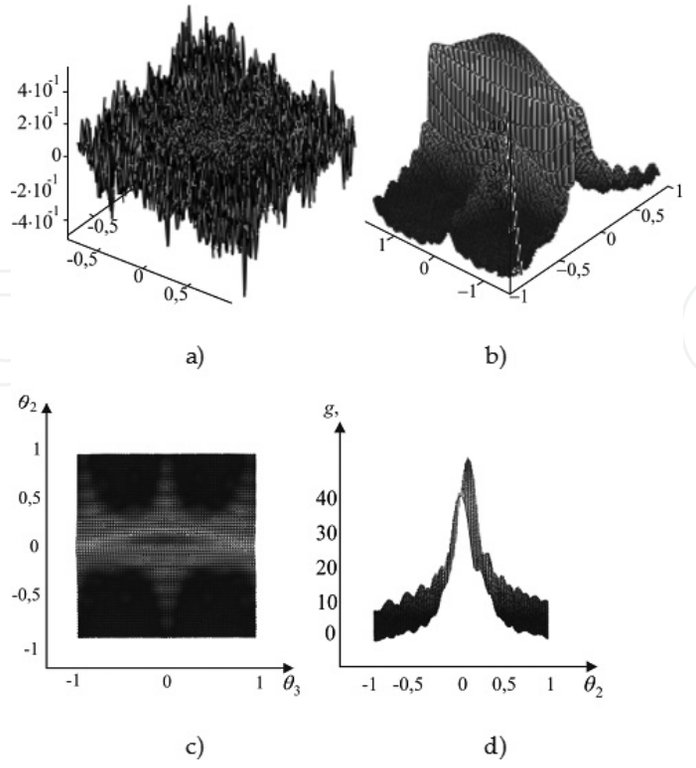

Figure 57. The fractal surface and the scattering indicatrix $g(\theta_2, \theta_3)$ when $\lambda = 30$ mm and $\theta_1 = 5°$: (a) fractal surface for $D = 2.2$; $N = M = 10$; $q = 2.7$; (b) $g(\theta_2, \theta_3)$; (c) $g(\theta_2, \theta_3)$, top view; (d) $g(\theta_2, \theta_3)$, side view.

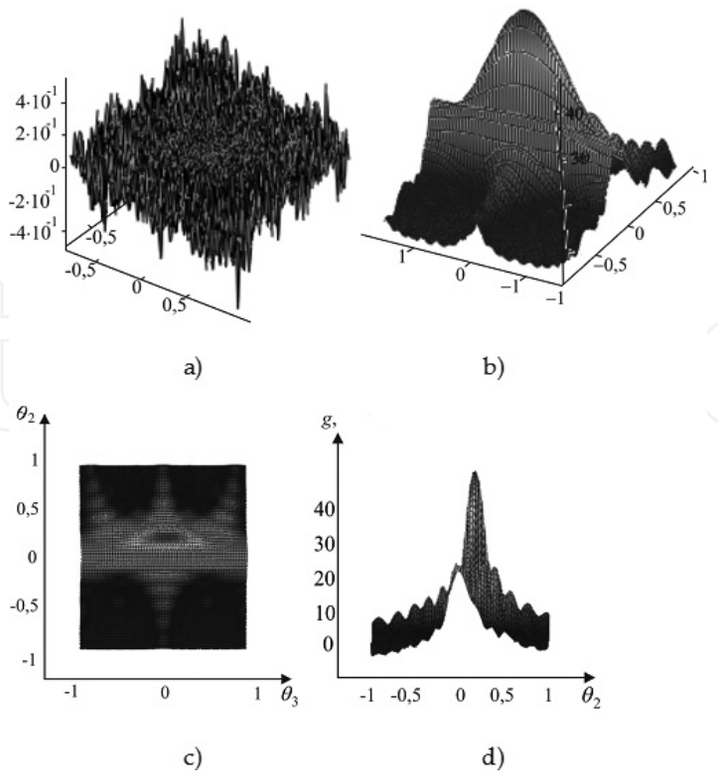

Figure 58. The fractal surface and the scattering indicatrix $g(\theta_2, \theta_3)$ when $\lambda = 30$ mm and $\theta_1 = 10°$: (a) fractal surface for $D = 2.2$; $N = M = 10$; $q = 2.7$; (b) $g(\theta_2, \theta_3)$; (c) $g(\theta_2, \theta_3)$, top view; (d) $g(\theta_2, \theta_3)$, side view.

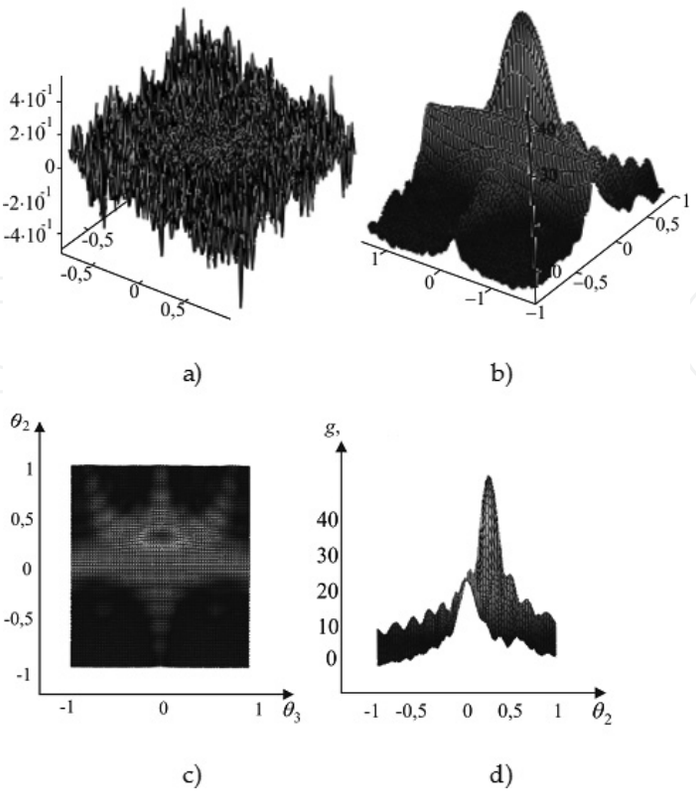

Figure 59. The fractal surface and the scattering indicatrix $g(\theta_2, \theta_3)$ when $\lambda = 30$ mm and $\theta_1 = 15°$: (a) fractal surface for $D = 2.2$; $N = M = 10$; $q = 2.7$; (b) $g(\theta_2, \theta_3)$; (c) $g(\theta_2, \theta_3)$, top view; (d) $g(\theta_2, \theta_3)$, side view.

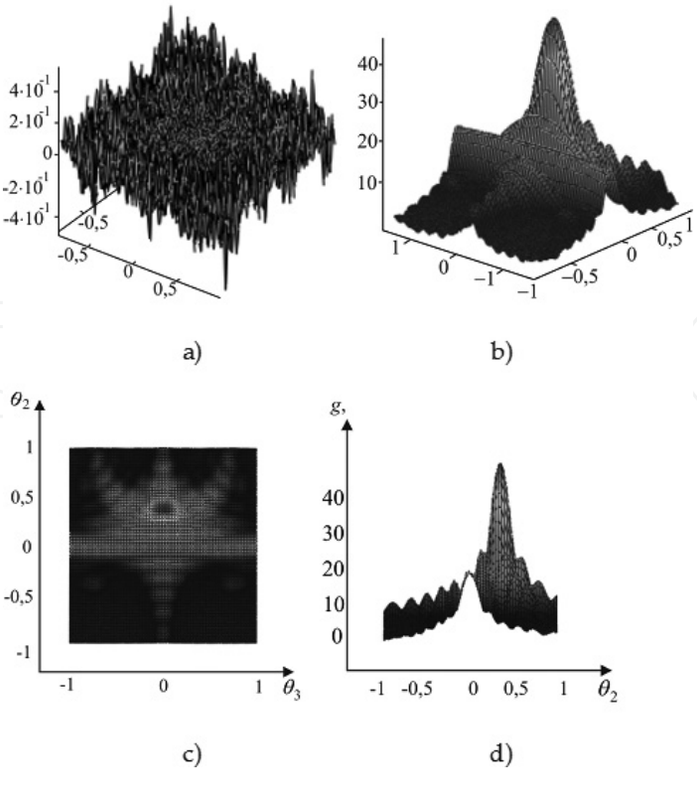

Figure 60. The fractal surface and the scattering indicatrix $g(\theta_2, \theta_3)$ when $\lambda = 30$ mm and $\theta_1 = 20°$: (a) fractal surface for $D = 2.2$; $N = M = 10$; $q = 2.7$; (b) $g(\theta_2, \theta_3)$; (c) $g(\theta_2, \theta_3)$, top view; (d) $g(\theta_2, \theta_3)$, side view.

http://dx.doi.org/10.5772/intechopen.68187

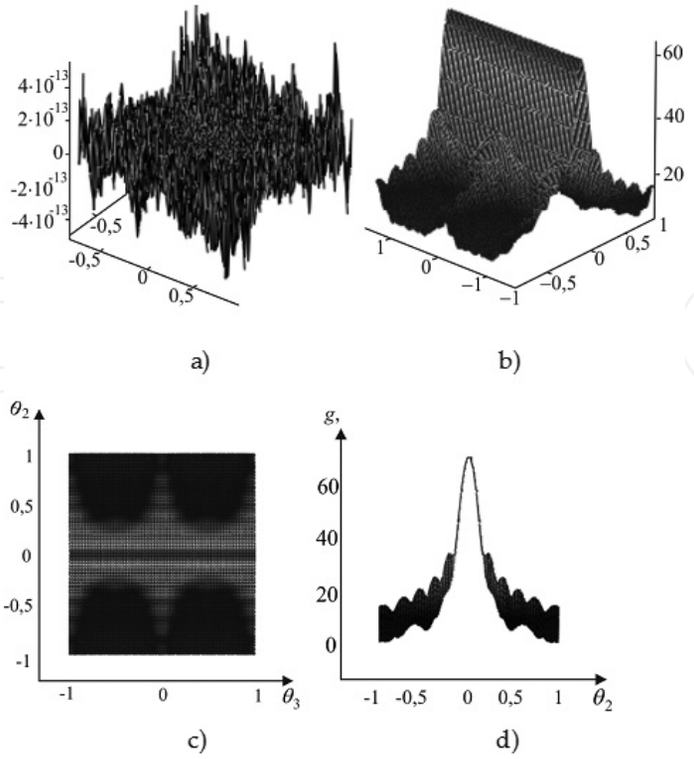

Figure 61. The fractal surface and the scattering indicatrix $g(\theta_2, \theta_3)$ when $\lambda = 30$ mm and $\theta_1 = 0°$: (a) fractal surface for $D = 2.2$; $N = M = 20$; $q = 2.7$; (b) $g(\theta_2, \theta_3)$; (c) $g(\theta_2, \theta_3)$, top view; (d) $g(\theta_2, \theta_3)$, side view.

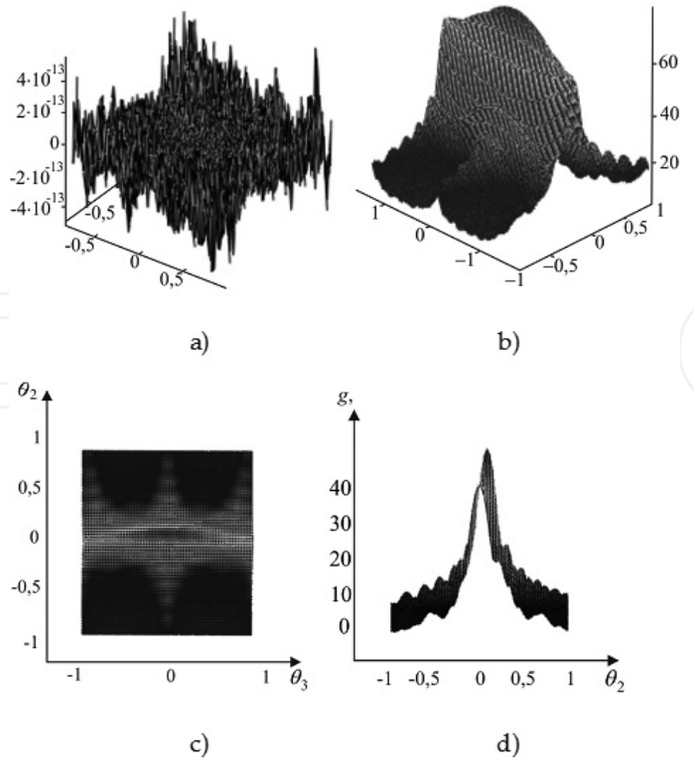

Figure 62. The fractal surface and the scattering indicatrix $g(\theta_2, \theta_3)$ when $\lambda = 30$ mm and $\theta_1 = 5°$: (a) fractal surface for $D = 2.2$; $N = M = 20$; $q = 2.7$; (b) $g(\theta_2, \theta_3)$; (c) $g(\theta_2, \theta_3)$, top view; (d) $g(\theta_2, \theta_3)$, side view.

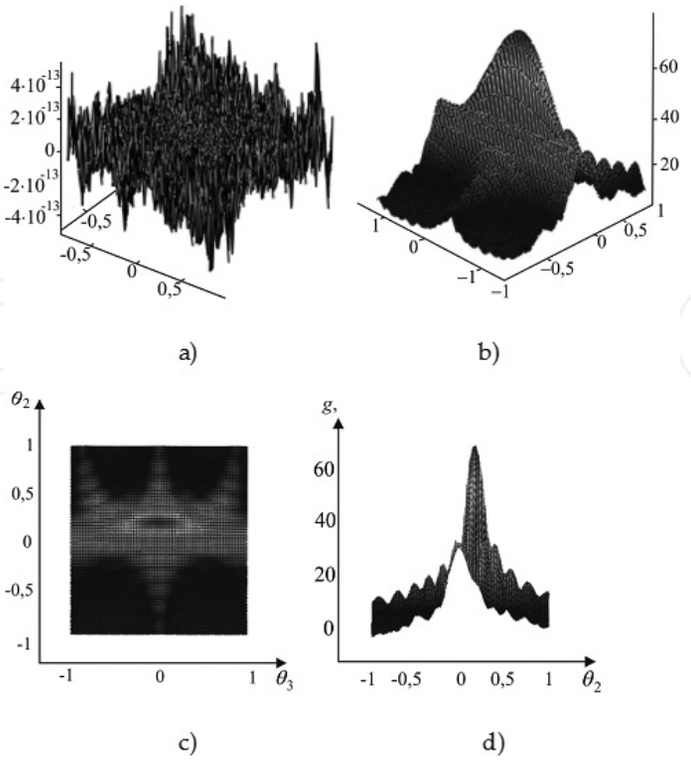

Figure 63. The fractal surface and the scattering indicatrix $g(\theta_2, \theta_3)$ when $\lambda = 30$ mm and $\theta_1 = 10°$: (a) fractal surface for $D = 2.2$; $N = M = 20$; $q = 2.7$; (b) $g(\theta_2, \theta_3)$; (c) $g(\theta_2, \theta_3)$, top view; (d) $g(\theta_2, \theta_3)$, side view.

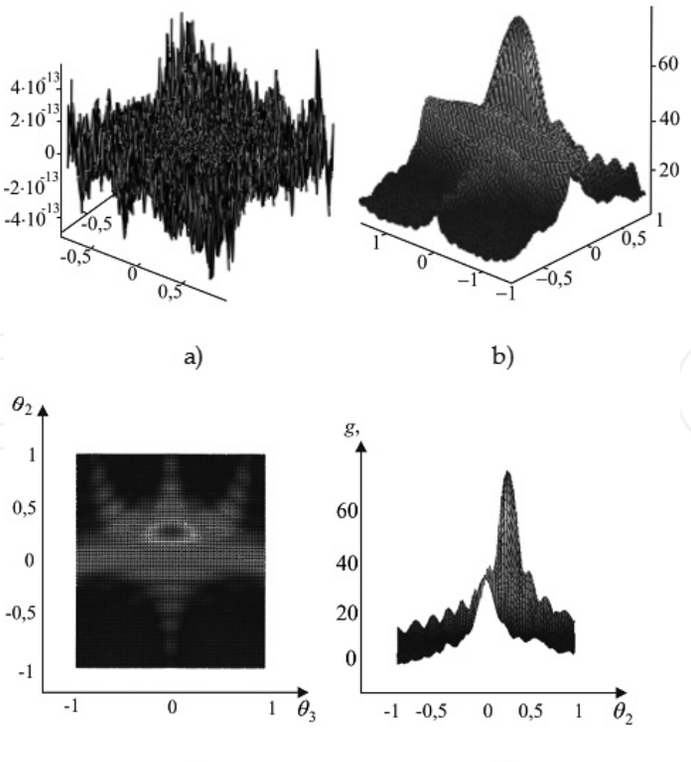

Figure 64. The fractal surface and the scattering indicatrix $g(\theta_2, \theta_3)$ when $\lambda = 30$ mm and $\theta_1 = 15°$: (a) fractal surface for $D = 2.2$; $N = M = 20$; $q = 2.7$; (b) $g(\theta_2, \theta_3)$; (c) $g(\theta_2, \theta_3)$, top view; (d) $g(\theta_2, \theta_3)$, side view.

http://dx.doi.org/10.5772/intechopen.68187

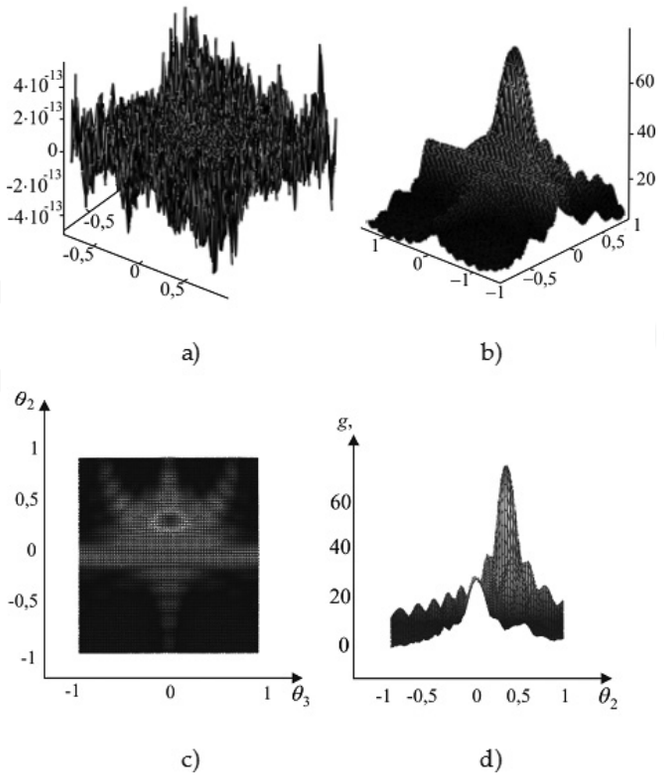

Figure 65. The fractal surface and the scattering indicatrix $g(\theta_2, \theta_3)$ when $\lambda = 30$ mm and $\theta_1 = 20°$: (a) fractal surface for $D = 2.2$; $N = M = 20$; $q = 2.7$; (b) $g(\theta_2, \theta_3)$; (c) $g(\theta_2, \theta_3)$, top view; (d) $g(\theta_2, \theta_3)$, side view.

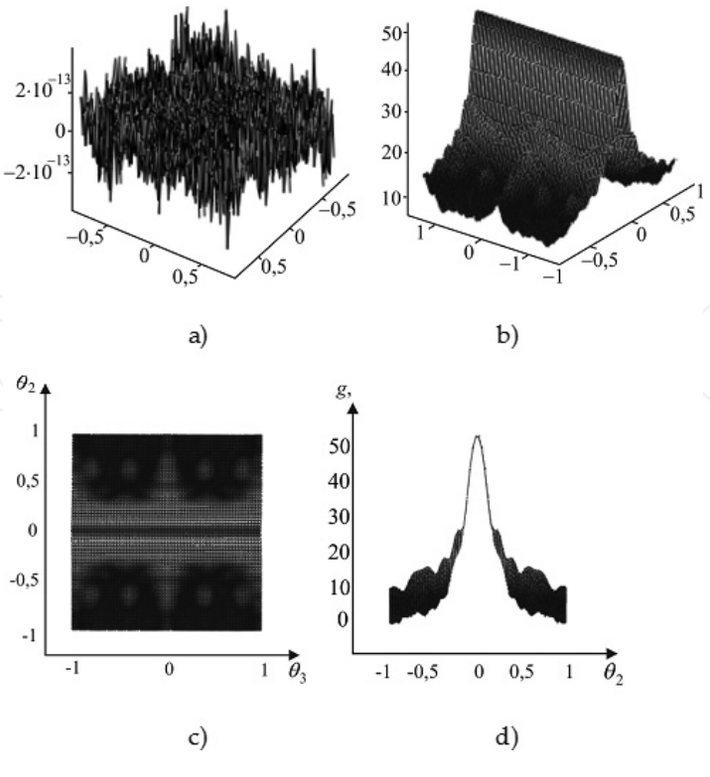

Figure 66. The fractal surface and the scattering indicatrix $g(\theta_2, \theta_3)$ when $\lambda = 30$ mm and $\theta_1 = 0°$: (a) fractal surface for $D = 2.5$; $N = M = 10$; $q = 2.7$; (b) $g(\theta_2, \theta_3)$; (c) $g(\theta_2, \theta_3)$, top view; (d) $g(\theta_2, \theta_3)$, side view.

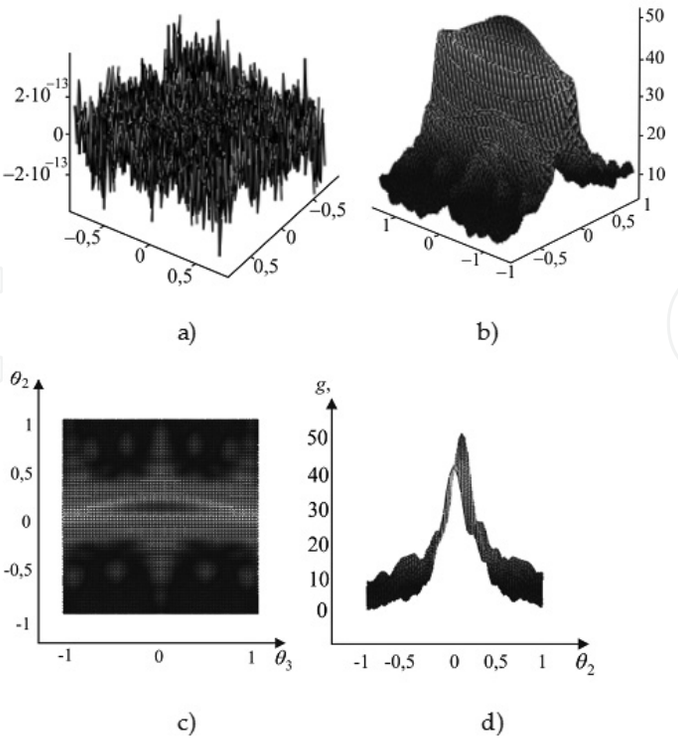

Figure 67. The fractal surface and the scattering indicatrix $g(\theta_2, \theta_3)$ when $\lambda = 30$ mm and $\theta_1 = 5°$: (a) fractal surface for $D = 2.5$; $N = M = 10$; $q = 2.7$; (b) $g(\theta_2, \theta_3)$; (c) $g(\theta_2, \theta_3)$, top view; (d) $g(\theta_2, \theta_3)$, side view.

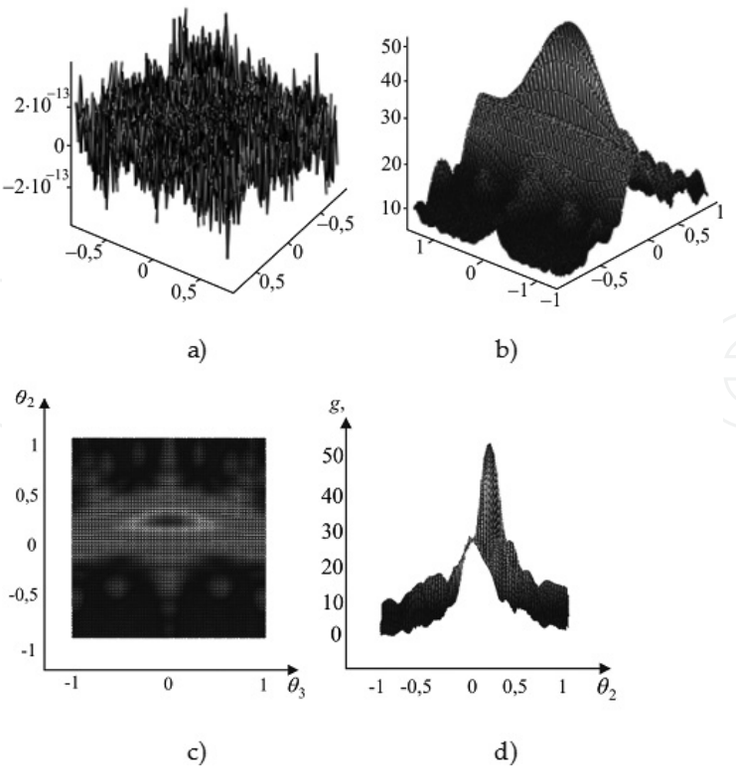

Figure 68. The fractal surface and the scattering indicatrix $g(\theta_2, \theta_3)$ when $\lambda = 30$ mm and $\theta_1 = 10°$: (a) fractal surface for $D = 2.5$; $N = M = 10$; $q = 2.7$; (b) $g(\theta_2, \theta_3)$; (c) $g(\theta_2, \theta_3)$, top view; (d) $g(\theta_2, \theta_3)$, side view.

http://dx.doi.org/10.5772/intechopen.68187

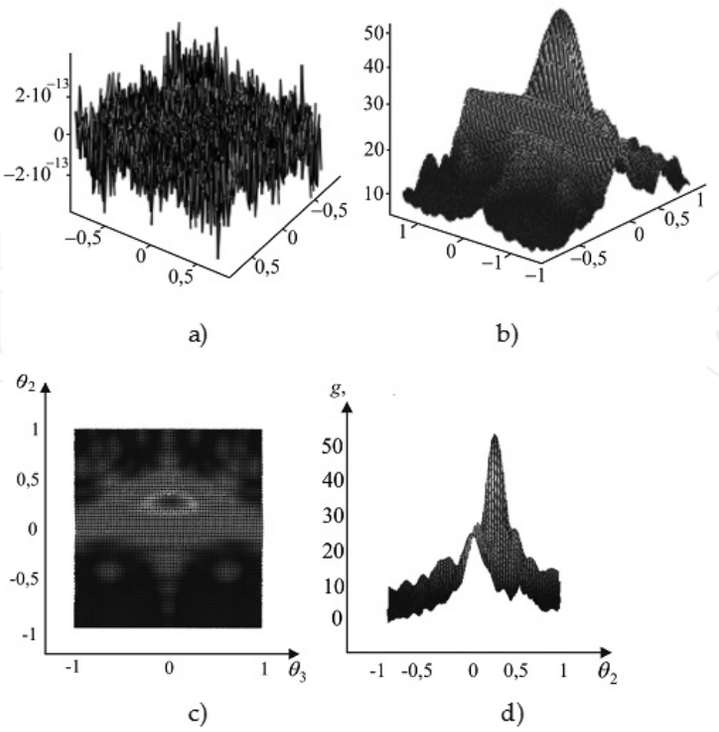

Figure 69. The fractal surface and the scattering indicatrix $g(\theta_2, \theta_3)$ when $\lambda = 30$ mm and $\theta_1 = 15°$: (a) fractal surface for $D = 2.5$; $N = M = 10$; $q = 2.7$; (b) $g(\theta_2, \theta_3)$; (c) $g(\theta_2, \theta_3)$, top view; (d) $g(\theta_2, \theta_3)$, side view.

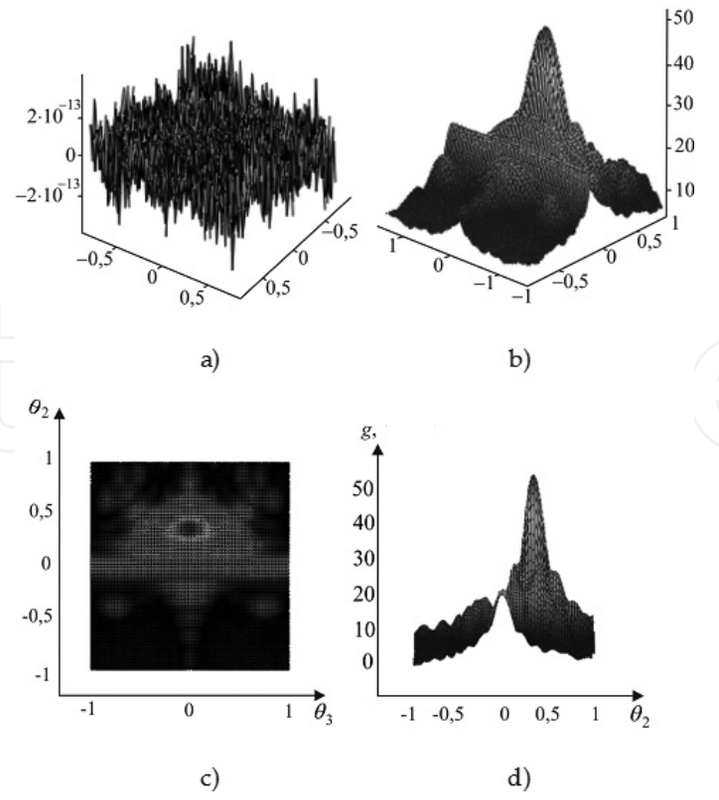

Figure 70. The fractal surface and the scattering indicatrix $g(\theta_2, \theta_3)$ when $\lambda = 30$ mm and $\theta_1 = 20°$: (a) fractal surface for $D = 2.5$; $N = M = 10$; $q = 2.7$; (b) $g(\theta_2, \theta_3)$; (c) $g(\theta_2, \theta_3)$, top view; (d) $g(\theta_2, \theta_3)$, side view.

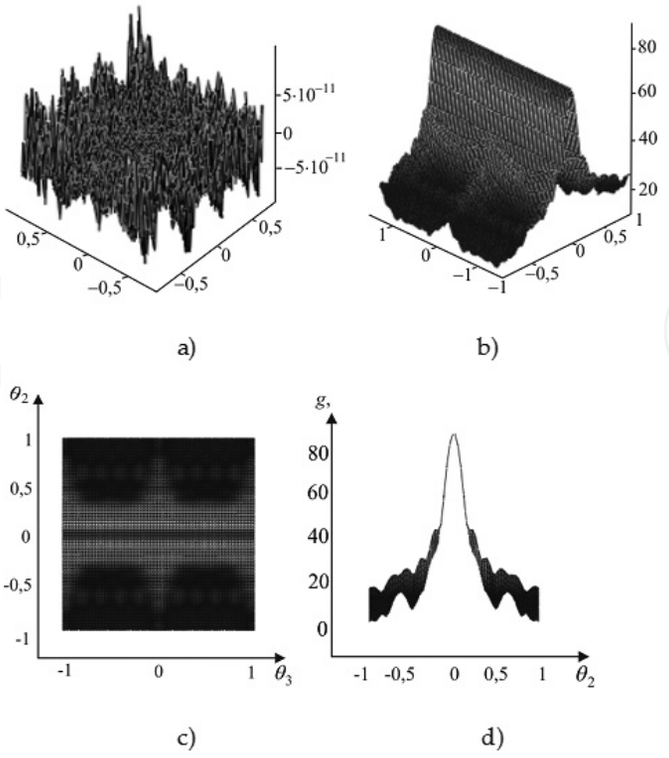

Figure 71. The fractal surface and the scattering indicatrix $g(\theta_2, \theta_3)$ when $\lambda = 30$ mm and $\theta_1 = 0°$: (a) fractal surface for $D = 2.5$; $N = M = 20$; $q = 2.7$; (b) $g(\theta_2, \theta_3)$; (c) $g(\theta_2, \theta_3)$, top view; (d) $g(\theta_2, \theta_3)$, side view.

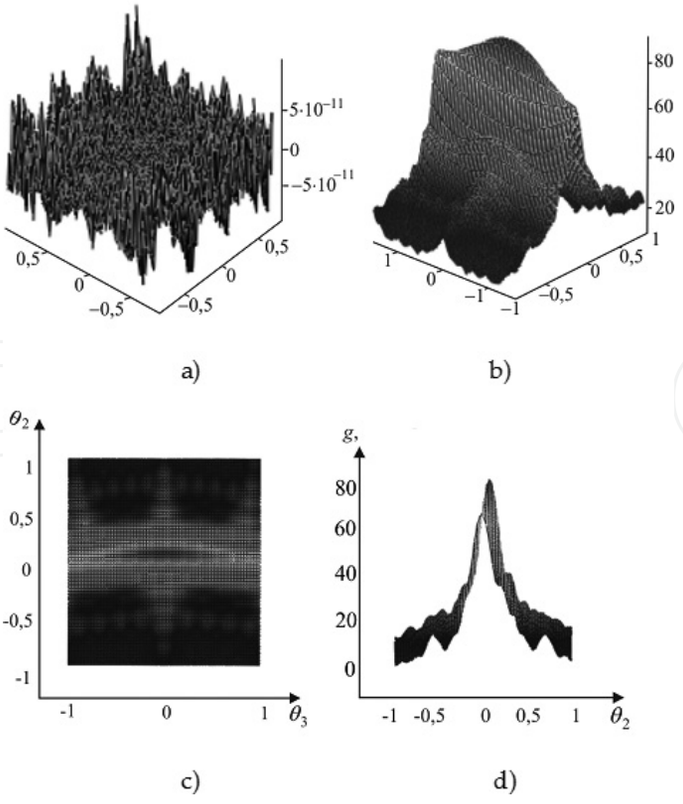

Figure 72. The fractal surface and the scattering indicatrix $g(\theta_2, \theta_3)$ when $\lambda = 30$ mm and $\theta_1 = 5°$: (a) fractal surface for $D = 2.5$; $N = M = 20$; $q = 2.7$; (b) $g(\theta_2, \theta_3)$; (c) $g(\theta_2, \theta_3)$, top view; (d) $g(\theta_2, \theta_3)$, side view.

http://dx.doi.org/10.5772/intechopen.68187

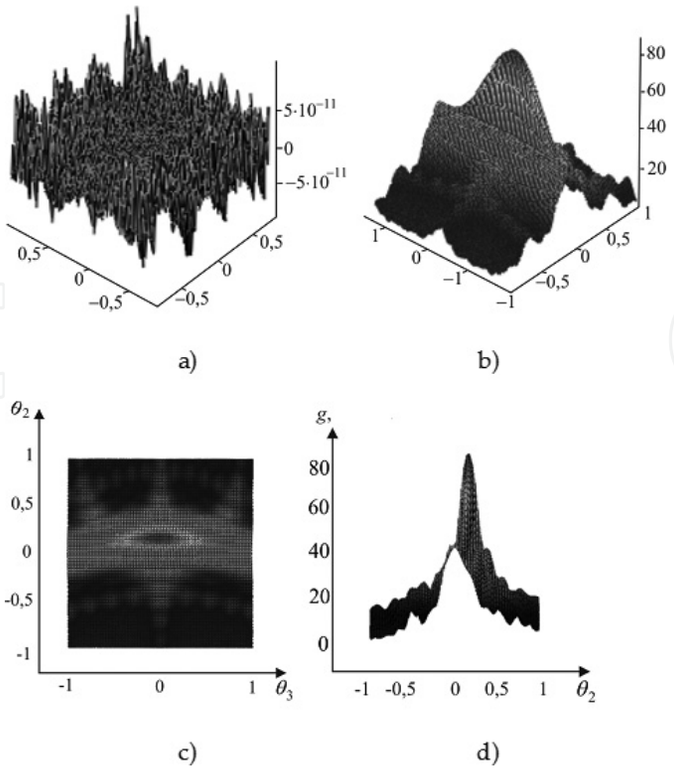

Figure 73. The fractal surface and the scattering indicatrix $g(\theta_2, \theta_3)$ when $\lambda = 30$ mm and $\theta_1 = 10°$: (a) fractal surface for $D = 2.5$; $N = M = 20$; $q = 2.7$; (b) $g(\theta_2, \theta_3)$; (c) $g(\theta_2, \theta_3)$, top view; (d) $g(\theta_2, \theta_3)$, side view.

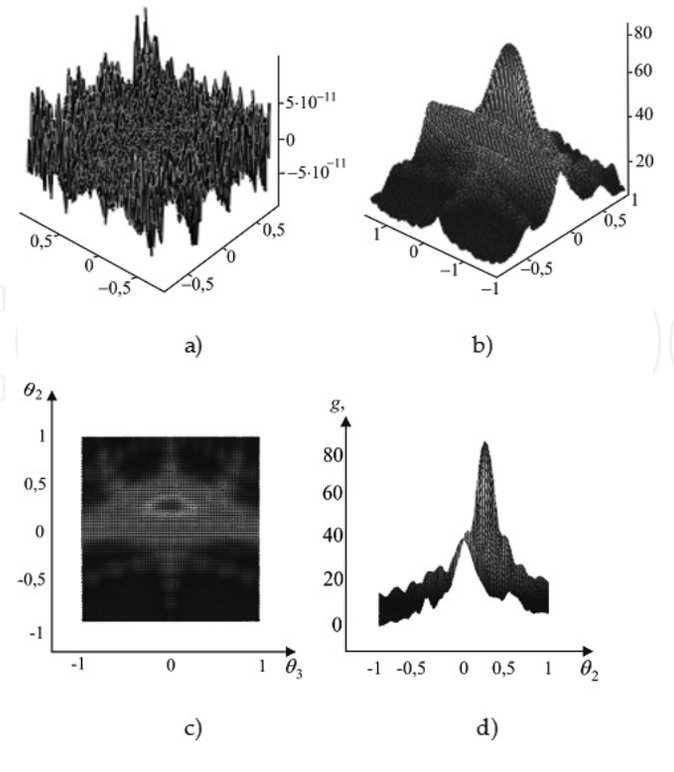

Figure 74. The fractal surface and the scattering indicatrix $g(\theta_2, \theta_3)$ when $\lambda = 30$ mm and $\theta_1 = 15°$: (a) fractal surface for $D = 2.5$; $N = M = 20$; $q = 2.7$; (b) $g(\theta_2, \theta_3)$; (c) $g(\theta_2, \theta_3)$, top view; (d) $g(\theta_2, \theta_3)$, side view.

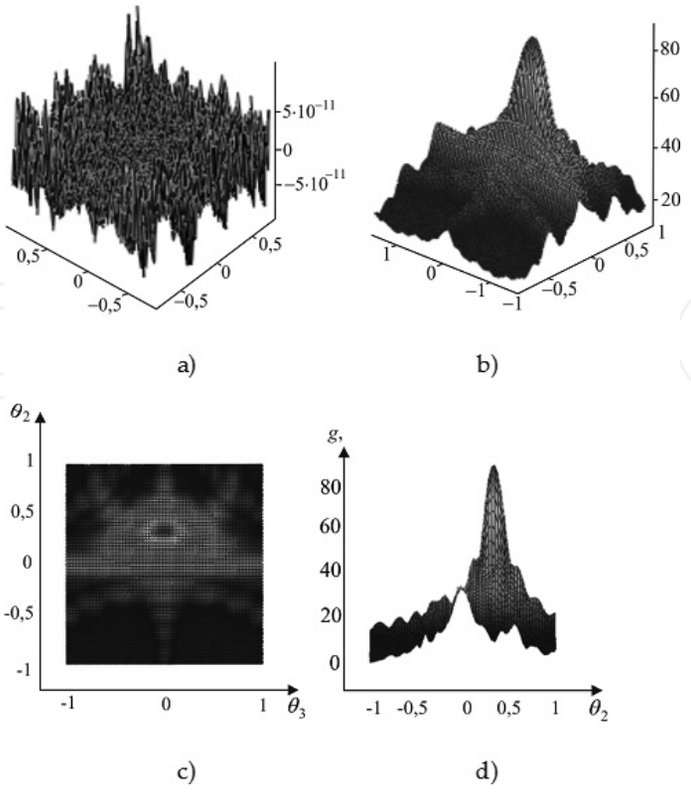

Figure 75. The fractal surface and the scattering indicatrix $g(\theta_2, \theta_3)$ when $\lambda = 30$ mm and $\theta_1 = 20°$: (a) fractal surface for $D = 2.5$; $N = M = 20$; $q = 2.7$; (b) $g(\theta_2, \theta_3)$; (c) $g(\theta_2, \theta_3)$, top view; (d) $g(\theta_2, \theta_3)$, side view.

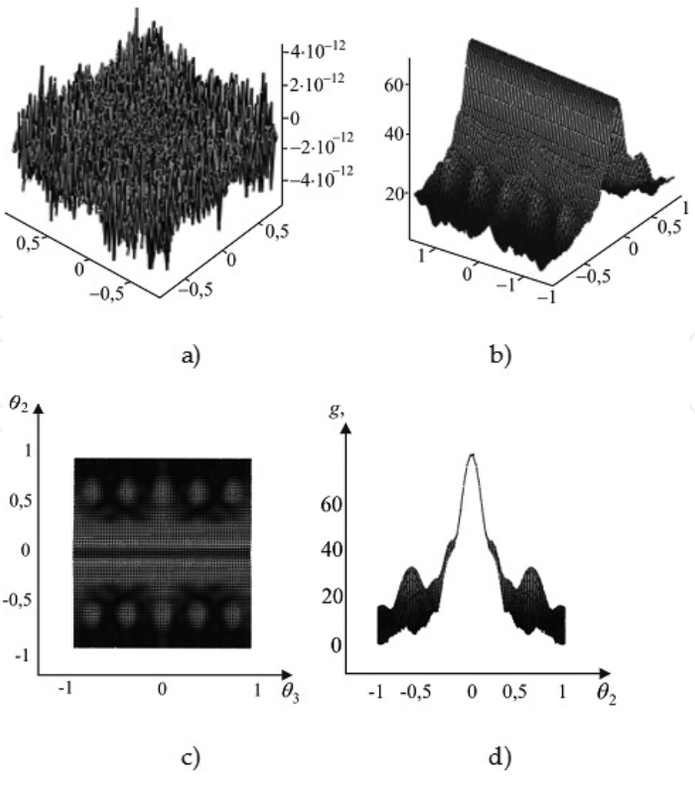

Figure 76. The fractal surface and the scattering indicatrix $g(\theta_2, \theta_3)$ when $\lambda = 30$ mm and $\theta_1 = 0°$: (a) fractal surface for $D = 2.8$; $N = M = 10$; $q = 2.7$; (b) $g(\theta_2, \theta_3)$; (c) $g(\theta_2, \theta_3)$, top view; (d) $g(\theta_2, \theta_3)$, side view.

http://dx.doi.org/10.5772/intechopen.68187

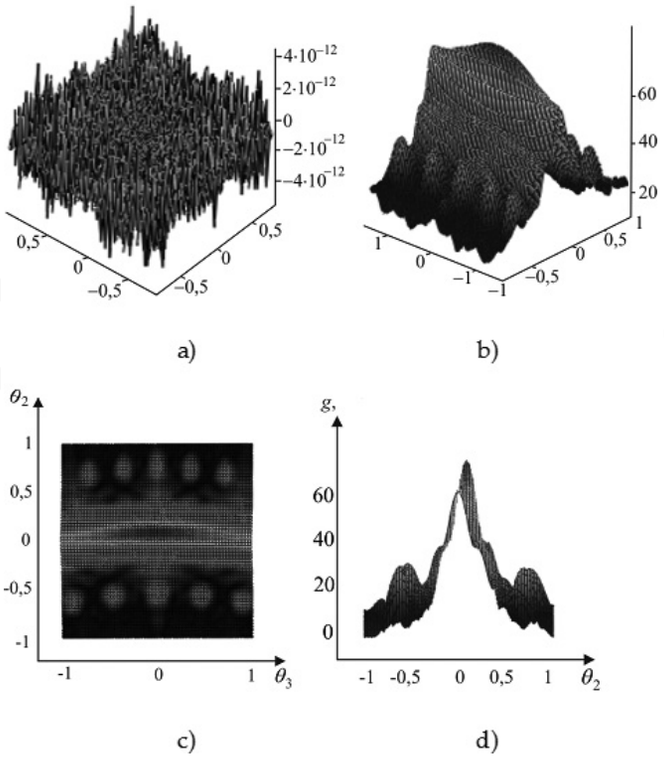

Figure 77. The fractal surface and the scattering indicatrix $g(\theta_2, \theta_3)$ when $\lambda = 30$ mm and $\theta_1 = 5°$: (a) fractal surface for $D = 2.8$; $N = M = 10$; $q = 2.7$; (b) $g(\theta_2, \theta_3)$; (c) $g(\theta_2, \theta_3)$, top view; (d) $g(\theta_2, \theta_3)$, side view.

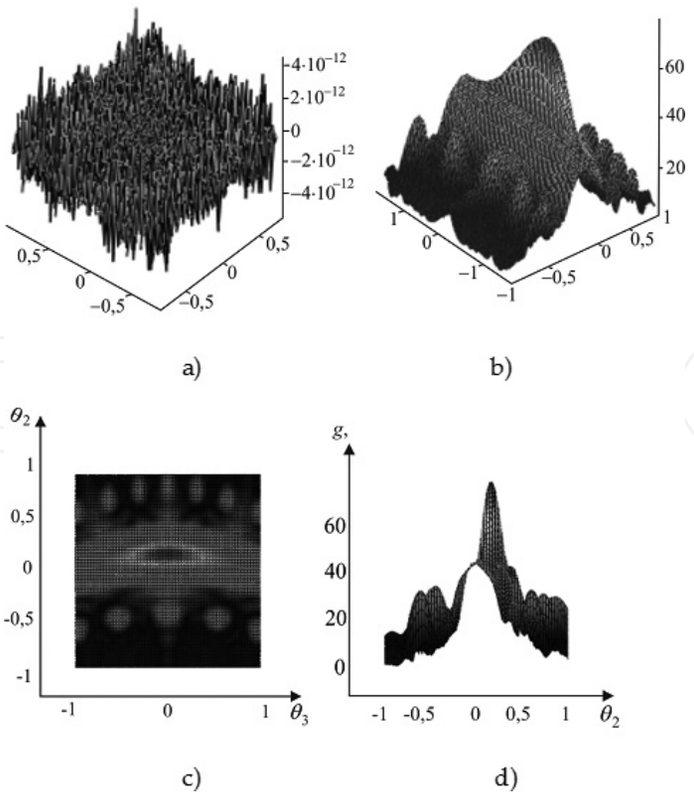

Figure 78. The fractal surface and the scattering indicatrix $g(\theta_2, \theta_3)$ when $\lambda = 30$ mm and $\theta_1 = 10°$: (a) fractal surface for $D = 2.8$; $N = M = 10$; $q = 2.7$; (b) $g(\theta_2, \theta_3)$; (c) $g(\theta_2, \theta_3)$, top view; (d) $g(\theta_2, \theta_3)$, side view.

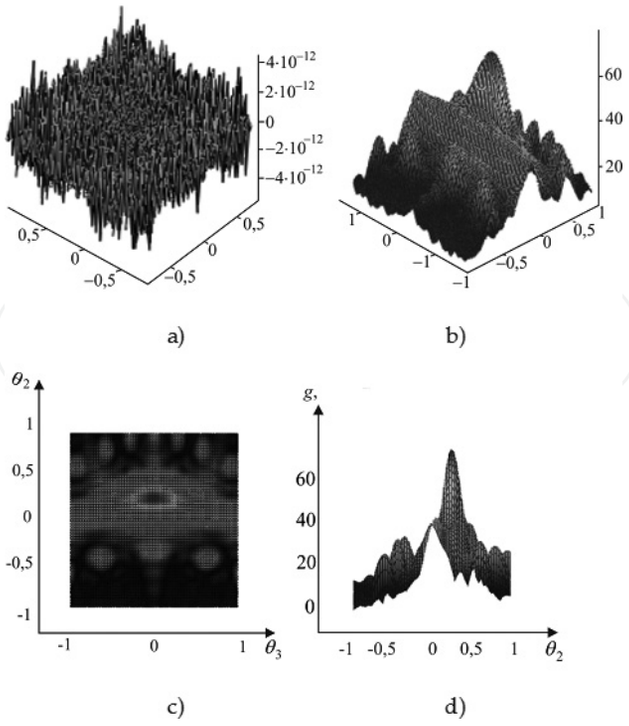

Figure 79. The fractal surface and the scattering indicatrix $g(\theta_2, \theta_3)$ when $\lambda = 30$ mm and $\theta_1 = 15°$: (a) fractal surface for $D = 2.8$; $N = M = 10$; $q = 2.7$; (b) $g(\theta_2, \theta_3)$; (c) $g(\theta_2, \theta_3)$, top view; (d) $g(\theta_2, \theta_3)$, side view.

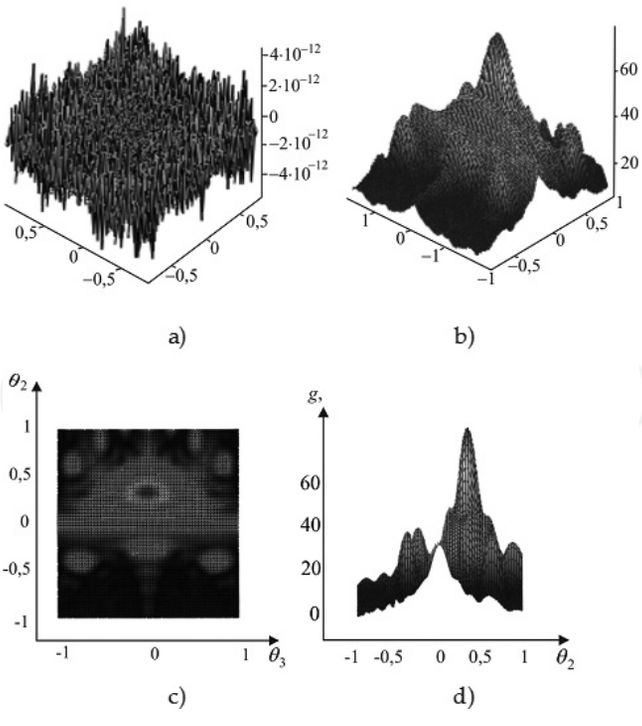

Figure 80. The fractal surface and the scattering indicatrix $g(\theta_2, \theta_3)$ when $\lambda = 30$ mm and $\theta_1 = 20°$: (a) fractal surface for $D = 2.8$; $N = M = 10$; $q = 2.7$; (b) $g(\theta_2, \theta_3)$; (c) $g(\theta_2, \theta_3)$, top view; (d) $g(\theta_2, \theta_3)$, side view.

http://dx.doi.org/10.5772/intechopen.68187

were calculated in the summer of 2006 for the wavelengths $\lambda = 2.2$ mm, $\lambda = 8.6$ mm and $\lambda = 3.0$ cm for the different values of fractal dimension D and different scattering geometry, respectively. It is significant to note that in this work there is only part of all of our theoretical results obtained for these courses. Some of results for this course that relates to "Fractal Electrodynamics" (this conception appeared for the first time in the USA in the monographs [66, 67]; see also native monographs [6, 7]) were published by us earlier in works [8, 15, 40].

8. Conclusion

Now on the basis of large scattering characteristics data array, we can arrive at some significant conclusions. When D has small value, the main part of energy is scattered in the specular direction. Side lobes appear due to Bragg scattering. The number of side lobes and their intensity increases with an increased value of fractal dimension D of the dispersive surface. Angular range of the side lobes also increases with an increase of D when higher spatial frequencies become significant. Radio wave that interacts with a fractal can be viewed as a yardstick to probe rough surfaces by means of spatial frequencies selection on the basis of Bragg diffraction conditions [6, 7]. In the case of small D values, classical and fractal approaches for scattered field solution coincide with each other. In practice, sizes of illuminated area must be at least two times greater than the main period of a surface structure in order to obtain fractal parameters information from scattering patterns.

Undoubtedly, fractal describing of the wave-scattering process [5–10, 15, 63, 72, 73, 77] will result in establishing new physical laws in the wave theory. Author is sure that the use of *fractal theory* and *determined chaos* jointly with *formalism of the apparatus of fractional operators* in the just considered problems allows to generate more valid radio physical and radar models that decrease significantly discrepancies between theory and measurements.

This work reviews in detail a variety of modern wave-scattering problems that appear in theoretical and applied areas of radio physics and radiolocation when the theory of *integer and fractional measuring* is used in general case. In other words, the use of *dissipative system dynamics formalism* (fractality, fractional operators, non-Gaussian statistics, distributions with heavy tales, mode of determined chaos, existing of strange attractors in the phase space of reflected signals, their topology, etc.) allows us to expect that classical problem of wave scattering by random mediums will be area of productive investigations in the future as before.

All results presented here are the priority ones in the world, and it is a basis material for the further development and foundation of practical application of fractal approaches in radio location, electronics, and radio physics and also for generating fundamentally new fractal elements/devices and fractal radio systems [5–48, 62, 63, 68–83]. These results can be applied widely for fractal antennas modeling, fractal frequency-selective structures modeling, solid-state physics, physics of nanostructures, and for the synthesis of nano-materials.

Acknowledgements

This work was supported in part by the project of International Science and Technology Center No. 0847.2 (2000–2005, USA), Russian Foundation for Basic Research (projects No. 05-07-90349, 07-07-07005, 07-07-12054, 07-08-00637, 11-07-00203) and also was supported in part by the project "Leading Talents of Guangdong Province," No. 00201502 (2016–2020) in the JiNan University (China, Guangzhou).

Author details

Alexander A. Potapov

Address all correspondence to: potapov@cplire.ru

1 Kotel'nikov Institute of Radio Engineering and Electronics of Russian Academy of Sciences, Moscow, Russia

2 JNU-IRE RAS Joint Laboratory of Information Technology and Fractal Processing of Signals, JiNan University, Guangzhou, China

References

[1] Bass FG, Fuks IM. Wave Scattering from Statistically Rough Surfaces. Oxford: Pergamon Press; 1979. p. 532

[2] Rytov SM, Kravtsov YA, Tatarskii VI. Introduction to Statistical Radiophysics. In: Rytov SM, editor. Moscow: Nauka; 1978. p. 464

[3] Ishimaru A. Wave Propagation and Scattering in Random Media. New York: Wiley-IEEE Press; 1999. p. 600

[4] Oleschko K, Korvin G, Balankin AS, Khachaturov RV, Flores L, Figueroa B, Urrutia J, Brambila F. Fractal scattering of microwaves from soils. Physical Review Letters. 2002;**89** (18):188501-1–188501-4

[5] Potapov AA. Earth Covering Image Synthesis in Optic and Millimeter Wave Bands [dissertation]. Moscow: IREE RAS; 1994. p. 436

[6] Potapov AA. Fractals in Radio Physics and Radar. Moscow: Logos; 2002. p. 664

[7] Potapov AA. Fractals in Radio Physics and Radar: Topology of Sample. Moscow: University Library; 2005. p. 848

[8] Potapov AA. Fractals and chaos as basis of new challenging technologies in modern radio systems. In: Cronover R, editor. Introduction to Fractal and Chaos. Moscow: Technosphere; 2006. pp. 374-479

[9] Podosenov SA, Potapov AA, Sokolov AA. Pulse Electrodynamics of Wide-Band Radio Systems. In: Potapov AA, editor. Moscow: Radiotekhnika; 2003. p. 720

[10] Bunkin BV, Reutov AP, Potapov AA, et al. Aspects of Prospective Radar. Moscow: Radiotekhnika; 2003. p. 512

[11] Bistrov RP, Potapov AA, Sokolov AV. Millimeter Band Radars with Fractal Processing. Moscow: Radiotekhnika; 2005. p. 512

[12] Nonlinear Radar: Collection of Articles (Library of Journal "Nonlinear World": Scientific Series "Fractals. Chaos. Probability"). Gorbachev AA, Koldanov AP, Potapov AA, Chigin EP, editors. Moscow: Radiotekhnika; 2005. p. 96

[13] Nonlinear Radar: Collection of Articles (Library of Journal "Nonlinear World": Scientific Series "Fractals. Chaos. Probability"). Gorbachev AA, Koldanov AP, Potapov AA, Chigin EP, editors. Moscow: Radiotekhnika; 2006. p. 168

[14] Nonlinear Radar: Collection of Articles (Library of Journal "Nonlinear World": Scientific Series "Fractals. Chaos. Probability"). Gorbachev AA, Koldanov AP, Potapov AA, Chigin EP, editors. Moscow: Radiotekhnika; 2007. p. 128

[15] Potapov AA. The textures, fractal, scaling effects and fractional operators as a basis of new methods of information processing and fractal radio systems designing. Proceedings of SPIE. 2009;**73740**:73740E-1–73740E-14

[16] Potapov AA, German VA. Detection of artificial objects with fractal signatures. Pattern Recognition and Image Analysis. 1998;**8**(2):226-229

[17] Potapov AA, German VA. Processing of optic and radar images of the earth surface by fractal methods. Journal of Communications Technology and Electronics. 2000;**45**(8):853-860

[18] Potapov AA. Fractals in radio physics and radio location: Fractal analysis of signals. Journal of Communications Technology and Electronics. 2001;**46**(3):237-246

[19] Potapov AA, German VA. Effects of deterministic chaos and strange attractor in the radar of dynamics systems of the vegetative cover type. Technical Physics Letters. 2002;**28** (7):586-588

[20] Potapov AA. Fractals in radiophysics and radar: Fundamental theory of wave scattering by a fractal surface. Journal of Communications Technology and Electronics. 2002;**47** (5):461-487

[21] Potapov AA. The fractal analysis in modern problems of radars and radiophysics. Radiotekhnika (Moscow). 2003;(8):55-66

[22] Potapov AA. New information technology in radar detection of low-contrast targets based on probabilistic texture and fractal features. Journal of Communications Technology and Electronics. 2003;**48**(9):1012-1029

[23] Reutov AP, Potapov AA, German VA. Strange attractors and fractals as a basis of new dynamics model of radar signals, scattering by vegetative cover. Nonlinear World (Moscow). 2003;**1**(1-2):12-27

[24] Potapov AA. Topology of sample. Nonlinear World (Moscow). 2004;**2**(1):4-13

[25] Potapov AA, German VA. Methods of measuring the fractal dimension and fractal signatures of a multidimensional stochastic signal. Journal of Communications Technology and Electronics. 2004;**49**(12):1370-1391

[26] Gorbachev AA, Potapov AA, Tarakankov SP. Distant diagnostic of dynamical systems based on electromagnetic waves nonlinear scattering. Nonlinear World (Moscow). 2004;**2**(5-6):310-314

[27] Potapov AA, Bulavkin VV, German VA, Vyacheslavova OF. The researching of micro structure surfaces with methods of fractal signatures. Technical Physics. 2005;**50**:560-575

[28] Bulavkin VV, Potapov AA, German VA, Vyacheslavova OF. The theory of fractals in problem of estimation surfaces. Russian Journal of Heavy Machinery. 2005;(6):19-25

[29] Potapov AA. The appliance of synergetic principles of nonlinear dynamic and fractals to development of the new information technologies for modern radio systems. Radiotekhnika (Moscow). 2005;(8):73-88

[30] Gulyaev YV, Nikitov SA, Potapov AA, Davydov AG. Design of fractal radio systems: Numerical analysis of electromagnetic properties of the Sierpinski fractal antenna. Journal of Communications Technology and Electronics. 2005;**50**(9):988-993

[31] Potapov AA, Il'yin EM, Chigin EP, German VA. Development and structure of the first etalon dictionary of fractal properties of target classes. Electromagnetic Phenomena. 2005;**5**(2(15)):107-142

[32] Opalenov YuV, Potapov AA. Fractal radar radonometry: Endomorphism of the radon's conception. Electromagnetic Phenomena. 2005;**5**(2(15)):143-159

[33] Kolesov VV, Potapov AA. Information technologies on dynamic chaos for telecommunication, radar and navigation systems. Electromagnetic Phenomena. 2005;**5**(2(15)):91-106

[34] Potapov AA, Potapov AA Jr, Potapov VA. The fractal capacitor, fractal operators, and fractal impedances. Nelineinyi Mir. 2006;**4**(4-5):172-187

[35] German VA, Potapov AA. Example of use of a hypothesis of self – similarity in a problem of detection of an acoustic signal. Nonlinear World (Moscow). 2006;**4**(4-5):204-207

[36] Potapov AA, German VA. The methods of fractal digital processing of weak signal and low contrast images. Avtometriya (Novosibirsk, Russia). 2006;**42**(5):3-25

[37] Potapov AA, German VA. The fractal non – parametric detector of radio signals. Radiotekhnika (Moscow). 2006;(5):30-36

[38] Gulyaev YV, Nikitov SA, Potapov AA, German VA. Concepts of scaling and fractal dimension in the design of a fractal detector of radio signals. Journal of Communications Technology and Electronics. 2006;**51**(8):909-916

[39] Potapov AA, Laktyunkin AV. Microwaves scattering on fractal surfaces as a new line of investigations. In: Proceedings of the Second European Conference on Antennas and

Propagation EuCAP 2007; 11-16 November 2007; The EICC, Edinburgh, UK. Edinburgh: The Institution of Engineering and Technology & EurAAP AISBL; 2007. p. MoPP.016. pdf. 6 pp

[40] Potapov AA. The theory of functionals of stochastic backscattered fields. Journal of Communications Technology and Electronics. 2007;**52**(3):245-292

[41] Laktyunkin AV, Potapov AA. Waves scattering dependence on the statistical parameters of classical and fractal rough surfaces. In: Proceedings of XXIX URSI General Assembly; 7-16 August 2008; USA, Chicago, Illinois. Chicago: University of Illinois at Chicago; 2008. p. BP16.1(228). pdf. 4 pp

[42] Potapov AA, Laktyunkin AV. Theory of the wave scattering by anisotropic fractal surface. Nonlinear World (Moscow). 2008;**6**(1):3-36

[43] Laktyunkin AV, Potapov AA. Radio waves scattering dependence on the statistical parameters of classical and fractal rough surfaces. In: Program 3rd European Conference on Antennas and Propagation EuCAP 2009; 23-27 March 2009; Berlin, Germany. Berlin: EurAAP; 2009. p. 24

[44] Laktyunkin AV, Potapov AA. Frequency and spatial features of waves scattering on fractals. In: Book of Abstracts 2nd International Conference (CHAOS' 2009) on Chaotic Modeling, Simulation and Applications; 01-05 June 2009; Chania, Crete, Greece. Chania: National and Kapodistrian University; 2009. p. 40

[45] Potapov AA. Can we build an adaptive fractal radio system? In: Proceedings of PIERS 2009 in Moscow "Progress in Electromagnetics Research Symposium"; 18-21 August, 2009; Moscow, Russia. Cambridge, MA: Electromagnetics Academy; 2009. pp. 1798-1802

[46] German VA, Potapov AA, Sykhonin EV. Fractal characteristics of radio thermal radiation of a different layer of atmosphere in a range of millimeter waves. In: Fractal Characteristics of Radio Thermal Radiation of a Different Layer of Atmosphere in a Range of Millimeter Waves; 18-21 August, 2009; Moscow, Russia. Cambridge, MA: Electromagnetics Academy; 2009. pp. 1813-1817

[47] Laktyunkin AV, Potapov AA. On frequency and spatial correlation of waves scattered by fractal surface. In: Program PIERS 2009 in Moscow "Progress in Electromagnetics Research Symposium"; 18-21 August, 2009; Moscow, Russia. Cambridge, MA: Electromagnetics Academy; 2009. p. 59

[48] Potapov AA. Fractals, scaling and fractal operators for radar problems: Fractal radio systems designing. In: Rohling H, editor. Proceedings of International Radar Symposium (IRS - 2009); 09-11 September, 2009; Hamburg, Germany. Hamburg: Technical University Hamburg-Harburg and German Institute of Navigation (TUHH and DGON); 2009. pp. 667-670

[49] Dyson F, Montroll E, Kas M, Fisher M. Stability and Phase Transitions. Moscow: Mir; 1973. p. 376

[50] Berry MV. Diffractals. Journal of Physics A. 1979;**12**(6):781-797

[51] Berry MV, Blackwell ZV. Diffractal echoes. Journal of Physics A. 1981;**14**(11):3101-3110

[52] Jaggard DL, Kim Y. Diffraction by band-limited fractal screens. Journal of Optical Society of America A. 1987;**4**:1055-1062

[53] Jaggard DL, Sun X. Scattering from fractally corrugated surfaces. Journal of Optical Society of America A. 1990;**7**:1131-1139

[54] Jakeman E. Fraunhofer scattering by a sub-fractal diffuser. Optica Acta. 1983;**30**:1207-1212

[55] Bertoni HL, Felsen LB, editors. Directions in Electromagnetic Wave Modeling. New York: Plenum Press; 1991. p. 560

[56] Jordan L, Hollins RC, Jakeman E. Experimental measurements of non-Gaussian scattering by a fractal diffuser. Applied Physics B. 1983;**31**:179-186

[57] Ball R, Blunt M. A fractal model for the impedance of a rough surface. Journal of Physics A. 1988;**21**:197-204

[58] Bourrely C, Chiappetta P, Torresani B. Light scattering by particles of arbitrary shape: A fractal approach. Journal of Optical Society of America A. 1986;**3**(2):250-255

[59] Sinha SK. Scattering from fractal structures. Physica D. 1989;**38**:310-314

[60] Jaggard DL, Sun X. Fractal surface scattering: A generalized Rayleigh solution. Journal of Applied Physics. 1990;**68**:5456-5462

[61] Lin N, Lee HP, Lim SP, Lee KS. Wave scattering from fractal surfaces. Journal of Modern Optics. 1995;**42**(1):225-241

[62] Potapov AA, Laktyun'kin AV. Frequency coherence function of a space-time radar channel forming images of an anisotropic fractal surface and fractal objects. Journal of Communications Technology and Electronics. 2015;**60**(9):962-969

[63] Alexander AP. Chaos theory, fractals and scaling in the radar: A look from 2015. In: Skiadas C, editor. The Foundations of Chaos Revisited: From Poincaré to Recent Advancements. Switzerland, Basel: Springer International Publishing; 2016. pp. 195-218

[64] Beckmann P, Spizzichino A. The Scattering of Electromagnetic Waves from Rough Surfaces. New York: Pergamon Press; 1963. p. 503

[65] Ogilvy JA. Theory of Wave Scattering from Random Rough Surfaces. Bristol: Adam Hilger; 1991. p. 292

[66] Jaggard DL. On Fractal Electrodynamics. In: Kritikos HN, Jaggard DL, editors. Recent Advances in Electromagnetic Theory. New York: Springer-Verlag; 1990. pp. 183-223

[67] Jaggard DL. Fractal electrodynamics: Wave interaction with discretely self – similar structures. In: Baum C, Kritikos HN, editors. Symmetry in Electrodynamics. London: Taylor & Francis; 1995. pp. 231-281

[68] Potapov AA. The global fractal method and the fractal paradigm in fundamental radar problems. In: Book of Abstracts International Conference on "Dynamics, Bifurcations and Strange Attractors" Dedicated to the Memory of L.P. Shil'nikov (1934–2011); July 1–5, 2013; Nizhni Novgorod, Russia. Nizhni Novgorod: Lobachevsky State University of Nizhni Novgorod; 2013. p. 98

[69] Potapov AA. The base of fractal antenna theory and applications: utilizing in electronic devices. In: Proceedings of the 2013 IX International Conference on Antenna Theory and Techniques; 16–20 September, 2013; Odessa, Ukraine. Odessa: Odessa National O.S. Popov Academy of Telecommunications; 2013. pp. 62-67

[70] Potapov AA. The global fractal method, fractal paradigm and the fractional derivatives method in fundamental radar problems and designing of revolutionary radio signals detectors. In: Zbornik Radova Konferencije MIT - Matematicke i informacione tehnologije; 5–14 September 2014; Vrnjackoj Banji od 5. do 9. septembra i u Becicima od 10. do 14. septembra 2013. godine. Kosovska Mitrovica: Prirodno-matematicki fakultet Ulverziteta u Pristini (Serbia); 2014. pp. 539-552

[71] Potapov Alexander A. Fractal radar: Towards 1980 – 2015. In: Proceedings of CHAOS 2015 International Conference; 26-29 May 2015; France. Paris: Henri Poincaré Institute; 2015. pp. 559-573

[72] Potapov AA, Rassadin AE. Feynman integrals, fractal paradigm and new point of view on hydroacoustics. Eurasian Physical Technical Journal. 2015;**12**(1(23)):3-13

[73] Podosenov SA, Potapov AA, Foukzon J, Menkova ER. Nonholonomic, fractal and linked structures in relativistic continuous media, electrodynamics, quantum mechanics and cosmology. In: Potapov AA, editor. 3 volumes. Moscow: Lenand; 2015. p. 1128

[74] Potapov AA. New conception of fractal radio device with fractal antennas and fractal detectors in the MIMO systems. In: Book of Abstracts 9th International Conference (CHAOS' 2016) on chaotic modeling, simulation and applications; 23-26 May 2016; Senate House, University of London, London, UK. London: University of London; 2016. p. 85

[75] Potapov AA, Laktyun'kin AV. Frequency coherence function of a radar channel forming images of a fractal surface and fractal objects. In: Book of Abstracts 9th International Conference (CHAOS' 2016) on Chaotic Modeling, Simulation and Applications; 23-26 May 2016; Senate House, University of London, London, UK. London: University of London; 2016. pp. 85-86

[76] Potapov AA, Potapov VA. Scaling of the fractals antennas. In: Book of Abstracts 9th International Conference (CHAOS' 2016) on Chaotic Modeling, Simulation and Applications; 23–26 May 2016; Senate House, University of London, London, UK. London: University of London; 2016. pp. 86-87.

[77] Potapov AA. The fractal - scaling radiolocation: Formation history 1980–2015. Chaotic Modeling and Simulation (CMSIM). 2016;(3):317-331

[78] Andrianov MN, Potapov AA. Increase efficiency of system of data transmission in fading channels using MIMO Systems. In: Shunjun W, editor. Proceedings of the 2016 CIE International Conference on Radar "Radar 2016"; October 10-12, 2016; China, Guangzhou. Beijing: Chinese Institute of Electronics (CIE); 2016. pp. 119-123

[79] Potapov AA, Zhang W. Simulation of new ultra-wide band fractal antennas based on fractal labyrinths. In: Shunjun W, editor. Proceedings of 2016 CIE International Conference on Radar "Radar 2016"; October 10-12, 2016; China, Guangzhou. Beijing: Chinese Institute of Electronics (CIE); 2016. pp. 319-323

[80] Potapov AA, German VA, Pahomov AA. Processing of images obtained from unmanned aerial vehicles in the regime of flight over inhomogeneous terrain with fractal-scaling and integral method. In: Shunjun W, editor. Proceedings of 2016 CIE International Conference on Radar "Radar 2016"; October 10-12, 2016; China, Guangzhou. Beijing: Chinese Institute of Electronics (CIE); 2016. pp. 585-587

[81] Potapov AA, Lazko FF. Gradients distribution matrices of and lacunarity in the capacity of texture measure of SAR and UAVs images. In: Shunjun W, editor. Proceedings of 2016 CIE International Conference on Radar "Radar 2016"; October 10-12, 2016; China, Guangzhou. Beijing: Chinese Institute of Electronics (CIE); 2016. pp. 605-608

[82] Potapov AA, German VA. A local dispersion method of measuring a fractal dimension and fractal signatures. In: Shunjun W, editor. Proceedings of 2016 CIE International Conference on Radar "Radar 2016"; October 10–12, 2016; China, Guangzhou. Beijing: Chinese Institute of Electronics (CIE); 2016. pp. 799-803

[83] Potapov AA. Strategic directions in synthesis of new topological radar detectors of low-contrast targets against the background of high-intensity noise from the ground, sea and precipitations. In: Shunjun W, editor. Proceedings of 2016 CIE International Conference on Radar "Radar 2016"; October 10-12, 2016; China, Guangzhou. Beijing: Chinese Institute of Electronics (CIE); 2016. pp. 692-696